ROLE OF LONG – RANGE ELECTRON - PHONON AND COULOMB INTERACTIONS IN HIGH - T_C CUPRATE SUPERCONDUCTORS

BY

TANUI PETER KIPROTICH

A THESIS SUBMITTED IN PARTIAL FULFILLMENT OF THE REQUIREMENTS FOR THE DEGREE OF DOCTOR OF PHILOSOPHY IN PHYSICS, SCHOOL OF SCIENCE UNIVERSITY OF ELDORET, KENYA

JANUARY 2016

DECLARATION

Declaration by the Candidate

This thesis is my original work and has not been submitted for any academic award in any institution; and shall not be reproduced in part or full, or in any format without prior written permission from the author and / or University of Eldoret.

Tanui Peter Kiprotich **Signature: _____Date: _____**

SC/D.PHIL /P/05/11

Declaration by Supervisors

This thesis has been submitted with our approval as university supervisors.

Prof. Khanna K.M. **Signature: _____ Date: _____**

Department of Physics

University of Eldoret

Prof. Tonui J.K. **Signature: _____ Date: _____**

Department of Physics

University of Eldoret

DEDICATION

This work is dedicated to my father, Joseph Tanui, my mother, Jane Tanui, my dear wife Rebecca Tanui, sons Kenan Kiplimo and Kilion Kimurgor, and daughters, Abital Jemeli and Adriel Jepkosgei.

ABSTRACT

Superconductivity is the disappearance of the electrical resistance of certain materials at certain critical temperatures called transition temperatures. This phenomenon was discovered in 1911 and is one of the most interesting and sophisticated discoveries in condensed matter physics. Superconducting materials have long been classified into two categories, viz low temperature (conventional) and high temperature (unconventional) supercunductors and the current work deals with the later type. High temperature superconductors have transition temperatures above 30 K (-243.15^0C) and are further grouped into pnictides and cuprates. Cuprates are copper oxide superconductors. This study investigated the role of long – range electron phonon and Coulomb interactions in high - T_c cuprate superconductors. In the study, the electron – phonon and Coulomb Hamiltonian was derived using frozen phonon method. The expectation value of the H_{epc} was calculated using second quantization and many body techniques. The equation for the energy of the system at ground state was obtained from the product of the expectation value of H_{epc} and the thermal activation factor, exp ($-E_1/kT$). The equation relating specific heat and absolute temperature was obtained from the first derivative of the energy of the system at ground state with respect to absolute temperature. The equation relating entropy and absolute temperature was obtained from the specific heat equation, using integral calculus. From the equations relating specific heat and entropy with absolute temperature, values of specific heat and entropy against absolute temperature were calculated. In these calculations, the onsite energy of copper (E_d) was fixed at 2.0 x 10^{-6} eV. The onsite energy of oxygen (E_p), hybridization energy of oxygen and copper bands (t_{pd}), the electron – phonon interaction energy, (g_{ep}) and energy due to repulsion of copper holes occupying the same orbital (u_d), were varied. From the results, it was found out that increase in the parameters E_d, t_{pd}, g_{ep} and u_d leads to increase in the transition temperature from 30 K to 90 K. It was further found that entropy and specific heat decrease with increase in the parameters. It can therefore be concluded that long range electron – phonon and Coulomb interactions increase the transition temperature of superconducting cuprates.

ACKNOWLEDGEMENTS

First and foremost, I thank the Almighty God for the wisdom that guided me to write this work. Secondly, I acknowledge the wise guidance and input from my supervisors, Professor K.M. Khanna (Professor of Physics, University of Eldoret) and Professor J.K. Tonui (Head, Department of Physics, University of Eldoret) for their dedicated assistance in doing this research work. I greatly benefited from their wide academic experience. They dedicated their precious time to reading my work and suggesting necessary corrections. I convey my sincere gratitude to the staff of the Department of Physics, University of Eldoret, for their constant encouragement while undertaking this research. I thank Professor Paul Samuel Francis (Chairperson, Department of Mathematics and Physics, University of Eastern Africa, Baraton), for his assistance. His knowledge in integral calculus was of great help. I will also not forget to acknowledge the moral support I received from my brothers and sisters. I acknowledge, in a special way, the spiritual and material support I received from my brother, Rev. Fr. Martin Kipkerich Tanui (Lecturer, Department of Social Sciences, University of Eldoret). To my friends and colleagues, thank you all for your encouragement. Finally, I thank my wife Rebecca Tanui for constantly encouraging me to continue writing even in times of difficulties.

TABLE OF CONTENTS

DECLARATION i
DEDICATION ii
ABSTRACT iv
ACKNOWLEDGEMENTS iii
TABLE OF CONTENTS v
LIST OF TABLES viii
LIST OF FIGURES ix
LIST OF APPENDICES xi
LIST OF ABBREVIATIONS AND ACRONYMS xii
LIST OF SYMBOLS xiii

INTRODUCTION 1
1.1 Background of the Study 1
1.2 The Discovery of Superconductivity 1
1.3 The Meissner Effect 3
1.4 Types of Superconductors 5
1.4.1 Type I Superconductors 5
1.4.2 Type II superconductors 6
1.5 Vortex States and Flux Pinning 7
1.6 BCS theory and Cooper Pairs 9
1.7 Statement of the Problem 12
1.8 Research Objectives 13
1.8.1 General Objective 13
1.8.2 Specific objectives 13
1.9 Significance of the Study 13
LITERATURE REVIEW 15
2.1 Introduction 15
2.2 Cuprate Superconductors 15
2.3 Conventional Superconductivity and high – T_c superconductivity. 18
2.4 Theoretical Models 21
2.4.1 Fermi – liquid Model 21
2.4.2 Hubbard Model 22
2.4.3 Frohlich – Coulomb Model 22
2.4.4. Coulomb Interaction and Hopping Model 24
2.4.5. t – J model 25
2.4.6 One-band Hubbard Model 26

2.4.7. Holstein Model 26
2.5. Electronic Structures of High Temperature Superconductors 26
2.6. Brief Summary of Some Latest ARPES Results 31
2.6.1Band Structure and Fermi Surface 32
2.6.2 Superconducting Gap 33
2.6.3. Time Reversal Symmetry Breaking 33
2.7. Electron-phonon Coupling in High Temperature Superconductors 34
2.7.1 Many – Body Effects 34
2.7.2 High critical transition temperature T_c 35
2.7.3 Isotope Effect in High Cuprate Superconductors 35
2.7.4 Transport Measurement 36
2.7.5 *d*-wave Symmetry of the Superconducting Gap 36
2.7.6 Structural Instability 37
2.7.7 Optical Spectroscopy and Raman Scattering 38
2.7.8 Neutron Scattering 41
2.7.9 Material and Structural Dependence 42
2.8. Electron-Phonon Interaction and Strong Electron Correlation 44
2.9. Weak Coupling – Perturbative and Self-Energy Description 48
2.10 Weak coupling and Non-interacting Electrons 49
2.10.1. Electron Self-energy 49
2.10.2 Electron-phonon Coupling 50
2.10.3 Anharmonic Apical Oxygen Vibrations in High T_c Superconductors 51
CHAPTER THREE 53
METHODOLOGY AND THEORETICAL DERIVATIONS 53
3.1 Introduction 53
3.2 The Frozen phonon method 53
3.3 The procedure for deriving electron – phonon interaction Hamiltonian 55
3.4 Derivation of Coulomb interaction Hamiltonian 61
3.5 The electron – phonon and Coulomb interaction Hamiltonian 63
CHAPTER FOUR 64
RESULTS AND DISCUSSIONS 64
4.1 Introduction 64
4.2 Calculation of the expectation value of the electron – phonon and Coulomb interaction Hamiltonian. 64

4.3 Effects of electron – phonon and Coulomb interactions on the transition temperature of high – T_c cuprate superconductors……...94

4.4 Effect of Various Parameters on Transition Temperature and Specific Heat..... 97

4.4.1 Effect of t_{pd} and g_{ep} on C_v and T_c(E_p = 3.5 x 10^{-6} eV and u_d = 2.5 x 10^{-6}eV) for YBaCuO. 97

4.4.2 Effect of t_{pd} and g_{ep} on C_v and T_c(E_p = 5.5 x 10^{-6} eV and u_d = 5.5 x 10^{-6}eV) for YBaCuO. 100

4.4.3 Effect of t_{pd} and g_{ep} on C_v and T_c (E_p = 7.5 x 10^{-6} eV and u_d = 6.5 x 10^{-6} eV) for YBaCuO. 103

4.5 Effects of Various Parameters on Transition Temperature and Entropy 106

4.5.1 Effect of t_{pd} and g_{ep} on S and T_c (E_p = 3.5 x 10^{-6} eV and u_d = 2.5 x 10^{-6} eV) for YBaCuO. 106

4.5.2. Effect of t_{pd} and g_{ep} on S and T_c (E_p = 5.5 x 10^{-6}eV and u_d = 5.5 x 10^{-6} eV) for YBaCuO. 109

4.5.3 Effect of t_{pd} and g_{ep} on S and T_c (E_p = 7.5 x 10^{-6} eV and u_d = 6.5 x 10^{-6} eV) for YBaCuO. 112

CHAPTER FIVE 115
CONCLUSION AND RECOMMENDATION.....115
5.1 Conclusion..... 115

5.2 Recommendations 116

REFERENCES 117
APPENDICES 132

LIST OF TABLES

Table 1.1: The critical temperatures of some superconductors(Dagotto, 1994)..... 3

Table C1: Numerical values of specific heat against temperature
(E_p = 3.5 x 10^{-6} eV and u_d = 2.5 x 10^{-6} eV) for YBaCuO. 142

Table C2: Numerical values of specific heat against absolute temperature
E_p = 5.5 x 10^{-6} eV and ud = 5.5 x 10^{-6} eV) 143

Table C3: Numerical values of specific heat against absolute temperature
(E_p = 7.5 x 10^{-6} eV and u_d = 6.5 x 10^{-6} eV) for YBaCuO. 144

Table C4:Numerical values of entropy agaisnt absolute temperature
(E_p = 3.5 x 10^{-6} eV and u_d = 2.5 x 10^{-6} eV) for YBaCuO……...145

Table C5: Numerical values of entropy against absolute temperature
(E_p = 5.5 x 10^{-6} eV and u_d = 5.5 x 10^{-6} eV) for YBaCuO. 146

Table C6: Numerical value of entropy against absolute temperature
(E_p = 7.5 x 10^{-6} eV and u_d = 6.5 x 10^{-6} eV) for YBaCuO. 147

LIST OF FIGURES

Figure 1.1: Variation of resistance of mercury with temperature (Onnes, 1911) 2

Figure 1.2: The Meissner effect (Meissner & Ochsenfeld, 1933) 4

Figure 1.3: Variation of induced magnetic field with external applied field for Type-I superconductor (Meissner & Ochsenfeld, 1933) 5

Figure 1.4: Variation of internal field with external field for Type-II superconductor (Sanchez & Navau, 2001) 6

Figure 1.5: Vortices (dark regions) in a type-II superconductor. Figure 1.5 (a) is 3 – dimensional view while figure 1.5 (b) is top view (Haugan *et al.*, 2004)..... 8

Figure 1.6: Coupling of a Cooper pair (Bardeen *et al.,* 1957) 10

Figure 2.1: Bonding in CuO2 plane (Pickett, 1989) 27

Figure 2.2: LDA calculated band structure of La_2CuO_4 (Pickett, 1989) 29

Figure 2.3: Experimentally measured Fermi surface and calculated Fermi surface in Pb-doped Bi2212 (Zhou *et al.,* 2007)..... 32

Figure 2.4: Anomalous softening of the B1g phonon when YBCO is cooled below T_c 38

Figure 2.5: Raman spectra of Hg1234 (Zhou *et al.,* 2007). 39

Figure 2.6: Variation of scattering intensity with energy shift in LSCO (Kim *et al.,* 2004). 40

Figure 2.7: Dispersion of the Cu-O bond-stretching vibrations (Ohkawa, 2007). 41

Figure 2.8: q dependence of B1g mode peak position at different temperatures in YBCO (Armitage, 2002)..... 42

Figure 2.9: Correlation between calculated range parameter r and observed T_c max..... 43

Figure 4.1: Variation of Specific Heat with temperature (E_p = 3.5 x 10^{-6} eV and u_d = 2.5 x 10^{-6} eV)..... 99

Figure 4.2: Variation of Specific heat with absolute temperature (E_p = 5.5 x 10^{-6} eV and u_d = 5.5 x 10^{-6} eV)..... 102

Figure 4.3: Variation of Specific Heat with absolute Temperature (E_p = 7.5 x 10^{-6} eV and u_d = 6.5 x 10^{-6} eV)..... 105

Figure 4.4: Variation of Entropy with absolute Temperature (E_p = 3.5 x 10^{-6} eV and u_d = 2.5 x 10^{-6} eV)..... 108

Figure 4.5: Variation of Entropy with absolute Temperature (E_p = 5.5 x 10^{-6} eV and u_d = 5.5 x 10^{-6} eV)..... 111

Figure 4.6: Variation of Entropy with absolute Temperature (E_p = 7.5 x 10^{-6} eV and u_d = 6.5 x 10^{-6} eV)..... 113

LIST OF APPENDICES

Appendix I: One Dimensional Electron – Phonon Transition Matrix Elements 132

Appendix II: Two Dimensions Electron – Phonon Transition Matrix Elements..... 138

Appendix III: Data for Specific Heat and Entropy against absolute Temperature……142

LIST OF ABBREVIATIONS AND ACRONYMS

AF	Antiferromagnetic
ARPES	Angle resolved photoemission spectroscopy
BCS	Bardeen, Cooper and Schrieffer
BEC	Bose – Einstein Condensate
CEIMC	Coupled electron – ion Monte Carlo
DFT	Density functional theory
DOS	Density of states
EPI	Electron phonon interaction
EPI	Electron-phonon interaction
FP	Frozen phonon
FS	Fermi surface
HTSC	High temperature superconductors
HTSC	High temperature superconductors
LDA	Local Density Approximation
LDC	Lattice dynamics calculation
MC	Monte Carlo
MD	Molecular dynamics
MRI	Magnetic resonance imaging
PES	Photoemission spectroscopy
QMC	Quantum Monte Carlo
SQUID	Superconducting quantum interference devices

LIST OF SYMBOLS

$\in_d$	or E_d	On – site energy of copper
m		Band mass
Δ_p		Binding energy
m^*		Carrier mass
ω		Phonon frequency
μ		Reduced mass of a pair of electrons
T_c		Critical temperature
$\alpha_{k,\sigma}$		Quasiparticle basis
U		Unitary transformation
γ		Electron – phonon interaction constant
ΔE		Energy gap
t_{pd}		Hybridization between copper and oxygen
M		Ion mass
M_D		Difference between the distorted and undistorted Hamiltonian
α		Isotope exponent
L		Lorenz number
λ_H		Magnetic field penetration depth
$\in_p$	or E_p	On – site energy of oxygen
u_{pd}		Oxygen – copper inter-site term
J_{pd}		Oxygen – copper spin exchange term
u_p		Oxygen on – site coupling term

u_d	Repulsion between holes occupying the same orbital
k	Thermal conductivity
C_n	Spinless fermionic operator
d_m	Spinless phononic operator
E_{LR}	Lattice relaxation energy
E_p	Polaronic level shift
k	Boltzmann constant
k	wave vector
zt	Half band width
ε_F	Fermi energy
λ	Dimensionless coupling constant
ΔE	Energy gap
$C_{\mathbf{n}}$	Spinless fermionic operator
$d_{\mathbf{m}}$	Spinless phononic operator
a	Lattice parameter
e_i	auxiliary boson
E_T	Charge transfer energy
λ	Electron – phonon dimensionless constant
B_c	Critical magnetic field
C_v	Specific heat
S	Entropy
Ω	Phonon energy
YBaCuO	Yttrium Barium Copper Oxide

CHAPTER ONE

INTRODUCTION

1.1 Background of the Study

Superconductivity is a phenomenon where electrical resistances of certain materials vanish completely at extremely low temperatures. It is among the most interesting and sophisticated discoveries in condensed matter physics in the twentieth century. Superconductivity has a number of applications, which includes superconducting quantum interference devices (SQUID), magnetic resonance imaging (MRI), scientific research and in magnetically levitated trains.

1.2 The Discovery of Superconductivity

Superconductivity was discovered by the Dutch physicist Heike Kamerlingh Onnes in 1911, three years after he liquefied helium (with boiling point of 4.2 K at standard pressure). Kamerlingh Onnes and one of his assistants discovered the phenomenon of superconductivity while studying the resistance of metals at low temperatures. They studied mercury because very pure samples could easily be prepared by distillation (Onnes, 1911). Figure 1.1 illustrates the phenomenon of superconductivity that was observed in mercury. As in many other metals, the electrical resistance of mercury decreased steadily upon cooling, but dropped suddenly at 4.2 K, and became undetectably small.

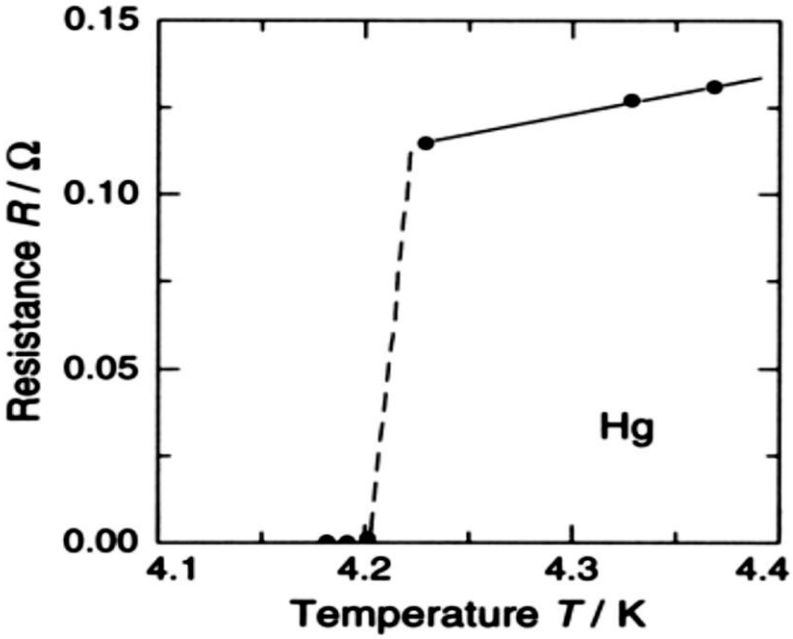

Figure 1.1: Variation of resistance of mercury with temperature (Onnes, 1911)

Soon after this discovery, many other elemental metals were found to exhibit zero resistance when their temperatures were lowered below a certain characteristic temperature of the material, called the critical temperature, T_c**.** The critical temperatures of some common superconducting materials are given in Table 1.1.

Table 1.1: The critical temperatures of some superconductors (Dagotto, 1994)

Element	T_c (K)	Element	T_c (K)	Element	T_c (K)
Al	1.19	Nb	9.2	Tc	7.8
Be	0.026	Np	0.075	Th	1.37
Cd	0.55	Os	0.65	Ti	0.39
Ga	1.09	Pa	1.3	Tl	2.39
Hf	0.13	Pb	7.2	U	0.2
Hg	4.15	Re	1.7	V	5.3
In	3.40	Rh	0.0003	W	0.012
Ir	0.14	Ru	0.5	Zn	0.9
La	4.8	Sn	3.75	Zr	0.55
Mo	0.92	Ta	4.39		
Compound	T_c (K)	Compound	T_c (K)	Compound	T_c (K)
Nb_3Sn	18.1	MgB_2	39	UPt_3	0.5
Nb_3Ge	23.2	$PbMo_6S_8$	15	UPd_2Al_3	2
Cs_3C_{60}	19	YPd_2B_2C	23	$(TMTSF)_2ClO_4$	1.2
Cs_3C_{60}	40	$HoNi_2B_2C$	7.5	$(ET)_2Cu[Ni(CN)_2]Br$	11.5
High-T_c superconductor		T_c (K)	High-T_c superconductor		T_c (K)
$La_{1.83}Sr_{0.17}CuO_4$		38	$Tl_2Ba_2Ca_2Cu_3O_{10+x}$		125
$YBa_2Cu_3O_{6+x}$		93	$HgBa2Ca_2Cu_30_{8+x}$		135
$Bi_2Sr_2Ca_2Cu_3O_{10+x}$		107	$Hg_{0.8}Tl_{0.2}Ba_2Ca_2Cu_30_{8.33}$		134

1.3 The Meissner Effect

In 1933, Meissner effect was discovered (Meissner & Ochsenfeld, 1933). This is a magnetic phenomenon in which a material excludes magnetic flux from its interior below its transition temperature. Figure 1.2 illustrates the difference between an ideal conductor and a superconductor when a magnetic field is applied.

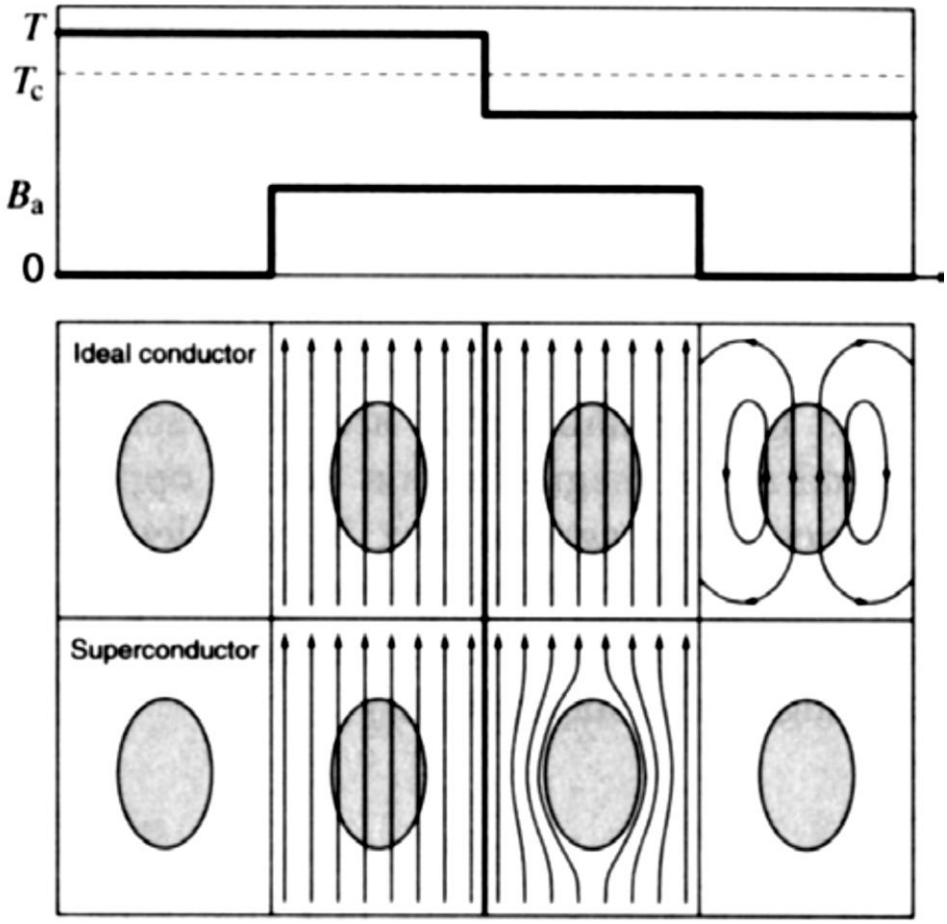

Figure 1.2: The Meissner effect (Meissner & Ochsenfeld, 1933)

The figure shows the behaviors of an ideal (normal) conductor and superconductor in the presence of external magnetic field above and below the critical temperature. At temperatures above T_C, the magnetic field penetrates both materials but at temperatures below T_C, the superconductor expels the magnetic field from inside it, while the ideal conductor maintains its interior field. The energy needed to expel the magnetic field by the superconductor comes from the exothermic superconducting transition. Switching off the field induces currents in the ideal conductor that prevent changes in the magnetic field inside it – by Lenz's law. However, the superconductor returns to its initial state, i.e. no magnetic field inside or outside it.

1.4 Types of Superconductors

Superconductors can be classified into type I and type II. High magnetic fields destroy superconductivity and restore the normal conducting state. Depending on the character of this transition, we may distinguish between type I and II superconductors.

1.4.1 Type I Superconductors

Fig. 1.3 illustrates the variation of internal magnetic field strength, B_i, with increasing applied magnetic field.

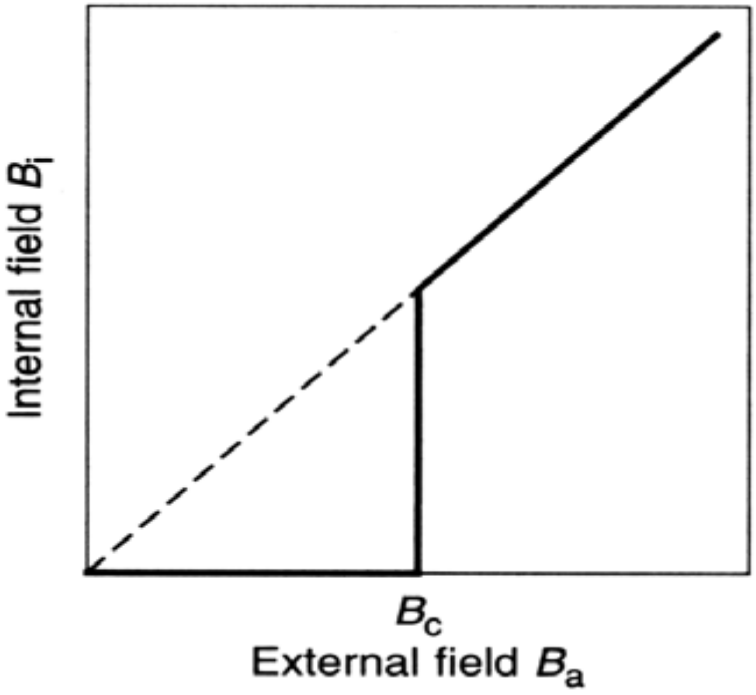

Figure 1.3: Variation of induced magnetic field with external applied field for Type-I superconductor (Meissner & Ochsenfeld, 1933)

From figure 1.3, the internal field is zero (as expected from the Meissner effect) until a critical magnetic field, B_c, is reached where a sudden transition to the normal state occurs. This results in the penetration of the applied field into the interior. Superconductors that undergo this abrupt transition to the normal state above a critical magnetic field are

known as type I superconductors. Most of the pure elements in Table (1.1) tend to be type I superconductors.

1.4.2 Type II superconductors

Fig. 1.4 shows how type II superconductors respond to an applied magnetic field.

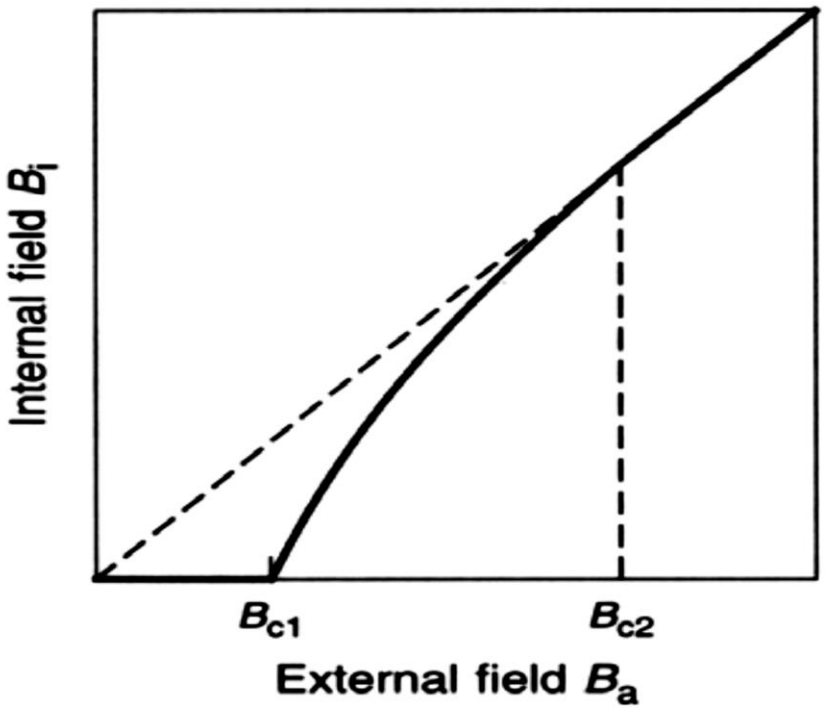

Figure 1.4: Variation of internal field with external field for Type-II superconductor (Sanchez & Navau, 2001)

An increasing field from zero results in two critical fields, $B_{c1}$and B_{c2}. At B_{c1}, the applied field begins to partially penetrate the interior of the superconductor. However, the superconductivity is maintained at this point. The superconductivity vanishes above the second, much higher, critical field, B_{c2}. For applied fields between B_{c1} and B_{c2}, the applied field is able to partially penetrate the superconductor, so the Meissner effect is incomplete, allowing the superconductor to accommodate very high magnetic fields.

Type II superconductors have useful technical applications because of the remnant magnetic field between the two transition regions. This is very useful particularly because of absence of electrical resistance, hence eddy current losses is minimal and provides a means of fabrication of very strong electromagnets. Most compounds given in Table 1.1 are type-II superconductors. Wires made from say niobium-tin (Nb_3Sn) have a B_{c2} as high as 24.5 Tesla – in practice it is lower. This makes them useful for applications requiring high magnetic fields, such as Magnetic Resonance Imaging (MRI) machines. The advantage of using superconducting electromagnets is that the current only has to be applied once to the wires, which are then formed into a closed loop and allow the current (and field) to persist indefinitely. As long as the superconductor stays below the critical temperature, the external power supply can be switched off. As a comparison, the strongest permanent magnets today may be able to produce a field close to 1 Tesla.

1.5 Vortex States and Flux Pinning

In type-II superconductors, there is partial penetration of the magnetic field in the form of a regular array of normal conducting regions (shown as the dark regions in Figure 1.5 (b).

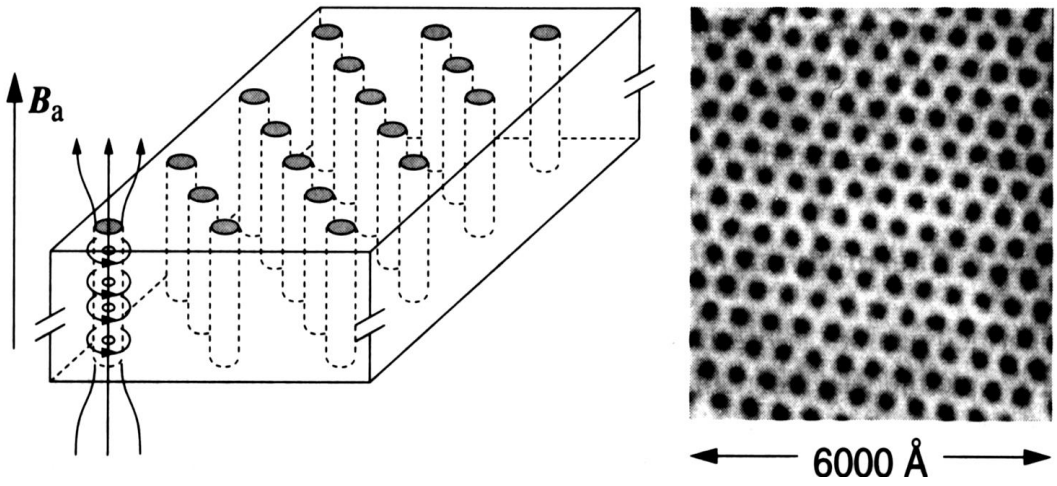

(a) (b)

Figure 1.5: Vortices (dark regions) in a type-II superconductor. (Haugan *et al.*, 2004)

These normal regions allow the penetration of the magnetic field in the form of thin filaments, usually called flux lines, fluxons, fluxoids or vortices. The vortices are aptly named because each is a "vortex" or swirl of electrical current (shown on Fig. 1.5 (a)) that are associated with this state. While in the vortex state, the material surrounding these normal conductors can have zero resistance and has partial flux penetration. Vortex regions are essentially filaments of normal conductor (non-superconducting) that run through the sample when an external applied magnetic field exceeds the lower critical field, B_{c1}. As the strength of the external field increases, the number of filaments increases until the field reaches the upper critical value, B_{c2}, the filaments crowd together and join up so the entire sample becomes normal. One can view a vortex as a cylindrical swirl of current surrounding a cylindrical normal conducting core that allows some flux to penetrate the interior of type-II superconductors. Thrusting a permanent magnet towards a type-II superconductor will cause the applied magnetic field at the

superconductor to be within the region of the two critical fields. This creates the vortex states shown on Fig. 1.5 (b). In principle, the motion of a levitating permanent magnet will cause these vortices to move. In practice, real materials (such as High T_c superconductors) have defects (missing or misplaced atoms, impurity atoms) in their crystal lattices. They are also composed of many crystals, all bound together, resulting in many crystal boundaries. The crystal defects and boundaries stop the motion of the vortices, which is known as flux pinning. This provides the stability of a levitating magnet. Pinning the motion of its magnetic field lines also means stopping the motion of the magnet. Note that flux pinning can only occur in type-II superconductors.

1.6 BCS theory and Cooper Pairs

According to classical physics, part of the resistance of a metal is due to collisions between free electrons and the crystal lattice's vibrations, known as phonons. In addition, part of the resistance is due to scattering of electrons from impurities or defects in the conductor. As a result, the question arose as to why this does not happen in superconductors.

A microscopic theory of superconductivity known as the Bardeen, Cooper and Schrieffer (BCS) theory was developed (Bardeen *et al.*,1957). The central feature of the BCS theory is that two electrons in the superconductor are able to form a bound pair called a Cooper pair if they somehow experience an attractive interaction between them. This notion at first sight seems counterintuitive since electrons normally repel one another because of their like charges. Figure 1.6 illustrates coupling of Cooper pairs.

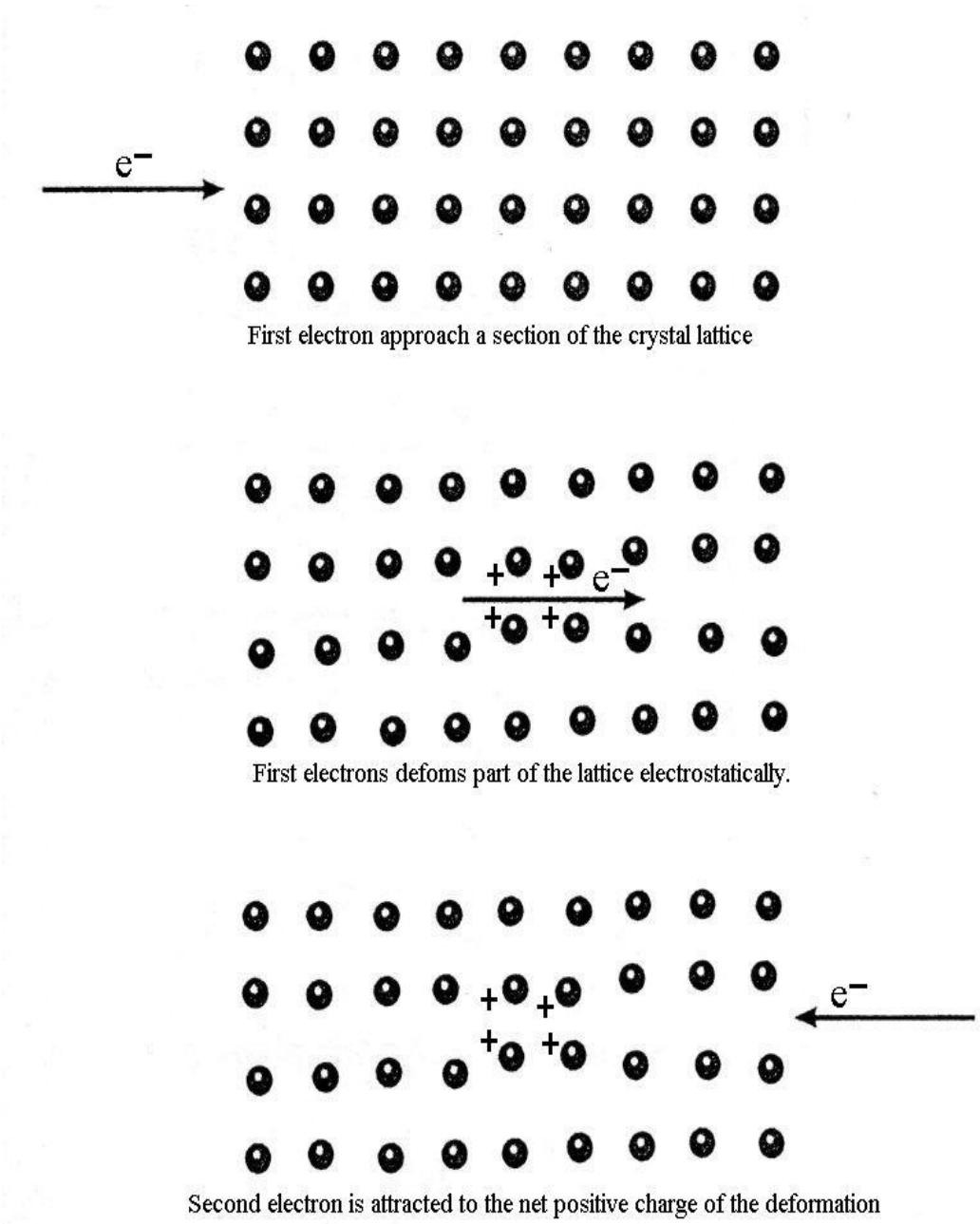

Figure 1.6: Coupling of a Cooper pair (Bardeen *et al.*, 1957)

An electron passes through the lattice and the positive ions are attracted to it, causing a distortion in their nominal positions. The second electron (the Cooper pair partner) comes along and is attracted by the displaced ions. Note that this second electron can only be attracted to the lattice distortion if it comes close enough before the ions have had a

chance to return to their equilibrium positions. The net effect is a weak delayed attractive force between the two electrons. This short lived distortion of the lattice is sometimes called a virtual phonon because its lifetime is too short to propagate through the lattice like a wave as a normal phonon would. From the BCS theory, the total linear momentum of a Cooper pair must be zero. This means that the electrons travel in opposite directions as shown in Figure 1.6. In addition, the nominal separation between the Cooper pair (called the coherence length) ranges from hundreds to thousands of ions separating them.

If electrons in a Cooper pair were too close, such as a couple of atomic spacing apart, the electrostatic (Coulomb) repulsion will be much larger than the attraction from the lattice deformation and so they will repel each other. Thus, there will be no superconductivity. A current flowing in the superconductor just shifts the total moment slightly from zero so that, on average, one electron in a Cooper pair has a slightly larger momentum magnitude than its pair. They do, however, still travel in opposite directions. The interaction between the electrons in a Cooper pair is transient. Each electron in the pair goes on to form a Cooper pair with other electrons, and this process continues with the newly formed Cooper pair so that each electron goes on to form a Cooper pair with other electrons. The end result is that each electron in the solid is attracted to every other electron forming a large network of interactions. If one of these electrons collides and scatters from atoms in the lattice, the whole network of electrons must be made to collide into the lattice, which is energetically too costly. The collective behaviour of all the electrons in the solid prevents any further collisions with the lattice. Nature prefers situations that spend a minimum of energy. In this case, the minimum energy situation is

to have no collisions with the lattice. A small amount of energy is needed to destroy the superconducting state and make it normal. This energy is called the energy gap.

Although a classical description of Cooper pairs has been given here, the formal treatment from the BCS theory is quantum mechanical. The electrons have wave-like behavior and are described by a wave function that extends throughout the solid and overlaps with other electron wave functions. As a result, the whole network of electrons behaves like one wave function so that their collective motion is coherent. In addition to having a linear momentum, each electron behaves as if it is spinning. This property is called spin. This does not mean that the electron is actually spinning, but behaves as though it is spinning. The requirement from the BCS theory is that spins of a Cooper pair be in opposite directions. Note that the explanation and pictorial representation of a Cooper pair presented here comes directly from BCS theory (Bardeen, *et al.,* 1957)

1.7 Statement of the Problem

Since the discovery of superconducting cuprates, many theories have been proposed to explain both normal and superconducting properties of these materials. However, there is no clear agreement on the appropriate theoretical description of these materials even in their normal states. It is generally believed that characterizing the cuprates above T_c is a necessary first step in unraveling the superconducting mechanism. Experimental observations and theoretical considerations point towards electron – phonon and Coulomb interactions in cuprates, which remain to be quantitatively addressed.

1.8 Research Objectives

1.8.1 General Objective

The general objective of this study was to evaluate the impact of electron – phonon and Coulomb interactions on superconducting properties of cuprates.

1.8.2 Specific objectives

i) To derive the electron – phonon and Coulomb interaction Hamiltonian using frozen phonon method

ii) To calculate the expectation value of the electron – phonon and Coulomb interaction Hamiltonian

iii) To determine the effect of electron – phonon and Coulomb interactions on the Transition Temperature of a high - T_c cuprate superconductor using Specific Heat and Entropy as parameters.

1.9 Significance of the Study

The electron – phonon and Coulomb interactions are of central importance for the electrical and thermal properties of solids, and its influence on high temperature superconductivity is the subject of intense research at present. However, the non – local nature of the interactions between valence electrons and lattice ions, compounded by vibrational modes present challenges for attempts to theoretically describe the physical properties of cuprates. Raman scattering study of the lattice dynamics in superlattices of high- temperature superconductors suggest a new approach to this problem. The superlattice geometry provides new opportunities for the electron - phonon interaction in complex materials. Experimental and theoretical studies of high – T_c superconductivity points to the possibility that the electron – phonon and Coulomb interactions have a

significant role in the behavior of high - T_c cuprate superconductors. This study, therefore, is essential because it explores the role played by electron – phonon and Coulomb interactions and unravel the quantitative theory that describes these interactions.

CHAPTER TWO

LITERATURE REVIEW

2.1 Introduction

Several experimental observations and theoretical studies have been done on superconductivity and published in refereed journals and books. In this chapter, important theories on superconductivity and literature review are presented.

2.2 Cuprate Superconductors

Superconductivity is a quantum mechanical phenomenon like magnetism. A modern and well accepted theory to explain superconductivity was developed by Bardeen, Cooper and Schrieffer in 1957 (Bardeen *et al.,* 1957) and is usually refereed to as the BCS theory. According to this theory, superconducting current was explained as a superfluid of Cooper pairs (pairs of electrons interacting through the exchange of phonons). Another point to note is that while low resistivity is a necessary condition for a material to be a superconductor, it is not sufficient.

Cuprates show a large number of interesting features. Apart from the exceptionally large superconducting transition temperature T_c, they exhibit antiferromagnetic (Kiryukhin *et al.,* 2001), pseudogap marginal Fermi liquid (Hwang *et al.,* 2004) and ordinary Fermi liquid phases (Varma *et al.,*1989) in addition to the superconducting phase. After the high-T_c cuprates had been discovered (Bednorz and Muller, 1986), there was initially much interest in the electron-phonon interaction (EPI). However, it was soon concluded that the EPI alone is too weak to explain high T_c superconductivity, in particular d-wave superconductivity, where the interest was focused purely on electronic models of these

compounds. More recently, there has been substantial experimental evidence that the EPI plays an appreciable role for a number of properties. Certain phonons show a large softening and broadening under doping (Pintschovius, 2005), suggesting a strong interaction with doped holes. This is, for instance, seen for the so-called half-breathing copper-oxygen bond stretching phonon, apical oxygen phonons and the oxygen B_{1g} buckling phonon. Photoemission spectroscopy (PES) experiments show the formation of small polarons for the undoped cuprates (Shen *et al.*,2007) and a kink in the nodal k-direction also suggests strong EPI (Gunnarsson & Rösch, 2008). While there is only a weak isotope effect on T_c for optimally doped samples, a strong isotope effect has been seen away from optimum doping (Chen *et al.,* 2007). Recent work suggests that a phonon mode plays a role in superconductivity (Xiang *et al.,* 2012) although other interpretations are possible (Pilgram *et al.,* 2006). In particular, an isotope effect has been observed (Gweon *et al.,* 2004). While the phonon contribution to superconductivity remains unclear, it seems clear that phonons can be important to study the properties of high – T_c superconductivity.

The EPI has been studied very extensively in the local density approximation (LDA) (Kohn & Sham, 1965) of the density functional formalism (Hohenberg *et al.,* 1964) , which is particularly appropriate for systems where correlation effects are not very strong. This approach has been shown to be very successful for conventional superconductors (Flores-Livas *et al.,* 2011). For cuprates (Pickett, 1989) a rather weak EPI was found, which alone would not be sufficient to explain the superconductivity (Savrasov & Anderson, 1996). However, the calculated width (Bohnen & Krauss, 2003)

of the half-breathing phonon is an order of magnitude smaller than the reported experimental value (Pintschovius & Braden, 1999), raising some questions about the accuracy of the LDA in this context(Reznik *et al.,* 2008). This is one of the reasons that the interest has recently focused on whether the interplay between the Coulomb interaction and the EPI can explain experimental signs of a strong EPI.

Due to the important effects of the Coulomb interaction in these systems, models such as the Hubbard and t-J models are often used. In these models phonons couple to charge fluctuations. Since charge fluctuations are strongly suppressed in the cuprates by the Coulomb interaction, an important issue is if this could mean that the EPI is actually suppressed.

In the so-called sudden approximation, angle resolved photoemission spectroscopy (ARPES) can be directly related to the one-electron Green's function. If superconductivity is due to bosons coupling to electrons and forming electron pairs, this coupling should show up in the one-electron Green's function. Due to the high interplay between electron-phonon and Coulomb interactions in cuprates energy- and k-resolution that can now be obtained in ARPES, a lot of interest has focused on ARPES recently.
ARPES experiments strongly indicate that small polarons are formed for undoped cuprates and there are signs of strong phonon side bands (Zhou *et al.,*2007). This indicates that there is a strong EPI for these systems. For weakly underdoped or optimally doped cuprates, ARPES experiments show quasiparticles, suggesting that there are no small polarons formed in these cases. However, there is still substantial spectral weight in

the energy range where phonon side bands would be expected, suggesting that the EPI is still substantial. There has been extensive work on polarons and bipolarons in metals, treating both electronic properties in general and superconductivity (Alexandrov & Mott, 1995).

Since experiments suggest that small polarons are not formed at dopings relevant for superconductivity, there was a focus on polaron formation for insulating systems. Due to the great interest in cuprates, there have been many reviews covering many aspects of these systems (Mandal *et al.*, 2014).

2.3 Conventional Superconductivity and high – T_c superconductivity.

Conventional Superconductivity can be understood as instability of a multi- electron system due to a phonon – mediated attractive interaction between the electrons resulting in the formation of Cooper pairs. Such systems could be understood on the basis of the weak coupling BCS Theory (Bardeen *et al.*, 1957). But in the case of Copper Oxide high-temperature superconductors (HTSC), which exhibit superconductivity at a much higher temperature (Bednorz & Müller,1986) than do conventional superconductors, it appears that established theories cannot explain the properties of HTSC and a new pairing mechanism has to be proposed. As a rule, the CuO_2 compounds are poor conductors, with one or two CuO_2 planes, which are separated by insulating oxide layers. It is believed that the CuO_2 layers form a charge reservoir with pairing interaction, and simultaneously these layers insulate the buffer layers(Gulacsi & Chan, 2001). It is well understood that due to the virtual charge excitations in oxygen-copper, an attraction appears at the oxygen ion sites.

CuO_2 planes or layers are regarded as the most important ingredients in achieving the high transition temperatures in superconductors. There appears to be a strong on-site attraction. A huge variation in the effective spin correlation is observed, and this changes sign with increasing oxygen-copper hopping. This can lead to changes in the on-site energies of oxygen (E_p) and copper (E_d). The energy gap ΔE for the charge transfer is

$$\Delta E = E_p - E_d \tag{2.1}$$

The hybridization enargy between copper and oxygen bands is represented by t_{pd}. The repulsion between the holes occupying the same $3d_{x^2-y^2}$ orbital is u_d. Consequently, the Hamiltonian will contain two new terms. One will be due to the oxygen-copper spin exchange, j_{pd}; and the second will be the oxygen-copper inter-site repulsion , u_{pd}, term. Thus there will be a new term in the Hamiltonian, and this will be the correlated oxygen-copper hopping term of the form $n_{\downarrow}(i,-a)^{\uparrow}\, p\left[p_{\downarrow}(i,-a)^{\uparrow} + d_{\downarrow}(j,a) + hc)\right]$ with a co-efficient denoted by t_{pd}^{p}.The presence of this new term will have a significant impact on the behavior of HTSC and in understanding the charge dynamics of the HTSC systems.

Hence in the second quantization notation, the Hamiltonian H can be written as

$$H = E_P \sum_i n_i^p + E_d \sum_j n_j^d + t_{pd} \sum_{i,j,a} \left(p_{i,a}^{+}\, d_{j,a} + hc \right) + u_d \sum_j n_{j,\uparrow}^d n_{j,\downarrow}^d \tag{2.2}$$

where p and d refer to the oxygen and copper ions, respectively. The first term in eq. (2.2) represents the energy of oxygen ions while the second term, the energy of the

copper ions (Gulacsi & Chan, 2001). The third term represents the energy due to the hybridization between copper and oxygen bands, and the fourth term represents the repulsion between the holes occupying the same copper orbital.

There are two new processes that can generate new terms, not present in the Hamiltonian given by equation (2.2). One of these new terms is a correlated oxygen-copper hopping term of the form

$$n^{p}_{i,-\lambda}(p^{+}_{i,a}d_{ja}+hc) \tag{2.3}$$

with a co-efficient denoted by; t^{p}_{pd}. The presence of the new term will have a significant impact on the behavior of HTSC and in understanding the charge dynamics of the HTSC systems. The second term will be completely new oxygen on-site coupling term represented by u_p and of the form

$$u_p \sum_i n^{p}_{i,\uparrow} n^{p}_{i,\downarrow} \tag{2.4}$$

The total Hamiltonian of the system will be the sum of equations (2.2) and the expressions (2.3) and (2.4) ; and the resultant Hamiltonian can be used to study the phenomena of the HTSC.

However, quite a large amount of research (Kaldis, *et al.*, 2012) in the field of high-temperature superconductivity suggests that the interaction in novel super-conductors is essentially repulsive and unretarted but it provides high-T_c without any phonons. On the other hand if it is assumed that Cooper pairing of repulsive fermions is possible, then the T_c of repulsive fermions is very low. Such models and BCS like theories fail to describe

the properties of high-T_c cuprates .It can therefore be said that models of this type are highly conflicting and confusing.

2.4 Theoretical Models

A number of theoretical models have been proposed to explain the mechanism of high temperature superconductivity. Some of the models are described below.

2.4.1 Fermi – liquid Model

A significant fraction of research in the field of high-temperature superconductivity suggests that the interaction in novel superconductors is essentially repulsive and unretarted, but it provides high T_c without any phonons (Anderson, 2004) .Earlier work (Kohn & Luttinger, 1965) showed that the Cooper pairing of repulsive fermions is possible. However, the same work showed that T_c of repulsive fermions is extremely low, well below the milliKelvin scale. Nevertheless, the BCS and BCS-like theories (including the Kohn–Luttinger consideration) heavily rely on the Fermi-liquid model of the normal state. This model fails in cuprates, so that there are no obvious reasons to discard the dogma, if the normal state is not the Fermi liquid. Strong on - site repulsive correlations (Hubbard *U*) are essential in undoped (parent) cuprates, which are *insulators* with an optical gap about 2 eV or so. Indeed, if repulsive correlations are weak, one would expect a metallic behaviour of a half-filled *d*-band of copper, or, at most, a much smaller gap caused by lattice and spin distortions (Gabovich *et al.,* 2001). It is a strong onsite repulsion of *d*-electrons which results in the “Mott” insulating state of parent cuprates. Different from conventional band structure insulators with completely filled or empty

Bloch bands, the Mott insulator arises from a potentially metallic half-filled band as a result of the Coulomb blockade of electron tunneling to neighbouring sites (Mott, 1990).

2.4.2 Hubbard Model

Hubbard model describes high-T_c superconductivity at finite doping. However some authors could not find any superconducting instability without an additional electron–phonon interaction (Sherman & Ambrose, 2000). Therefore, it has been concluded that model of this kind are highly conflicting and confuse the issue by exaggerating the magnetism rather than clarifying it (Alexandrov, 2007). There is another serious problem with the Hubbard-U approach to high-temperature superconductivity in the cuprates. The characteristic (magnetic) interaction, which might be responsible for the pairing in the Hubbard model, is the spin exchange interaction, $J = 4t^2/U$, of the order of 0.1 eV. It turns out much smaller than the (intersite) Coulomb repulsion and the unscreened long-range (Frohlich) electron–phonon interaction each of the order of 1 eV, routinely neglected within the approach. There is virtually no screening of electron–phonon interactions with *c*-axis polarised optical phonons in cuprates because the upper limit for the out-of-plane plasmon frequency = 200 cm^{-1} (Bozovic *et al.,* 1994) is well below the characteristic phonon frequency, $\omega \approx 400–1000$ cm^{-1}. Because of the poor screening, the magnetic interaction remains small compared with the Frohlich interaction at any doping. Hence, any realistic approach to superconductivity and heterogeneity in cuprates should treat the Coulomb and unscreened electron – phonon interactions on the same footing.

2.4.3 Frohlich – Coulomb Model

The “Frohlich– Coulomb” model was developed to deal with the strong Coulomb and long-range electron–phonon interactions in cuprates and other doped oxides (Alexandrov,

2003). The model Hamiltonian explicitly includes the long-range electron–phonon and Coulomb interactions as well as the kinetic and deformation energies. The implicitly present large Hubbard term prohibits double occupancy and removes the need to distinguish fermionic spins. Introducing spinless fermionic, $c_{\mathbf{n}}$, and phononic, $d_{\mathbf{m}}$, operators, the Hamiltonian of the model is written as

$$H = \sum_{n,n'} [\, t(\mathbf{n}-\mathbf{n}')c_n^+ c_{n'} + V_c(\mathbf{n}-\mathbf{n}')c_n^+ c_{n'}^+ c_{n'} c_n \,] \\ - \omega \sum_{\mathbf{n},\mathbf{m}} g(\mathbf{m}-\mathbf{n})\, e u_{m-n} c_n^+ c_n (d_m^+ + d_m) + \omega \sum_m (d_m^+ d_m + \frac{1}{2}) \qquad 2.5$$

where **e** is the polarization vector of the vibration coordinate, $\mathbf{u_{m-n}} \equiv (\mathbf{m} - \mathbf{n})/|\mathbf{m} - \mathbf{n}|$ is the unit vector in the direction from electron **n** to the ion **m**, $g(\mathbf{m} - \mathbf{n})$ is a dimensionless electron – phonon coupling function, and $V_c(n-n')$ is the intersite Coulomb repulsion. $g_\alpha(\mathbf{m} - \mathbf{n})$ is proportional to the force acting between an electron on site **n** and an ion **m**. For simplicity, we assume that all the phonon modes are dispersionless with frequency ω_α. The Hamiltonian, Eq. (2.5), can be solved analytically in the extreme case of the strong electron – phonon interaction with the electron – phonon dimensionless coupling constant $\lambda = E_p/zt > 1$ using $1/\lambda$ multi-polaron expansion technique (Alexandrov, 2003). Here $E_p = \sum_{n\alpha} \omega_a g_\alpha^2(n)(e_\alpha - u_n)^2$, is the polaronic level shift about 1 eV and zt is the half bandwidth in a rigid lattice.

The model shows a phase transition depending on the ratio of the intersite Coulomb repulsion V_c and the polaronic (Franc–Condon) level shift E_p (Alexandrov & Kornilovitch,2002). The ground state is a polaronic Fermi liquid at large Coulomb

repulsion, a bipolaronic high-temperature superconductor at intermediate Coulomb repulsions, and a charge-segregated insulator at weak repulsion. The model predicts superlight bipolarons with a remarkably high superconducting critical temperature. It describes many other properties of the cuprates in particular the isotope effects, normal state thermomagnetic transport and real-space modulations of the single-particle density of states (DOS).

2.4.4. Coulomb Interaction and Hopping Model

The Coulomb interaction plays an important role in the cuprates. A frequently used model for describing this is the three-band model (Emery, 1987), which includes a Cu_{x2-y2} 3d orbital and two O orbitals in a CuO_2 plane. The model includes the Cu-O hopping integrals and the Coulomb interaction between two electrons on the Cu orbital given by the Hamiltonian

$$H_{three-band} = \varepsilon_d \sum_{i\sigma} c_{i\sigma}^{+} c_{i\sigma} + \varepsilon_o \sum_{i\delta\sigma} a_{i\delta\sigma}^{+} a_{i\delta\sigma} + t_{pd} \sum_{i\delta\sigma} P_\delta (c_{i\sigma}^{+} a_{i\delta\sigma} + H.c) + U \sum_i n_{i\uparrow} n_{i\downarrow} \tag{2.6}$$

where ε_d and ε_O are the energies of the Cu and O atoms, respectively. δ describes the O atom positions in the unit cell and runs over (a/2, 0) and (0, a/2) in the second term and over (±a/2, 0) and (0,±a/2) in the third term, where 'a' is the lattice parameter. $P_{-\delta} = -P_\delta$, $P_\delta = 1$ for δ = (a/2, 0) and $P_\delta = -1$ for δ = (0, a/2), $c_{i\sigma}^{+}$ creates a Cu electron with spin σ, $a_{i\delta\sigma}^{+}$ creates an O electron and $n_\sigma = c_{i\sigma}^{+} c_{i\sigma}$. U is the Coulomb interaction and t_{pd} is a hopping integral.

2.4.5. t – J model

From Coulomb interaction and hopping model, the t-J model was derived (Zhang & Rice, 1988), where each site corresponds to a Cu atom in the CuO_2 plane. In the undoped system, corresponding to all Cu atoms being in d_9 configurations, each site is occupied by one hole. In a hole doped system, the holes go primarily onto the O sites. Such an O hole forms a Zhang-Rice singlet with a Cu hole (Zhang & Rice, 1988). A Zhang-Rice singlet is described by an empty site in the t-J model.

The corresponding Hamiltonian is

$$H_{t-J} = -t \sum_{\langle i\, j\rangle \sigma} (\breve{c}^{+}_{i\sigma} \breve{c}_{j\sigma} + H.c) + J \sum_{\langle i\, j\rangle} (S_i \,.\, S_j - \frac{1}{4} n_i n_j) \qquad (2.7)$$

where <ij> refers to a sum over nearest neighbor pairs, and $c^{+}_{i\sigma}$ creates a hole of spin σ on site i if this site was previously empty. S_i is the spin and $n_i = \sum_{\sigma} \breve{c}^{+}_{i\sigma} \breve{c}_{i\sigma}$ is the number of holes on sites i.

The breathing (oxygen bond-stretching) phonons have attracted much interest due to the observation of an anomalous softening and broadening of these phonons when the system is doped (Graf *et al.*, 2008). That these phonons may have a strong coupling can be understood by noticing that the formation of the Zhang-Rice singlet in the t-J model involves a large energy of the order of several eV. For a system without phonons and a fixed number of doped holes, this energy only enters as an uninteresting constant. If phonons are added, however, the singlet energy can be modulated by the phonons. This is the case for the breathing phonons, where the O atoms in the CuO_2 plane move in the direction of the Cu atoms, thereby changing the bond lengths. This directly modulates the Cu-O hopping integrals t_{pd} (in a three-band model) determining the Zhang-Rice singlet

energy and leads to a substantial coupling. This has been discussed by several groups (Horsch and Khaliullin, 2005). A general formula for this coupling was given (Rosch and Gunnarson, 2004), considering both the modulation of the Cu-O hopping integrals and shifts of the levels due to Coulomb interactions. It was found that the main coupling is an on-site coupling due to the modulation of the Cu-O hopping integrals. One reason for this result is that the hopping integrals in the t-J model, obtained after the O levels have been projected out, are about an order of magnitude smaller than the on-site singlet energy. This strongly favors the on-site electron-phonon interaction over the coupling to the t-J hopping integrals (Sentef *et al.*, 2013).

2.4.6 One-band Hubbard Model

This model is often used and the Hamiltonian is given by

$$H_{Hub} = -t \sum_{<ij>\sigma} (c^{+}_{i\sigma} c_{ij} + H.c.) + U \sum_{i} n_{i\uparrow} n_{i\downarrow} \tag{2.8}$$

The t-J model can also be derived from the Hubbard model in the large U limit if certain terms are neglected (Auerbach, 2012).

2.4.7. Holstein Model

Often, the electron-phonon interaction is treated in a Holstein model, where there is an on-site coupling to one local Einstein phonon per site. This corresponds to a **k** and **q** independent coupling

$$g_{Hol}(k,q) = g_0 \tag{2.9}$$

where g_0 is the coupling constant, and a **q** independent phonon frequency $\omega_{q,Hol} = \omega_{ph}$.

2.5. Electronic Structures of High Temperature Superconductors

A common structural feature of all cuprate superconductors is the CuO_2 plane which is responsible for the low lying electronic structure. The CuO_2 planes are sandwiched between various block layers which serve as charge reservoirs to dope CuO_2 planes (Maekawa, 2012). For the undoped parent compound, such as La_2CuO_4, the valence of Cu is 2+, corresponding to $3d^9$ electronic configuration. Since the Cu^{2+} is surrounded by four oxygens in the CuO_2 plane and apical oxygen(s) or halogen(s) perpendicular to the plane, the crystal field splits the otherwise degenerate five *d*-orbitals, as schematically shown in Figure 2.1 (Pickett, 1989).

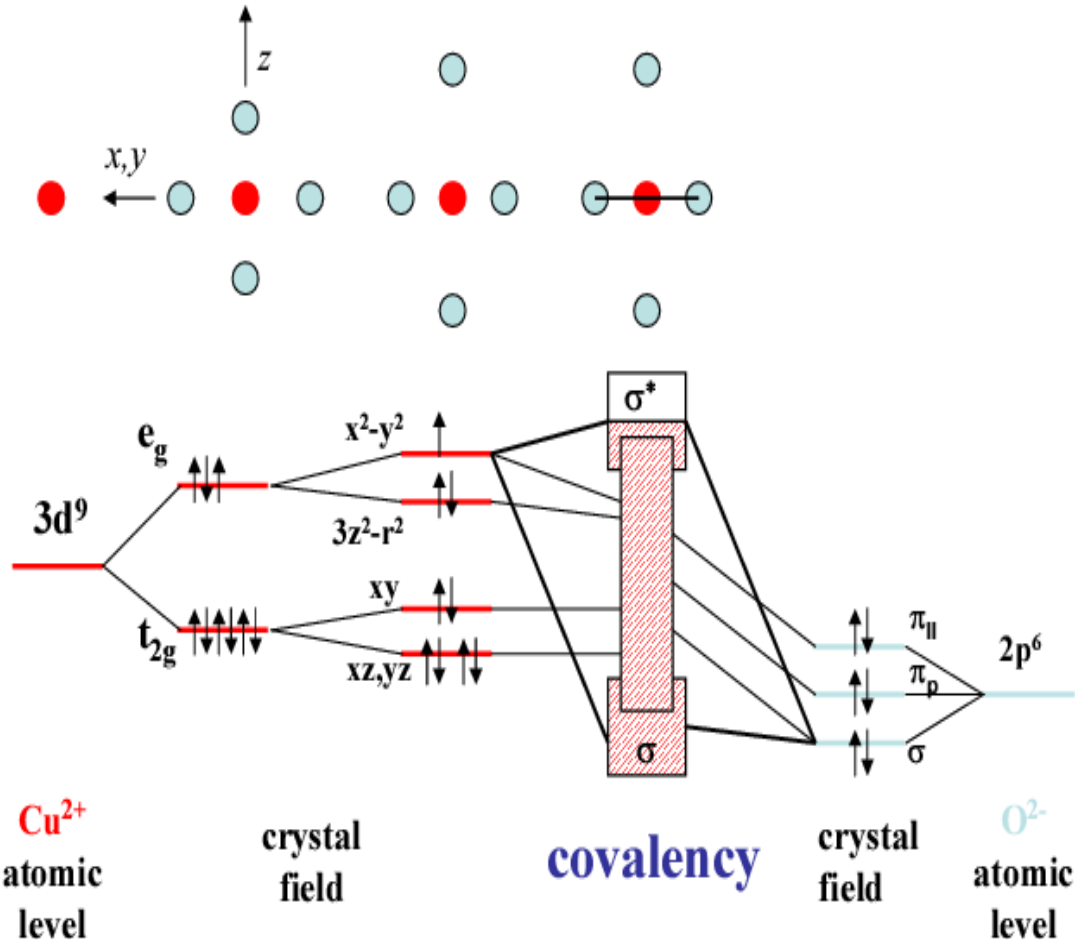

Figure 2.1: Bonding in CuO_2 plane (Pickett, 1989)

The atomic Cu 3d level is split due to the cubic crystal field into e_g and t_{2g} states. There is a further splitting due to an octahedral crystal field into $x^2 - y^2$, $3z^2 - r^2$, xy, and xz, yz states. For divalent Cu which has nine 3d electrons, the uppermost $x^2 - y^2$ level is half filled, while all other levels are completely filled. There is a strong hybridization of the Cu states, particularly the $x^2 - y^2$ states, with the O 2p states thus forming a half-filled two dimensional Cu 3 d_{x2-y2} -O $2p_{x,y}$ antibonding $dp\sigma$ band. The hybridization of the other 3d levels is smaller and is indicated in Figure (2.1) only by a broadening $2p_{x,y}$ character.

The four lower energy orbitals, including xy, xz, yz and $3z^2 - r^2$, are fully occupied, while the orbital with highest energy, x^2-y^2, is half-filled. Since the energies of the Cu d-orbitals and O 2p-orbitals are close, there is a strong hybridization between them. As a result, the topmost energy level has both Cu $d_{x^2-y^2}$and O $2p_{x,y}$ character. The same conclusion is also drawn from band structure calculations (Pickett, 1989).

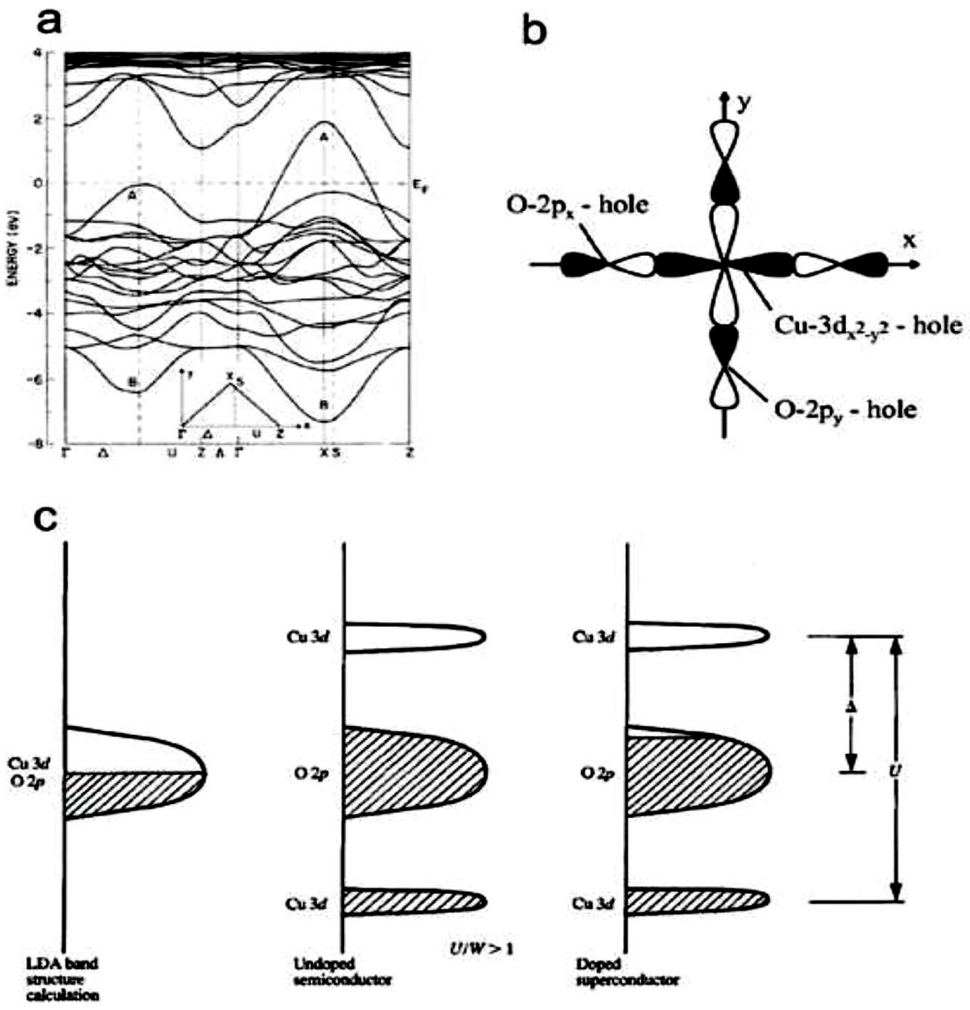

Figure 2.2: LDA calculated band structure of La_2CuO_4 (Pickett, 1989)

In Figure 2.2(a), the band labeled B is bonding band between Cu- $3d_{x2-y2}$ and O - 2p states while the band labeled A is the corresponding antibonding band that is half-filled; Figure 2.2(b) is the Schematic of Zhang- Rice singlet state; Figure 2.2 (c) is the Schematic energy diagrams for undoped and doped CuO_2 planes. (c1) is the band picture for a half-filled (undoped) CuO_2 plane (Fermi liquid); (c2) is the charge-transfer insulating state of the CuO_2 plane with split Cu 3d bands due to on-site Coulomb repulsive interaction U.

The O 2p band is separated by a charge transfer energy E_T from the upper Cu 3d band; (c3) and (c4) show rigid charge transfer energy bands doped with holes and electrons, respectively; (c4). Formation of mid-gap states inside the charge transfer gap.

According to both simple valence counting (Fig.2.1) and band structure calculation (Fig.2.2a), the undoped parent compound is supposed to be a metal. However, strong Coulomb interactions between electrons on the same Cu site make it an antiferromagnetic insulator with an energy gap of 2 eV (Lee *et al*, 2006). The basic theoretical model for the electronic structure most relevant to our discussion is the multi-band Hubbard Hamiltonian (Sénéchal *et al.,2002*) containing d states on Cu sites, p states on O sites, hybridization between Cu-O states, hybridization between O-O states, and Coulomb repulsion terms. In terms of hole notation, i.e., starting from the filled-shell configuration ($3d^{10}$, $2p^6$) corresponding to a formal valence of $Cu^{1+}$and O^{2-}, the general form of the model can be written as (Wagner *et al*., 1991):

$$H = \sum_{i\sigma} \varepsilon_d d^+_{i\sigma} d_{i\sigma} + \sum_{i\sigma} \varepsilon_p p^+_{i\sigma} p_{i\sigma} + \sum_{<li>\sigma} t_{pd} p^+_{i\sigma} d_{i\sigma} + h.c. + \sum_i U_d n_{i\uparrow} n_{i\downarrow} + \sum_{<il'\sigma>} t_{O-O} p^+_{i\sigma} d_{l'\sigma} + h.c. + \sum_{<il>\sigma\sigma'} U_{pd} n_{l\sigma} n_{i\sigma'+} \sum_l U_{pd} n_{l\downarrow} n_{l\downarrow} \quad (2.10)$$

where the operator $d^+_{i\sigma}$ creates Cu ($3d_{x^2-y^2}$)holes at site i, and $p^+_{l\sigma}$ creates O(2p) holes at the site i. U_d is the onsite Coulomb repulsion between two holes on a Cu site. The third term accounts for the direct overlap between Cu-O orbitals. The fifth term describes direct hopping between nearest-neighbor oxygens, and U_{pd} in the sixth term is the nearest

neighbor Coulomb repulsion between holes on Cu and O atoms. Qualitatively, this model gives the energy diagram in Fig.2.2c.

Simplified versions of model Hamiltonians have also been proposed. Notably among them are the single-band Hubbard model (Anisimov *et al.*, 2004) and t-J model (Sirker & Klümper, 2002). The t-J Hamiltonian can be written in the following form (Bazak, 2013):

$$H_{tJ} = -t \sum_{<ij>\sigma} \left(\vec{c}^{+}_{i\sigma} \vec{c}_{j\sigma} + J \sum_{<ij>} \left(S_i . S_j - \hat{n}_{i\uparrow} \hat{n}_{j\downarrow} / 4 \right) \right) \qquad (2.11)$$

where the operator $\vec{c}^{+}_{i\sigma} = c^{+}_{i\sigma}(1 - \hat{n}_{i,-\sigma})$ excludes double occupancy, J = $4t^2/U$ is the antiferromagnetic exchange coupling constant, S_i is the spin operator, $\hat{c}_{i,-\sigma}$ is the projected annihilation operator, $c_{i,\sigma}$ is the annihilation operator for the electron and $n_{i,\sigma} = c^{+}_{i,\sigma} c_{i,\sigma}$. Since the hopping process may also involve the second (t′) and third (t”) nearest neighbor, an extended t-J model, the t− t ′−t”−J model, has also been proposed (Tohyama & Maekawa, 2000).

2.6. Brief Summary of Some Latest ARPES Results

Angle resolved photoemission spectroscopy (ARPES) has provided key information on the electronic structure of high temperature superconductors, including the band structure, Fermi surface, superconducting gap, and pseudogap. These topics are well

covered in recent reviews (Campuzano *et al.,* 2004). A brief summary of some of the latest developments not include before are given as follows.

2.6.1Band Structure and Fermi Surface

The bi-layer splitting of the Fermi surface is well established in the overdoped Bi2212 (Ding *et al.,* 2001) as shown in Fig.2.3 and also suggested to exist in under doped and optimally doped Bi2212 (Chuang *et al.*,2004). Recent measurements also show that there is a slight splitting along the (0,0)-(π,π) nodal direction. The measurement on four-layered $Ba_2Ca_3Cu_4O_8F_2$ has identified at least two clear Fermi surface sheets (Zhou *et al.,* 2007).

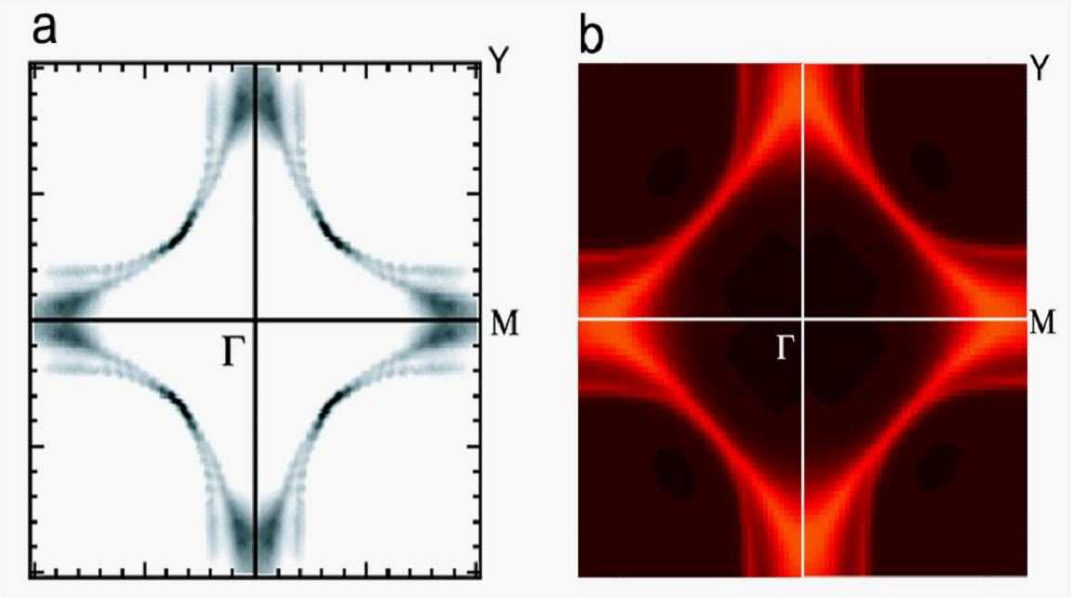

Figure 2.3: Experimentally measured Fermi surface and calculated Fermi surface in Pb-doped Bi2212 (Zhou *et al.*, 2007).

2.6.2 Superconducting Gap

Since the first identification of an anisotropic superconducting gap in Bi2212 (Schabel, 1998), subsequent measurements on the superconductors such as Bi2212(Kordyuk,2003), Bi2201(Sato,2001), Bi2223(Muller, 2002), YBa2Cu3O7−δ (Zhang *et al.*,2006), LSCO(Ino *et al.*,1999) have established a universal behavior of the anisotropic superconducting gap in these hole-doped superconductors which is consistent with d-wave pairing symmetry (although it is still an open question whether the gap formed is a simple d-wave-like $\Delta(k)=\Delta_0[\cos(kxa)-\cos(kya)]$ or higher harmonics of the expansion should be included). The measurements on electron-doped superconductors also reveal an anisotropic superconducting gap (Matsui, 2005). One interesting issue is, if a material has multiple Fermi surface sheets, whether the superconducting gap on different Fermi surface sheets is the same. This issue traces back to superconducting $SrTiO_3$ where it was shown from tunneling measurements that different Fermi surface sheets may show different Fermi surface gaps (Yokoya *et al*., 2001). With the dramatic advancement of the ARPES technique, different superconducting gaps on different Fermi surface sheets have been observed in 2H-$NbSe_2$ (Yokoya,2006) and MgB_2(Lorenz,2006). For high-T_c materials, Bi2212 shows two clear FS sheets, but no obvious difference of the superconducting gap has been resolved (Zhou *et al*., 2006).

2.6.3. Time Reversal Symmetry Breaking

It has been proposed theoretically that, by utilizing circularly polarized light for ARPES, it is possible to probe time-reversal symmetry breaking that may be associated with the pseudogap state in the underdoped samples (Li *et al.*, 2010). The observation of such an effect had been reported earlier (Kaminski *et al.*, 2002). However, this observation is not

reproduced by another group (Borisenko *et al.,* 2004) and the subject remain controversial (Lu, 2012).

2.7. Electron-phonon Coupling in High Temperature Superconductors

It is well-known that, in conventional superconductors, electron-phonon (el-ph) coupling is responsible for the formation of Cooper pairs (Bardeen *et al.,* 1957). The discovery of high temperature superconductivity in cuprates was actually inspired by possible strong electron-phonon interaction in oxides owing to polaron formation or in mixed-valence systems (Bednorz & Müller, 1986). However, shortly after the discovery, a number of experiments led some researchers to believe that electron-phonon coupling may not be relevant to high temperature superconductivity (Reznik, 2006). But now there are many experimental observations and theoretical calculations that emphasize the effectiveness of EPI (Plakida, 2010).

2.7.1 Many – Body Effect

The many-body effect refers to interactions of electrons with other entities, such as other electrons, or collective excitations like phonons, magnons, and so on. It has been recognized from the very beginning that many-body effects are key to understanding cuprate physics. Due to its proximity to the antiferromagnetic Mott insulating state, electron-electron interactions are extensively discussed in the literature (Yoshida *et al.,* 2007). This study will mostly review the recent progress in understanding of electrons interacting with bosonic modes, such as phonons. This progress stems from improved sample quality, instrumental resolution, as well as theoretical development. In a complex system like the cuprates, it is not possible to isolate various degrees of freedom as the interactions mix them together. One may discuss the electron-boson interactions in this

spirit, and will comment on the interplay between electron-phonon and Coulomb interactions whenever appropriate. Here, bosonic modes refer to collective modes with sharp collective energy scale such as the optical phonons and the famous magnetic resonance mode seen in some cuprates (Yu *et al*.,2010), but not the broad excitation spectra such as those from the broad electron/spin excitations as these issues have been discussed in previous reviews. Furthermore, it is believed the effects due to sharp mode coupling seen in cuprates are caused by phonons rather than the magnetic resonance. The reason for not attributing the observed effect to magnetic resonance will become apparent from the rest of the write up. With more limited data, different groups have taken the view that the magnetic resonance is the origin of the boson coupling effect. For this reason, one may focus more on our own results in reviewing the issues of electron-phonon interaction in cuprates. The electron-phonon interactions can be characterized into two categories: (i). Weak coupling where one can still use the perturbative self-energy approach to describe the quasiparticle and its lifetime and mass; (ii). Strong coupling and polaron regime where this picture breaks down.

2.7.2 High critical transition temperature T_c

So far, the highest T_c achieved in cuprate superconductors is 135 K in $HgBa_2Ca_2Cu_3O_8$ (Uchida, 2015). Such a high-T_c was not expected in simple materials using the strongly coupled version of BCS theory, or the McMillan equations (Dal Conte, 2012).

2.7.3 Isotope Effect in High Cuprate Superconductors

The discovery of superconductivity in $La_{2-x}Ba_xCuO_4$ (Bednorz & Muller, 1986) prompted a burst of experimental and theoretical investigations in these systems in order to clarify the microscopic pairing mechanism for high temperature superconductivity.

However, the mechanism is still highly controversial because the opinions as regards the role of electron - phonon interaction vary widely (Hardy, *et al.,* 2009). Also, the unprecedentedly high transition temperatures in some cuprates were difficult to reconcile with the conventional phonon mediated mechanism which could account for a maximum T_C of 30K (Pasupathy, 2008). Existence of short coherence length raises further challenges against BCS theory. Cuprates have a complex structure as compared to elemental superconductors and essentially have layered character, confirmed by the anisotropy of their properties. Usually, cuprates consist of four layers: (a) Conducting layer (i.e CuO_2 planes), (b) separating Layer typically like Ca or Y, (c) bridging layer typically like BaO, LaO or SrO, and (d) additional layer like BiO, HgO or TlO. Superconductivity is believed to take place in CuO_2 planes which are present in all high T_C superconductors, but the number of CuO_2 planes varies among the different families of cuprates, ranging from a single-layer up to an infinite-layer structure. Thus, the existence of layer structure introduces complexity in the investigation of isotope effect in cuprates.

2.7.4 Transport Measurement

The linear resistivity-temperature dependence in optimally doped samples and the lack of a saturation in resistivity over a wide temperature range have been taken as an evidence of weak electron-phonon coupling in the cuprate superconductors (Johnston *et al*., 2010).

2.7.5 *d*-wave Symmetry of the Superconducting Gap

The electron-phonon interaction, which plays a vital role in conventional superconductors, may not account fully for superconductivity in the cuprates. A natural

explanation for the *d*-wave gap symmetry and for the magnitude and doping dependence of T_c has been given in terms of an effective spin spin interaction (*t*-*J* model) between the carriers on the border of a Mott transition and antiferromagnetism. As in the original BCS theory we consider an effective pairing Hamiltonian but now for the exchange interaction rather than the electron-phonon interaction. For a single tight-binding band near half filling on the border of the Mott transition, we consider the Hamiltonian

$$H_{eff} = -t\sum_{<ij>}(c^{+}_{j\sigma}c_{i\sigma} + hc) + J_{eff}\sum_{ij} S_i S_j \qquad (2.12)$$

where <*ij*>denotes sum over nearest neighbor, (*nn*) pairs of sites, t_{eff} is the effective *nn* hopping matrix element, J_{eff}(>0) is the effective exchange constant, $c_{i\sigma}$ destroys an electron of spin index σ on atomic site *I* and S_i is the electron spin on site *i*.

2.7.6 Structural Instability

It is generally believed that sufficiently strong electron-phonon coupling to yield high T_c will result in structural instability (Pasupathy, 2008). Although none of these observations can decisively rule out the electron - phonon coupling mechanism in high-T_c superconductors, overall they suggest a different approach. Instead, strong electron-electron correlation has been proposed to be the mechanism of high-T_c superconductivity (Cuk *et al.,* 2005).This approach is attractive since *d*−wave pairing is a natural consequence. Furthermore, the high temperature superconductors evolve from antiferromagnetic insulating compounds where the electron-electron interactions are strong (Comanac *et al*., 2008). However, there is a large body of experimental evidence also showing strong electron-phonon coupling in high-temperature superconductors (Kordyuk, 2011).

2.7.7 Optical Spectroscopy and Raman Scattering

Raman scattering (Le Tacon, *et* al., 2006) and infrared spectroscopy (Dubroka, 2011) reveal strong electron-phonon interaction for certain phonon modes. In $YBa_2Cu_3O_{7-\delta}$, it has been found that, the B_{1g} phonon, which is related to the out-of-plane, out-of-phase, in plane oxygen vibrations , exhibits a Fano-like lineshape (Fig.2.4) and shows an abrupt softening upon entering the superconducting state (Graf., 2008).

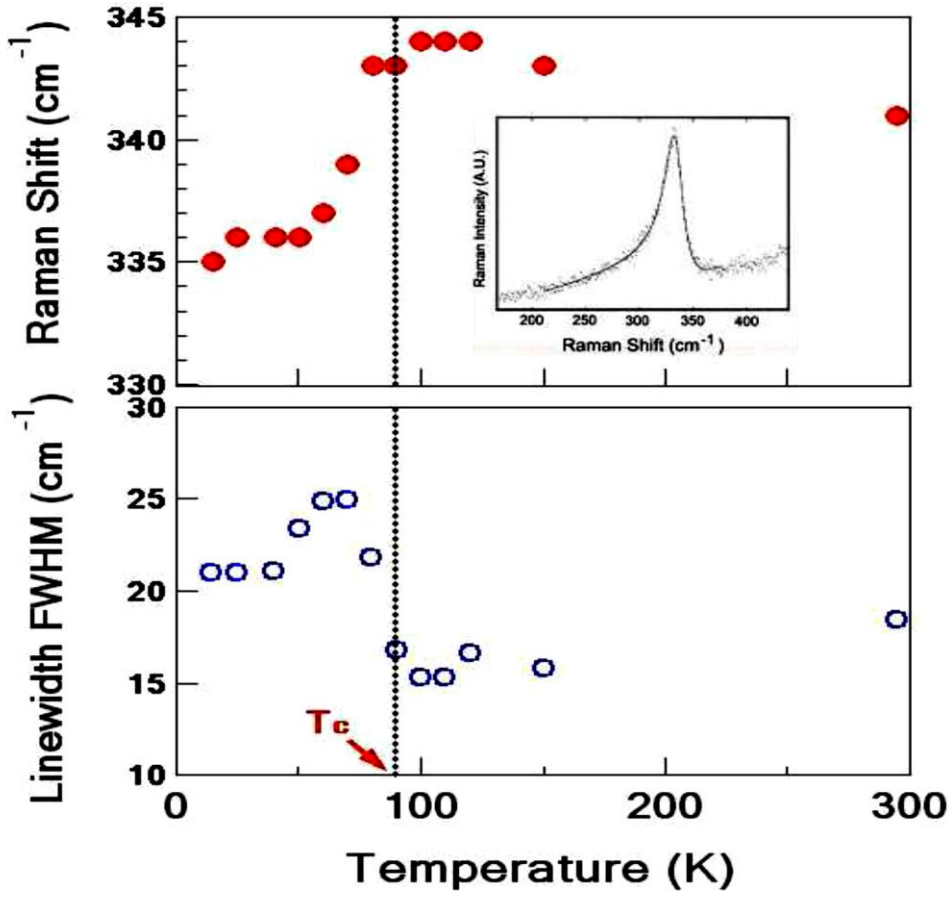

Figure 2.4: Anomalous softening of the B_{1g} phonon when YBCO is cooled below T_c (Zhou *et al.*, 2006)

In Fig. (2.4), the inset shows the fit of a Fano function to the phonon peak at T=72K. (Zhou *et al.*, 2006). The A_{1g}modes, as found in $HgBa_2Ca_3Cu_4O_{10}$ (Hg1234) (Hadjiev,1998) and in $HgBa_2Ca_2Cu_3O_8$ (Hg1223)(Zhou, 1997), exhibit especially strong superconductivity-induced phonon softening(Fig.2.5).

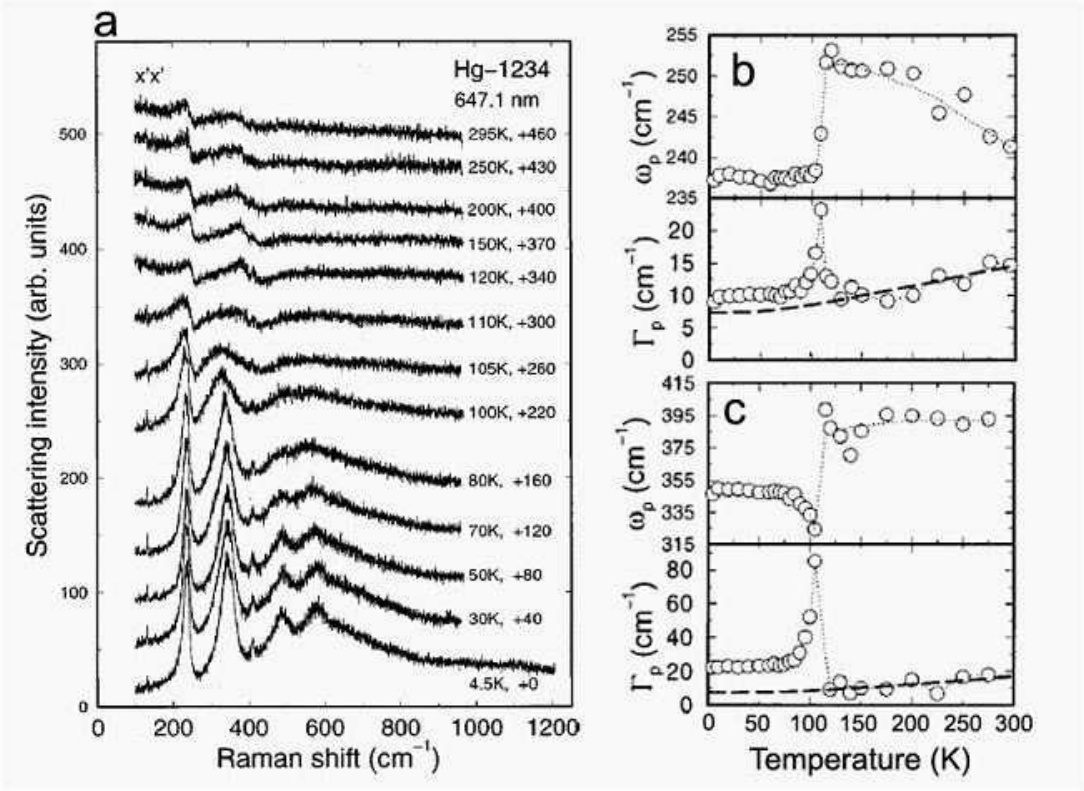

Figure 2.5: Raman spectra of Hg1234 (Zhou *et al.*, 2007).

Figure 2.5 shows a giant superconductivity-induced mode softening across T_c=123 K . The modes at 240 cm^{-1} and 390 cm^{-1} correspond to A_{1g} out-of-plane, in-phase vibration of oxygen in the CuO_2 planes. Upon cooling from room temperature to 4.5 K, the 240 cm^{-1} A_{1g} mode shows an abrupt drop in frequency at T_c from 253 to 237 cm^{-1} and the 390 cm^{-1} mode drops from 395 to 317 cm^{-1}(Zhou *et al.*, 2007).

Infrared reflectance measurements on various cuprates found that the frequency of the Cu-O stretching mode in the CuO_2 plane is very sensitive to the distance between copper and oxygen (Carbone *et al*., 2010)

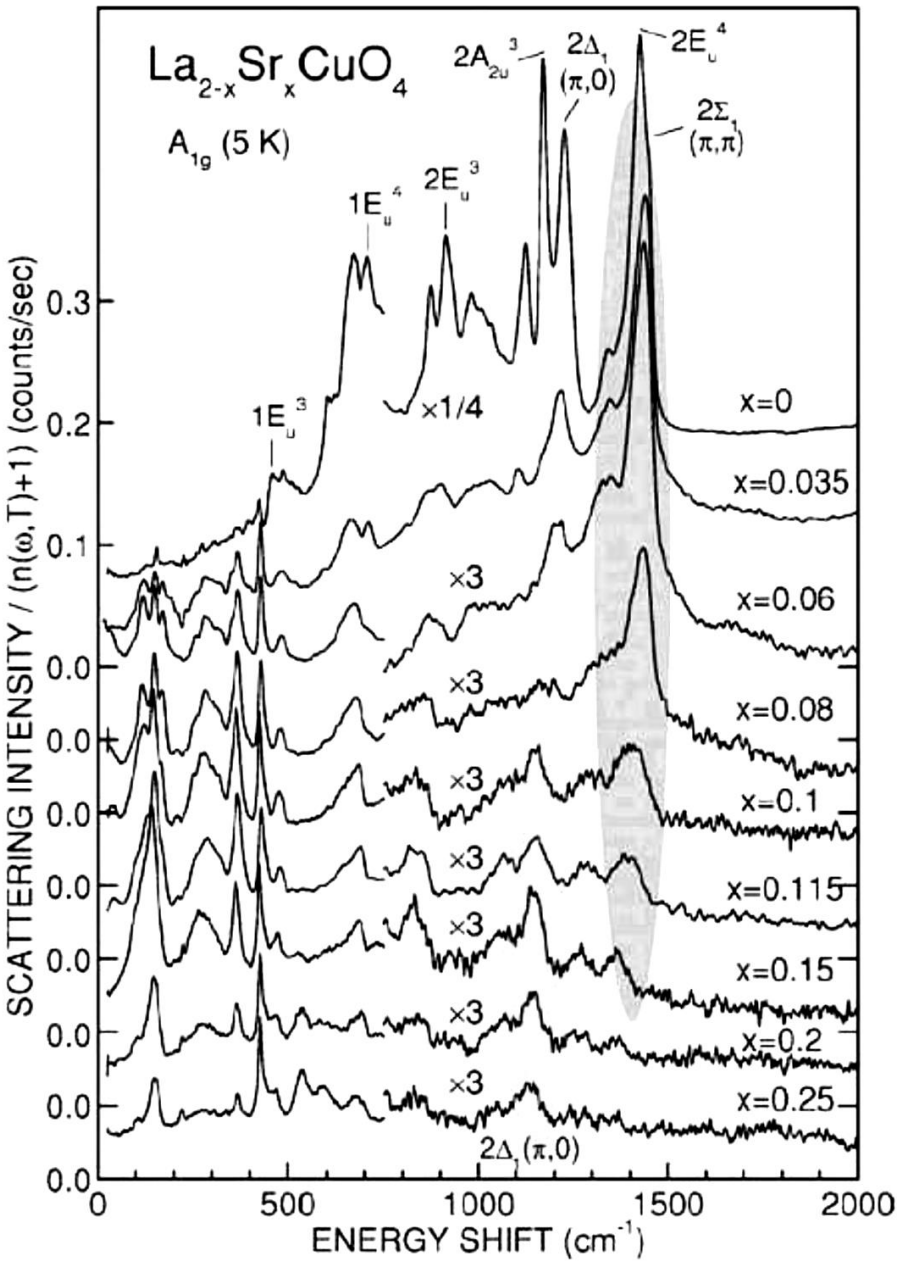

Figure 2.6: Variation of scattering intensity with energy shift in LSCO (Kim *et al.*, 2004).

The sharp structures in Figure 2.6 at high frequency are signals from multiphonon processes, which can only occur if the electron-phonon interaction is very strong (Gadermaier, 2010). One can see that this effect is very strong in undoped and deeply underdoped regime, and gets weaker with doping increase.

2.7.8 Neutron Scattering

Neutron scattering measurements have provided rich information about electron-phonon coupling in high temperature superconductors (Reznik, 2012).

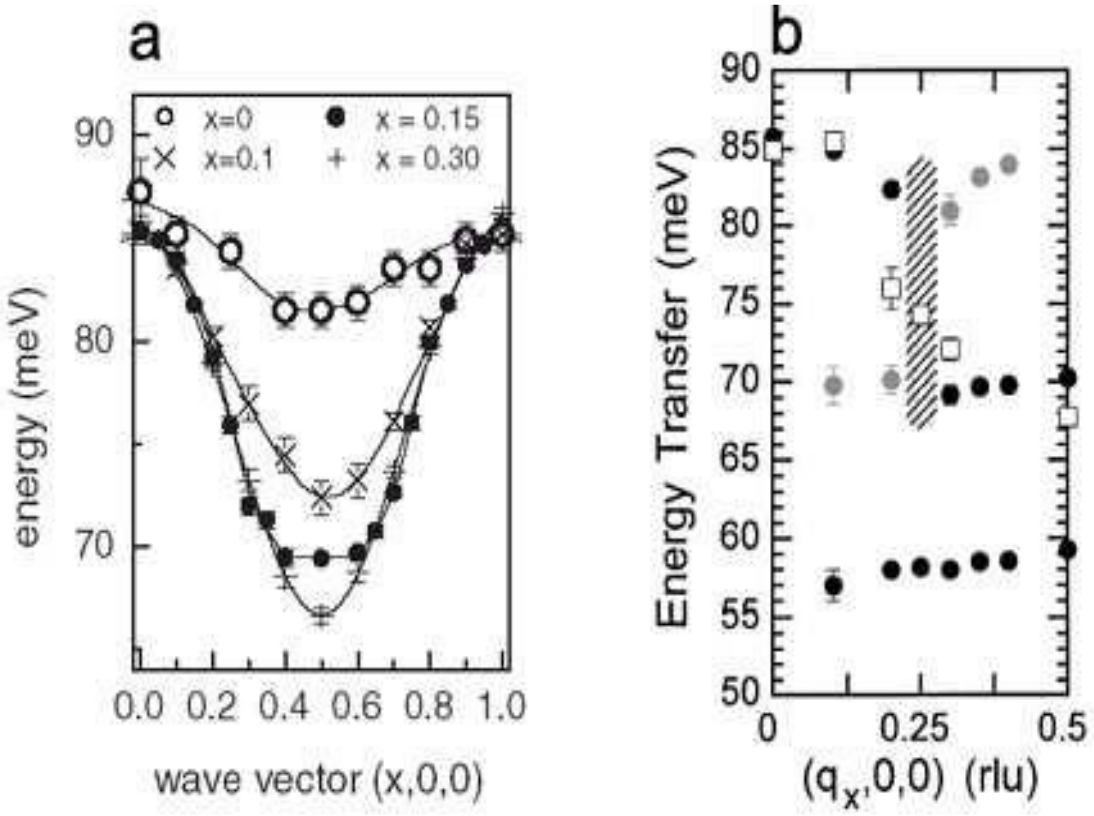

Figure 2.7: Dispersion of the Cu-O bond-stretching vibrations (Ohkawa, 2007).

As seen from Figure 2.7, the in-plane "half-breathing" mode exhibits strong frequency renormalizations upon doping along (001) direction (Ohkawa, 2007). In $La_{1.85}Sr_{0.15}CuO_4$, it is reported that, at low temperature, the half-breathing mode shows a

discontinuity in dispersion (Fig.2.7b) (Mc Queen, 1999). In YBCO, neutron scattering indicates that the softening of the B_{1g} mode upon entering the superconducting state is not just restricted near q=0, as indicated by Raman scattering (Fig.2.6), but can be observed in a large part of the Brillouin zone (Fig.2.7) (Fong, 1995).

2.7.9 Material and Structural Dependence

There is a strong material and structural dependence to the high-T_c superconductivity (Armitage, 2002), as exemplified in Figure 2.8 below.

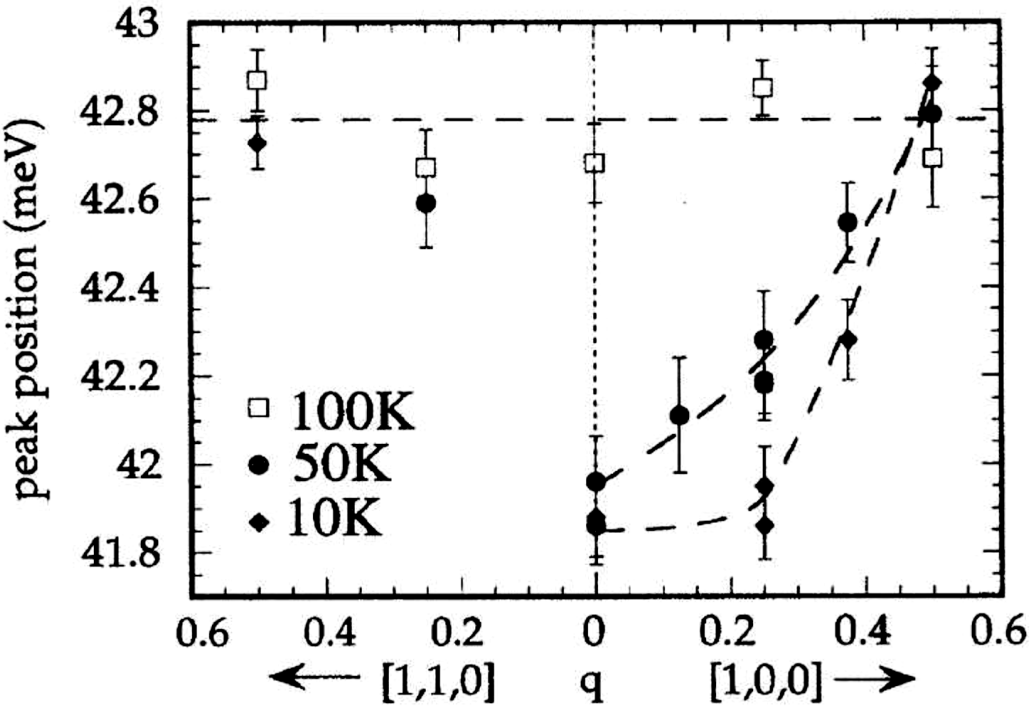

Figure 2.8: q dependence of B1g mode peak position at different temperatures in YBCO (Armitage, 2002)

In Fig. 2.9, the range parameter, r is controlled by the energy of the axial orbital, a hybrid between Cu 4s, apical-oxygen 2pz, and farther orbitals (Pavarini *et al.*, 2001). Filled squares represent single-layer materials and most bonding sub - band for multilayer while

empty squares represent most antibonding sub - band. Half-filled squares represent nonbonding sub - band. Dotted lines connect sub - band values. Bars give kz dispersion of r in primitive tetragonal materials.

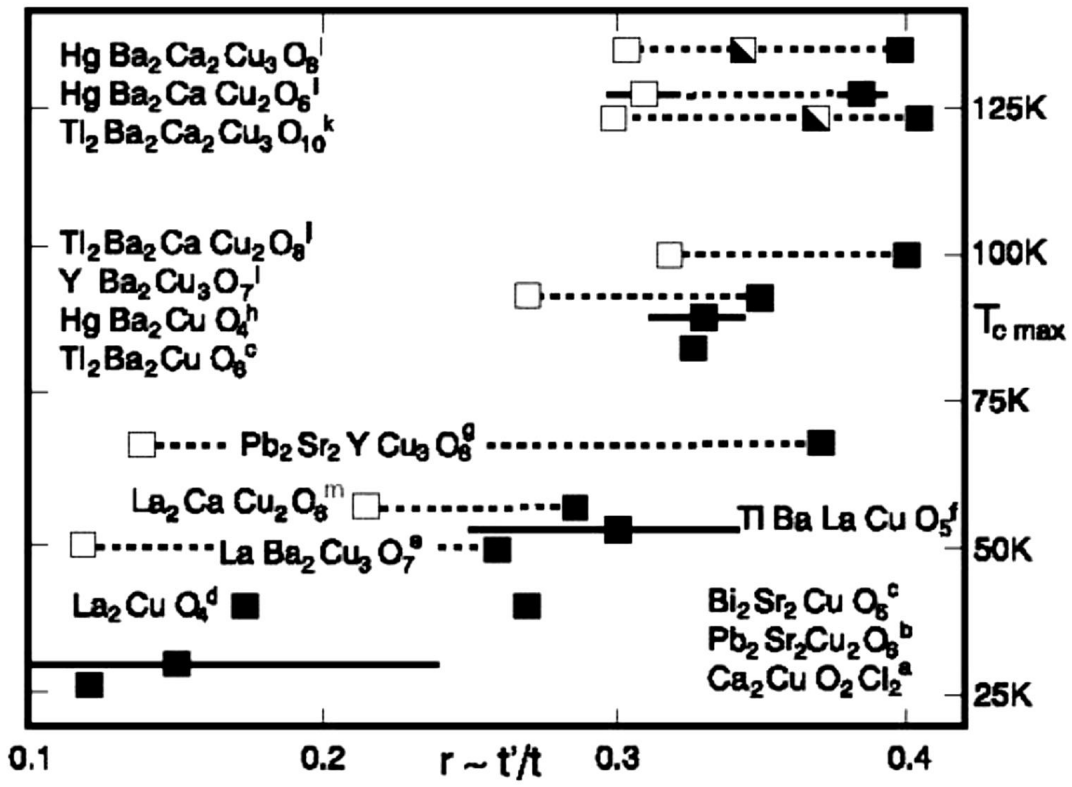

Figure 2.9: Correlation between calculated range parameter r and observed T_c max

Empirically it is found that, for a given homologous series of materials, the optimal T_c varies with the number of adjacent CuO_2 planes, n, in a unit cell: T_c goes up first with n, reaching a maximum at n=3, and goes down as n further increases. For the cuprates with the same number of CuO_2 layers, T_c also varies significantly among different classes. For example, the optimal T_c for one-layered $(La_{2-x}Sr_x)CuO_4$ is 40K while it is 95K for one-layered $HgBa_2CuO_4$. These behaviors are clearly beyond simplified models that consider CuO_2 planes only, such as the t−J model. In fact, such effects were taken as evidence against theoretical models based on such simple models and in favor of the interlayer

tunneling model (Leggett, 1996). Although the interlayer tunneling model has inconsistencies with some experiments, the issue that the material dependence cannot be explained by single band Hubbard and t-J model remains to be true.

The above results suggest that the lattice degree of freedom plays an essential role. However, the role of phonons has not been scrutinized as much, in particular in regard to the intriguing question of whether high- T_c superconductivity involves a special type of electron- phonon coupling. In other words, the complexity of electron-phonon interaction has not been as carefully examined as some of the electronic models. As a result, many naive arguments are used to argue against electron - phonon coupling as if the conclusions based on simple metals are applicable here. Recently, a large body of experimental results from angle-resolved photoemission, as we review below, suggest that electron-phonon coupling in cuprates is not only strong but shows behaviors distinct from conventional electron-phonon coupling. In particular, the momentum dependence and the electron-phonon interaction are very important.

2.8. Electron-Phonon Interaction and Strong Electron Correlation

Theory of electron – phonon interaction in the presence of strong electron correlation has not been developed. Given both interactions are important in cuprates, it is difficult to have a good way to address these issues. In fact, it is believed that an important outcome of this research is the stimulus to develop such a theory. In the meantime, the strategy is to separate the problem in different regimes and see to what extent a heuristic understanding of the experimental data can be developed. Such empirical findings can serve as a guide for comprehensive theory. The theories of electron-phonon coupling in condensed matter have been developed rather separately for metals and insulators. In the

former case, the dominant energy scale is the kinetic energy or the Fermi energy ε_F on order of $1 - 10$eV, and the phonon energy $\sim 1{-}100$meV is much smaller. The Fermi degeneracy protects the many-body fermion system from perturbations and only the small energy window near the Fermi surface responds. Therefore even if the lattice relaxation energy $E_{LR}= g^2/\omega$ for the localized electron is comparable to the kinetic energy ε_F the electron - phonon coupling is essentially weak and the perturbative treatment is justified. The dimensionless coupling constant λ is basically the ratio of E_{LR}/ε_F, which ranges $\lambda \sim= 0.1 - 2$ in the usual metals. In the diagrammatic language, the physics described above is formulated within the framework of the Fermi liquid theory (Clarke *et al.*, 1995). The electron-electron interaction is taken care of by the formation of the quasi-particle, which is well-defined near the Fermi surface, and the electron –phonon vertex correction is shown to be smaller by the factor of Ω/ε_F and can be neglected. Therefore the multi-phonon excitations are reduced and the single-loop approximation or at most the self-consistent Born approximation is enough to capture the physics well, i.e., Migdal-Eliashberg formalism. When a carrier is put into an insulator, on the other hand, it stays near the bottom of the quadratic dispersion and its velocity is very small. The kinetic energy is much smaller than the phonon energy, and the carrier can be dressed by a thick phonon cloud and its effective mass can be very large. This is called the phonon polaron. Historically the single carrier problem coupled to the optical phonon through the long range Coulomb interaction, i.e., Fr¨ohlich polaron, is the first studied model, which is defined in the continuum. When one considers the tight-binding models, which is more relevant to the Bloch electron, the bandwidth W plays the role of ε_F in the above metallic case. Then again we have three energy scales, W, E_{RL}, and Ω . Compared with the

metallic case, the dominance of the kinetic energy is not trivial, and the competition between the itinerancy and the localization is the key issue in the polaron problem, which is controlled by the dimensionless coupling constant $\lambda = E_{RL}/W$. Another dimensionless coupling constant is $S = E_{RL}/\Omega$, which counts the number of phonon quanta in the phonon cloud around the localized electron. This appears in the overlap integral of the two phonon wavefunctions with and without the phonon cloud as:

$$<\text{phonon vacuum} \mid \text{phonon cloud}> \propto e^{-S} \tag{2.13}$$

This factor appears in the weight of the zero-phonon line of the spectral function of the localized electron, and S can be regarded as the maximum value for the number of phonons N_{ph} near the electron. In a generic situation, N_{ph} is controlled by λ, and there are cases where N_{ph} shows an (almost) discontinuous change from the itinerant undressed large polaron to the heavily dressed small polaron as λ increases. This is called the self trapping transition. Here a remark on the terminology “self-trapping” is in order. Even for the heavy mass polaron, the ground state is the extended Bloch state over the whole sample and there is no localization. However a small amount of disorder can cause the localization. Therefore in the usual situation, the formation of the small polaron implies the self-trapping, and we use this language to represent the formation of the thick phonon clouds and huge mass enhancement. In cuprates, it is still a mystery why the transport properties of the heavily underdoped samples do not show the strong localization behavior even though the ARPES shows the small polaron formation. The electron - phonon coupling in cuprates depends on the hole doping concentration, momentum and energy. The half-filled undoped cuprate is a Mott insulator with antiferromagnetic ordering, and a single hole doped into it can be regarded as the polaron subjected to the

hole-magnon and hole-phonon interactions. At finite doping, but still in the antiferromagnetic (AF) order, the small hole pockets are formed and the hole kinetic energy can be still smaller than the phonon energy. In this case the polaron picture still persists. The main issue is to what range this continues. One scenario is that once the antiferromagnetic order disappears the metallic Fermi surface is formed and the system enters the Migdal-Eliashberg regime. However, there are several physical quantities such as the resistivity, Hall constant, optical conductivity, which strongly suggest that the physics still bears a strong characteristic of doped holes in an insulator rather than a simple metal with large Fermi surface. Therefore the crossover hole concentration x_c between the polaron picture and the Migdal - Eliashberg picture remains an open issue. Probably, it depends on the momentum/energy of the spectrum. For example, the electrons have smaller velocity and are more strongly coupled to the phonons in the anti-nodal region near $(\pm\pi, 0)$, $(0,\pm\pi)$, remaining polaronic up to higher doping, while in the nodal region, the electrons behave more like the conventional metallic ones since the velocity is large along this direction. Furthermore, the low energy states near the Fermi energy are well described by Landau's quasi-particle and Migdal- Eliashberg theory, while the higher energy states do not change much with doping even at $x \approx 0.1$ (Anderson *et al.,* 2004) suggestive of polaronic behavior. In any event, the dichotomy between the hole doping picture and the metallic (large) Fermi surface picture is the key issue in the research of high T_c superconductors.

2.9. Weak Coupling – Perturbative and Self-Energy Description

First, the Migdal-Eliashberg regime is reviewed, in which the electron-phonon interaction results in single-phonon excitations and can be considered as a perturbation to the bare band dispersion. In this case, dominant features of the mode coupling behavior can be captured using the following form for the self-energy:

$$E(k,w) = T/N \sum_{q,v} g^2(k,q) D(q,w) \tau_3 \hat{G}(k-q, iw-iv) \tau_3 \qquad (2.14)$$

where $D(q,w) = \frac{2\Omega_q}{w^2 - \Omega_q^2}$ is the phonon propagator, Ω_q is the phonon energy, T is temperature, N is the number of particles and τ_3 is the Pauli matrix and $\hat{G}$ is the corresponding Green's function.

In this form of the self-energy, corrections to the electron-phonon vertex, g, are neglected as mentioned above (Reizer, 1989). Furthermore, we assume only one-iteration of the coupled self-energy and Green's function equations. In other words, in the equation for the self- energy, E, we assume bare electron and phonon propagators, G_0 and D_0. With these assumptions, the imaginary parts of the functions Z, χ, and φ, denoted as Z_2, χ_2, and φ_2, are:

$$Z_2(k,\omega)\omega = \sum g^2(k,q)(\pi/2)\left\{\begin{array}{c}\left[\begin{array}{l}\delta\left(\omega-\Omega_q-E_{k-q}\right)\\+\delta\left(\omega-\Omega_q+E_{k-q}\right)\end{array}\right]\\\left[f\left(\Omega_q-\omega\right)+n\left(\Omega_q\right)\right]\\+\left[\begin{array}{l}-\delta\left(\omega+\Omega_q-E_{k-q}\right)\\+\delta\left(\omega+\Omega_q+E_{k-q}\right)\end{array}\right]\left[\begin{array}{l}f\left(\Omega_q+\omega\right)\\+n\left(\Omega_q\right)\end{array}\right]\end{array}\right\} \tag{2.15}$$

where *f(x),n(x)*, are the Fermi, Bose distribution functions and E_k is the superconducting state dispersion,

$$E_k^2 = \varepsilon_k^2 + \Delta_k^2 \tag{2.16}$$

The above equations are essentially those of Eliashberg theory for strongly-coupled superconductors. Although λ can be large (>1), i.e., "strongly-coupled", the vertex corrections and multi-phonon processes are still negligible due to the Fermi degeneracy and small $\Omega/E_F/$ (Wolf, 2011).

2.10 Weak coupling and Non-interacting Electrons

2.10.1. Electron Self-energy

The electron-phonon interaction is often studied assuming that the electrons are non-interacting. This is a quite unrealistic assumption for the cuprates, where the electron-electron interaction is crucial. Below, nevertheless some of the results (Calandra & Mauri, 2007) for this case are given, since they provide a basis for discussing similarities and deviations for strongly correlated systems.

The electrons are described by the Hamiltonian

$$H_{non} = \sum_{k\sigma} \varepsilon_k c^{+}_{k\sigma} c_{k\sigma} \tag{2.18}$$

where ε_k is the energy for the wave vector **k** and σ is the spin index. The electrons are assumed to couple to phonons via the Holstein model (Macridin *et al.*, 2012). The retarded electron self – energy to lowest order in the coupling for T = 0, it is given by (Calandra & Mauri, 2007)

$$E(k,\omega) = \frac{1}{N} g^2 \sum_q \left[\frac{f(\varepsilon_{k+q})}{\omega + \omega_{ph} - \varepsilon_{k+q} + i\delta} + \ln \frac{1 - f(\varepsilon_{k+q})}{\omega - \omega_{ph} - \varepsilon_{k+q} + i\delta} \right] \tag{2.19}$$

where N is the number of sites, f(ε) is the Fermi function and δ is a positive infinitesimal (later small) quantity. N(ε) = 1/B is assumed to be constant, where N(ε) is the density of states (DOS) per spin and B is the band width. The band is assumed to be half-filled and to extend from -B/2 to B/2.

2.10.2 Electron-phonon Coupling

Two-dimensional (2d) correlated models with EPI are often compared with the 2d Holstein model to determine the effects of correlation on the EPI. A 2d Holstein model at half-filling with only nearest neighbor hopping is unstable to an infinitesimal EPI due to perfect nesting. Therefore the comparison is often made to a Holstein model with just a single electron at the bottom of the band (Mischenko, 2009). Often a t-J model doped with one hole is studied, suggesting similarities with a Holstein model with a single electron. The half-filled Holstein model, however, is of particular interest, since the relevant antibonding Cu-O band in the cuprates is close to half-filling.

2.10.3 Anharmonic Apical Oxygen Vibrations in High T_c Superconductors

It is well established that most of the high T_c superconductors have *Cu–O* layers sandwitched between layers of other materials (Klemm, 2012). The charge carriers are electrons and the pairing mechanism between the electrons is exotic. The electronic pairing in exotic superconductors is such that three electrons take part in the superconducting current and that they interact with each other through harmonic forces (Khanna & Kirui, 2002). Two of these electrons form a bound pair while the third one is a polarization electron which hops from one lattice site to another lattice site of similar symmetry. Studies that have been done in photo – induced Raman Scattering (Nyawere & Khanna, 2011) have confirmed that there exists strong anharmonic nature of apical oxygen vibrations. When the spectral function of electron – phonon interaction is compared with the phonon spectrum in bismuth compounds it is noted that, both low frequency vibrations (buckling mode) and high frequency vibrations (breathing mode) contribute to the electron – phonon coupling.

It is therefore assumed that the polarization electron causes perturbation with respect to the apical oxygen vibrations leading to the contraction of $Cu_p - O_3$ bond. The unperturbed Hamiltonian is given by

$$H^{'} = \beta x^3 + \gamma x^4 \tag{2.20}$$

where β and γ may or may not depend on temperature.

The eigenvalues and eigenfunctions of the unperturbed harmonic oscillator Hamiltonian are given by

$$H_o|n,0> = \epsilon_n^0 |n,0> \tag{2.21}$$

where

$$\epsilon_n^0 = \left(n + \frac{1}{2}\right)\hbar\omega, \qquad \text{n = 0,1,2,} \tag{2.22}$$

and

$$|n,0\rangle = N_n H_n(\xi)\exp\left(-\frac{1}{2}\xi^2\right) \tag{2.23}$$

are the hermite polynomials such that,

$$N_n = \left(\frac{\alpha}{n!2^n\sqrt{\pi}}\right)^{1/2}; \quad \xi = ax\ ; \qquad \alpha^2 = \frac{\mu\omega}{\hbar} \tag{2.24}$$

where ω is the phonon frequency and μ is the reduced mass of the pair of electrons interacting harmonically.

When the system is perturbed, the eigenvalue equation to be solved is,

$$H|n\rangle = \epsilon_n |n\rangle \tag{2.25}$$

Where H is the perturbed Hamiltonian of the entire system such that

$$H = H_0 + H' = -\frac{\hbar^2}{2\mu}\nabla^2 + \frac{1}{2}\mu\omega^2 + H' \tag{2.26}$$

CHAPTER THREE

METHODOLOGY AND THEORETICAL DERIVATIONS

3.1 Introduction

This chapter presents the method used and the procedure for deriving the electron – phonon and Coulomb interaction Hamiltonian.

3.2 The Frozen phonon method

The electron – phonon interaction Hamiltonian may be written using the frozen phonon method (Yildirim, 2013). This technique is often applied to deduce electron – phonon coupling in the context of more conventional band structure approaches which are highly numerical. Here, we proceed somewhat more analytically. The starting point is the three – band Hubbard Hamiltonian which describes the copper oxide plane. Following earlier work (McMahan *et al.,* 1988), a model Hamiltonian which includes a next – nearest – neighbor interaction i.e oxygen – oxygen overlap may be constructed as

$$H = \sum_{j,\eta,\sigma} \varepsilon_p C^{\eta^+}_{j,\sigma} C^{\eta}_{j,\sigma} + \sum_{i,\sigma} \varepsilon^0_d D^+_{i,\sigma} D_{i,\sigma} + \sum_{<ij>,\eta,\sigma} V_{i,j} (C^{\eta^+}_{j,\sigma} D_{i,\sigma} + D^+_{i,\sigma} C^{\eta}_{j,\sigma}) + \sum_{<jl>(\eta \neq \eta'),\sigma} t_{j,l} (C^{\eta^+}_{j,\sigma} C^{\eta'}_{l,\sigma} + C^{\eta'^+}_{l,\sigma} C^{n}_{j,\sigma}) + \sum_i U_d n_{i,\uparrow} n_{i,\downarrow} \quad (3.1)$$

where ε_p and ε^0_d are oxygen and copper energy levels, $C^{\eta^+}_{j,\sigma}$ *and* $C^{\eta}_{j,\sigma}$ are creation and annihilation operators for the oxygen electrons at site *j* and spin σ respectively, $D^+_{i,\sigma}$ *and* $D_{i,\sigma}$ are the creation and annihilation operators for the copper electrons at site *i* and spin σ respectively. The hopping interaction $V_{i,j}$ is between neighbouring copper and oxygen sites, while $t_{j,l}$ describes the transfer between two nearest – neighbour oxygen sites, and $n_{i,\sigma} = D^+_{i,\sigma} D_{i,\sigma}$. Here, $n(= x, y)$ represents two oxygen orbitals (p_x and

p_y) and $< jl > (n \neq n')$ denotes the nearest neighbouring orbitals $n and\ n'$ at sites $j and\ l$, respectively. The Coulomb repulsion between electrons on Copper sites is U_d.

It is generally assumed that U_d is the largest energy scale in the problem. At infinite U_d, a mean – field theory may be derived using the auxiliary boson (e_i) approach; this model has been extensively studied (Kim *et al.*, 1991) and in slightly different variations, by others (Newns, *et al.*, 1988). It is based on a 1/N expansion, where N is the spin degeneracy of the Copper and Oxygen sites. Here, one works in the electron picture. This allows one to take semirealistic values for the parameters in Eq. (3.1) and still preserve the Mott localization at half-filling. This localization arises from a suppression of the renormalized hybridization.

In the limit of infinite U_d, we introduce an auxiliary boson, e_i which corresponds to the Cu^{3+} valence state, in which the $d_{x^2-y^2}$ state is empty. The fermion operator $d_{i,\sigma}$ represents a Cu^{2+} state with spin σ . In this case, the $d_{x^2-y^2}$ is half full. Imposing a constraint via a Lagrange multiplier, λ_i at each site that there being no double occupancy of the $d_{x^2-y^2}$ requires that

$$\sum_{\sigma} d^{+}_{i,\sigma} d_{i,\sigma} + e^{+}_{i} e_i = 1 \tag{3.2}$$

In the mean- field limit, the operator e_i (auxiliary boson) is replaced by its expectation value e_0 which is spatially uniform and similarly λ_i is replaced by the average λ_0 so that the mean - field Hamiltonian may be written as

$$\begin{aligned} H_{mf} = & \sum_{j,\eta,\sigma} \varepsilon_p C^{\eta^{+}}_{j,\sigma} C^{\eta}_{j,\sigma} + \sum_{i,\sigma} \varepsilon_d d^{+}_{i,\sigma} d_{i,\sigma} + \sum_{<ij>,\eta,\sigma} Ve_o (C^{\eta^{+}}_{j,\sigma} d_{i,\sigma} + H.c) \\ & + \sum_{< jl >,\eta \neq \eta',\sigma} t (C^{n^{+}}_{j,\sigma} C^{n'}_{l,\sigma} + H.c) \end{aligned} \tag{3.3}$$

Finally, the parameters e_0 and λ_0 may be obtained by minimizing the resulting mean – field free energy. A diagonalization of the Hamiltonian in eqn. (3.3) for the case of zero oxygen - oxygen overlap t = 0 yields a simple dispersion relation $E_k^{\pm}$ for the renormalized band structure

$$E_k^{\pm} = \frac{\varepsilon_p + \varepsilon_d}{2} \pm \left[\left[\frac{\varepsilon_p - \varepsilon_d}{2} \right]^2 + r_0^2 \gamma_k^2 \right] = e_d \pm r_0 \gamma_k (\cot\theta_k)^{\pm 1} \tag{3.4}$$

In eqn. (3.4), $\varepsilon_d = \varepsilon_d^0 + \lambda_0$, $r_0 = e_0 V$, and the dispersion is given by

$$\gamma_k^2 = 4\left[\cos^2 \frac{k_x a}{2} + \cos^2 \frac{k_y}{2} \right] \tag{3.5}$$

The dispersion given by eq. (3.5), arises entirely from the hopping terms between copper and oxygen orbitals. Associated with the eigen energies of the mean – field Hamiltonian are the eigenstates $\alpha_{k,\sigma}, \beta_{k,\sigma}$ *and* $\delta_{k,\sigma}$ which correspond to the antibonding, bonding and non bonding states respectively. We consider the case of non zero *t* so that E_k does not reduce to a simple expression.

3.3 The procedure for deriving electron – phonon interaction Hamiltonian

The procedure for deriving the electron – phonon interaction Hamiltonian using the frozen – phonon method involves a standard sequence of steps applied to a renormalized band structure. First, the frozen phonon, with wave vector **q** , is introduced as a static displacement of ions within the 2 D copper – oxide plane. Next, the electronic dispersion is recomputed in the presence of this distortion. Comparison with the electronic energy in the undistorted lattice indicates a mixing of states having wave vector **k** with those of

k + q. The associated transition matrix element is readily related to the electron – phonon coupling at wave vector **q**.

The standard frozen – phonon calculation can be extended to include the strong Coulomb correlations which are believed to lead to the insulating state of the cuprates at half filling. These Coulomb correlations are incorporated via the renormalized band structure which can be derived from Eq. (3.3) and its extension in the presence of a frozen phonon. To provide an overview of the general formulation, a simpler example, which focuses on a 1 D model containing both Cu and O components, is presented in Appendix A.

The electron – phonon Hamiltonian is written in terms of a vector representation of the quasiparticle basis operator $\Phi_{k,\sigma}$. These basis operators, deduced from a diagonalization of the Hamiltonian (Eq. 3.3), are the eigenstates $\alpha_{k,\sigma}, \alpha_{k+q,\sigma}, etc.,$. The difference between the distorted and undistorted Hamiltonian is called $\mathbf{M}_D$, which is directly related to the electron – phonon coupling. A natural basis for representing this difference matrix is the band representation, $C^{\eta}_{k,\sigma}$ *and* $d_{k,\sigma}$, corresponding to the various oxygen and copper electron operators. Thus, $\mathbf{M}_D$ contains contributions from changes in the copper - oxygen hybridization, the d – band centre of gravity, and the oxygen – oxygen overlap. The values of these shifts are linear in the ionic displacement and their 'bare' values can be deduced (Sherrington & Von Molnar, 1975). Conversion of $\mathbf{M}_D$ to the quasiparticle basis $\alpha_{k,\sigma}$ involves a unitary transformation *U*.

In the strong - U_d limit, the matrix $\mathbf{M}_D$ is self – consistently derived. In this way, important screening effects enter a renormalization of the 'bare shifts' in the copper – oxygen hybridization and *d* – band center of gravity. These self – consistently obtained

(Coleman, 2007) screening contributions are parametrized in terms of the quantities e_0 and λ_0.

In order to make analytical progress, the ionic component can be simplified by considering only the zone edge ($\mathbf{q} = \mathbf{X} = \pi/a$) phonons. These X phonons appear to couple most effectively since they lead to strong perturbations in the crystalline potential associated with the charge transfer between like atoms. In contrast to these longitudinal modes, correlation effects deriving from the transverse modes at $\mathbf{q} = \mathbf{X}$ are not as dramatic since they maintain the equivalence of like atoms. Because there is a large number of **X** phonons in two dimensions, we build on the lattice – dynamics calculation (Succi, 2001). In La_2CuO_4 in the tetragonal phase, a potential induced breathing model shows that there are 21 modes, 4 of which are unstable. Ignoring the 4 unstable modes (since their associated motions seem to couple only weekly to the electronic degrees of freedom), the remaining 17 modes are categorized by considering only the motion of those copper and oxygen ions which are in the plane. 2D models do not distinguish modes which involve motion of atoms, other than those in the plane. In this way, six distinct types of 2 D copper – oxygen phonon modes are found (Von Stetten *et al*., 1988). Following this frozen – phonon (FP) procedure, we calculate the renormalized band structure and the quasiparticle states in the distorted (**X** – mode) lattice can be calculated. The distorted Hamiltonian in the infinite U_d limit is written in terms of auxiliary boson operators as

$$H_{FP}^{2d} = \sum_{i,n,\sigma} \varepsilon_{d,n}^{0} d_{i,n,\sigma}^{+} d_{i,n,\sigma} + \sum_{i,m,\eta} \varepsilon_{p,m}^{\eta} C_{i,m,\sigma}^{\eta^{+}} C_{i,m,\sigma}^{\eta} + \sum_{i,n,\sigma} V_n (d_{i,n,\sigma}^{+} e_{i,n} \sum_{\delta,m,\eta} C_{i+\delta,m\sigma}^{\eta} + H.c.)$$

$$+ \frac{1}{2} \sum_{i,m,m',\sigma} \left[C_{i,m,\sigma}^{\eta^{+}} \sum_{\delta(\eta' \neq \eta)} t_{\delta} C_{i+\delta,m',\sigma}^{\eta'} + H.c \right] \tag{3.6}$$

where the index n = 1,2 denotes two positions for the copper orbitals and the indices m (=1,2) denote two unequal oxygen sites. As in the undistorted case, the operators e_{in}^{+} and d_{in}^{+} create Cu^{3+} and Cu^{2+} states, respectively, whereas $C_{i,m,\sigma}^{\eta^{+}}$ creates an electron at the m^{th} oxygen site within the i^{th} unit cell. The constraint equation is imposed on each copper site

$$\sum_{\sigma} d_{i,n,\sigma} d_{i,n,\sigma} + e_{i,n} e_{i,n} = 1 \tag{3.7}$$

A renormalized band structure is directly obtained from equation (3.6) by replacing the boson operators by their corresponding expectation values and introducing equation (3.7) via a Lagrangian multiplier.

Following the details described in Appendix A for the simple 1 D case, one can express the quasiparticle operators as

$$\Phi_{k,\sigma} = \begin{bmatrix} \alpha_{k,\sigma} \\ \alpha_{k+Q,\sigma} \\ \delta_{k,\sigma} \\ \delta_{k+Q,\sigma} \\ \beta_{k,\sigma} \\ \beta_{k+Q,\sigma} \end{bmatrix} = U \begin{bmatrix} d_{1,k,\sigma} \\ d_{2,k,\sigma} \\ C_{1,k,\sigma}^{x} \\ C_{2,k,\sigma}^{x} \\ C_{1,K,\sigma}^{y} \\ C_{2,k,\sigma}^{y} \end{bmatrix} \tag{3.8}$$

where the operators α, β and δ destroy a quasiparticle in the antibonding, nonbonding and bonding bands respectively.

Within this field approximation, the difference between the Hamiltonian corresponding to the distorted H_{FP}^{2d} and the undistorted $, H_0$, cases may be readily deduced from equations(3.3) and (3.6) as:

$$H_{e-ph} = H_{FP} - H_0 = \sum_{k,\sigma} \Phi_{k,\sigma}^{+} \overline{M}_D \Phi_{k,\sigma} + \sum_n \lambda_n (e_n^2 - 1) - 2\lambda_0 (e_0^2 - 1) \qquad (3.9)$$

where the λ_n's are the Lagrange multipliers introduced to satisfy the constraint equation (3.7) and $\overline{M}_D = U.M_D.U^+$ is the transformed distortion matrix which includes 'screening' effects via the parameters e_n and λ_n.

In this method, the focus is on intraband scatterings between $\alpha_{k,\sigma}$ and $\alpha_{k+X,\sigma}$ because these states near E_F are strongly scattered by the ionic displacement. Furthermore, other contributions such as interband scattering require higher energies than a phonon can provide. These intraband terms are written as

$$H_{eph} = \sum_{k,\sigma} \hat{g}_X (\alpha_{k,\sigma}^{+} \alpha_{k+X,\sigma} + \alpha_{k+X,\sigma}^{+} \alpha_{k,\sigma}) \qquad (3.10)$$

Here, the electron - phonon coupling in the quasiparticle basis is

$$\hat{g}_X = \left\langle \alpha_{k,\sigma} \left| H_{e-ph} \right| \alpha_{k+X,\sigma} \right\rangle \qquad (3.11)$$

We may express this matrix element in terms of phonon creation and annihilation operators $a_{X,v}^{+}$ and $a_{X,v}$ respectively, for a wave vector **X** with quantized displacement (h=1) as

$$\hat{g}_{X,v} = g_{X,v} \left[\frac{1}{2N_0 M_{X,v} \omega_{X,v}} \right]^{\frac{1}{2}} (a_{X,v}^{+} + a_{-X,v}) \qquad (3.12)$$

where the electron – phonon transition matrix element is

$$g_{X,v} = \lim_{\delta R \to 0} \left\langle \alpha_{k,\sigma} \left| \frac{\delta H}{\delta R} . \hat{\varepsilon}_{X,v} \right| \alpha_{k+X,\sigma} \right\rangle \tag{3.13}$$

and $\hat{\varepsilon}_{X,v}$ is the polarization vector for a normal mode *v*, N_0 is the number of ions in each unit cell, $\boldsymbol{M}_{X,v}$ is the reduced mass corresponding to a phonon mode ($\boldsymbol{X}$,*v*), $\omega_{X,v}$ is a normal mode frequency.

The electron – phonon matrix element in equation (3.13) can now be evaluated in terms of changes in the 'bare' Hamiltonian parameters which arise from a lattice distortion. Hybridization between copper $3d_{x^2.y^2}$ and oxygen *2p* orbital distance is highly anisotropic (Kim *et al.,* 1991). A small distortion along the longitudinal direction (parallel to the bonding axis) leads to significant changes in hybridization. This can be represented as linearly proportional to the ionic displacement when the distortion is small (Appendix B)

$$V_n(R+\delta R) - V(R) \approx \frac{\delta V}{\delta R}\delta R = -7V\frac{\delta R}{a} \tag{3.14}$$

and

$$t(R+\delta R) - t(R) \approx -2t(R)\frac{\delta R}{a} \tag{3.15}$$

Along the transverse direction (perpendicular to the bonding axis), however, the change in hybridization is almost negligible. These changes in V ultimately lead to changes in the variational parameters such as e_n and λ_n. These parameters have been calculated self – consistently, and they are found to vary linearly with displacement about the equilibrium or undistorted values e_0 and λ_0:

$$e_n \approx e_0 \pm \frac{\delta e_0}{\delta R}\delta R \tag{3.16}$$

and

$$\lambda_1 - \lambda_2 \approx \frac{\delta\lambda_0}{\delta R}\delta R \tag{3.17}$$

where $\delta e_0/\delta R$ and $\delta\lambda_0/\delta R$ are the Coulomb interaction – induced screening responses. These functions depend on E_F and their concentration dependence may be calculated using a somewhat simplified analysis. First, we change the amplitude of the static displacement of either the copper or oxygen ions is changed and then e_n and λ_n are calculated from the mean – field equations for H_{FP}^{2d} at each E_F. Finally, $\delta e_0/\delta R$ and $\delta\lambda_0/\delta R$ are extracted by comparing e_n and λ_n to e_0 and λ_0 as a function of the displacement.

3.4 Derivation of Coulomb interaction Hamiltonian.

It is clearly established that the high temperature superconductivity [HTSC] cannot be explained by using the BCS theory. A new type of pairing mechanism between the electrons has to be invoked to explain the properties of high - T_c superconductors.

The structure of these HTSC compounds is explained in the section (2.5). It is also emphasized that there exists a pairing interaction between the charges in the charge reservoir; and there exists an attractive term at the oxygen ion sites as a result of oxygen virtual charge excitations. It seems such interactions are relevant to study the properties of high - T_c superconductors. The resulting oxygen-copper hopping due to attractive term leads to the changes in the onsite energies of oxygen (E_p) and copper (E_d). The hybridization between copper and oxygen bands is represented by (t_{pd}) and the repulsion between the holes occupying the same copper orbital is(u_d).

Using second quantization and many body techniques, the Hamiltonian H_c (Coulomb interaction Hamiltonian) for the assembly can be written as,

$$H_c = E_p \sum_i n_i^p + E_d \sum n_n^j + t_{pd} \sum_{i,j,\sigma} (d_{j\sigma}^+ + h.c.) + u_d \sum_n n_{i\uparrow}^j n_{j\downarrow}^d \tag{3.18}$$

where p and d operators refer to the oxygen and copper ions, respectively. Each term in equation (3.18) can be written in terms of the creation and annihilation operators. Here n_i^p refers to the number of electrons at the site i for oxygen, and n_j^d refers to the numbers of electrons at the site j for copper.

$$n_i^p = a_{ip}^+ a_{ip} \text{ and } n_j^d = a_{jd}^+ a_{jd} \tag{3.19}$$

Due to hybridization between copper and oxygen bands we have the term $(d_{j\sigma}^+)$ and this term can be written as $((a_{ip}^+ a_{jd} + a_{jd}^+ a_{ip})$ .The term d represents the repulsion between the holes occupying the same copper orbital. Let the creation and annihilation operators for holes be represented by 'b'. We can then write dropping spin orientation

$$n_i^d n_j^d = b_{jd}^+ b_{id}^+ b_{ip} b_{jp} \tag{3.20}$$

which means the holes on repulsion in copper orbital go to oxygen from the site j in copper to the site i in oxygen, and the opposite can also happen. Now the creation of a hole results due to the disappearance of the electron, and the destruction of a hole means the appearance (creation) of an electron. To convert eq. (3.18) into a set of creation and annihilation operators for the electrons, this can be written as,

$$H_c = E_p \sum_i a_{ip}^+ a_{ip} + E_d \sum_j a_{jd}^+ a_{jd} + t_{pd} \sum_{ij} (a_{ip}^+ a_{jd} + a_{jd}^+ a_{ip}) + u_d \sum_{ji} a_{jd}^+ a_{jd}^+ a_{ip} a_{ip}$$

(3.21)

3.5 The electron – phonon and Coulomb interaction Hamiltonian

The electron – phonon and Coulomb interaction Hamiltonian, H_{epc} is obtained from the sum of eq. (3.10) and (3.21) as

$$H_{epc} = g_{ep}\sum_{k,\sigma}(\alpha^{+}_{k,\sigma}\alpha_{k+X,\sigma} + \alpha^{+}_{k+X,\sigma}\alpha_{k,\sigma}) + E_p\sum_i a^{+}_{ip}a_{ip} + E_d\sum_j a^{+}_{jd}a_{jd} + t_{pd}\sum_{ij}(a^{+}_{ip}a_{jd} + a^{+}_{jd}a_{ip}) + u_d\sum_{ji} a^{+}_{jd}a^{+}_{jd}a_{ip}a_{ip}$$

(3.22)

where g_{ep} is the energy for electron – phonon interaction.

CHAPTER FOUR

RESULTS AND DISCUSSIONS

4.1 Introduction

In this section, the expectation value of the H_{epc} is calculated and the results on the effect of the electron – phonon and Coulomb Hamiltonian on transition temperature, specific heat and entropy are presented. Numerical values of specific heat against absolute temperature and those of entropy against absolute temperature were calculated and tabulated.

The results for specific heat and entropy against absolute temperature are presented. From the graphs specific heat against absolute temperature, the transition temperatures, T_c, were obtained. The effects of the various parameters on transition temperature, specific heat and entropy are presented.

4.2 Calculation of the expectation value of the electron – phonon and Coulomb interaction Hamiltonian.

The expectation value of H_{epc} given in Eq. (3.22) was calculated by writing the trial wave function for such a system. The trial wave function was written as,

$$\Psi = (a_i a_i + a_j^+ a_j^+)(u + v a_i^+ a_i^+)\left|n,0\right\rangle \tag{4.1}$$

and its conjugate was

$$\Psi^* = \left\langle n,0\right|\left(u + v a_i a_i\right)\left(a_j a_j + a_i^+ a_i^+\right) \tag{4.2}$$

Using the trial wave function and its conjugate, the expectation value of the H_{epc} was written as;

$$E_n = \left\langle \Psi \right| \mathrm{H_{epc}} \left| \Psi \right\rangle \tag{4.3}$$

Eqs. (4.1), (4.2) were substituted in eq. (4.3) to obtain

$$E_n = \langle n,0 | \left(u + v a_i a_i\right)\left(a_j a_j + a_i^+ a_i^+\right) \begin{bmatrix} E_p a_{ip}^+ a_{ip} \\ +E_d a_{jd}^+ a_{jd} \\ +t_{pd}(a_{ip}^+ a_{jd} + a_{jd}^+ a_{ip}) \\ +u_d a_{jd}^+ a_{jd}^+ a_{ip} a_{ip} \\ +g_{ep}(a_{k\sigma}^+ a_{k+X,\sigma} + a_{k+X,\sigma}^+ a_{k\sigma}) \end{bmatrix} (a_i a_i + a_j^+ a_j^+)(u + v a_i^+ a_i^+ | n,0\rangle$$

(4.4)

The expectation value of the electron – phonon and Coulomb Hamiltonian was calculated using second quantization and many body techniques to obtain the coefficients of E_p, E_d, t_{pd}, u_d *and* g_{ep} from eq. (4.4) .

The terms containing E_p were obtained from eq. (4.4) as follows;

$$\langle n,0|(u+va_ia_i)\left(a_ja_j+a_i^+a_i^+\right)\left[E_pa_{ip}^+a_{ip}\right](a_ia_i+a_j^+a_j^+)(u+va_i^+a_i^+|n,0\rangle$$
$$=\langle n,0|(ua_ja_j+ua_i^+a_i^++va_ia_ia_ja_j+va_ia_ia_i^+a_i^+)\left[E_pa_{ip}^+a_{ip}\right](ua_ia_i+va_ia_ia_i^+a_i^+$$
$$+ua_j^+a_j^++va_j^+a_j^+a_i^+a_i^+)|n,0\rangle$$
$$=\langle n,0|\begin{bmatrix}\left\{ua_ja_j(E_pa_{ip}^+a_{ip})\right\}+\left\{ua_j^+a_j^+(E_pa_{ip}^+a_{ip})\right\}+\left\{(va_ia_ia_ja_j)(E_pa_{ip}^+a_{ip})\right\}\\+\left\{va_ia_ia_i^+a_i^+(E_pa_{ip}^+a_{ip})\right\}\end{bmatrix}$$
$$(ua_ia_i+va_ia_ia_i^+a_i^++ua_j^+a_j^++va_j^+a_j^+a_i^+a_i^+)|n,0\rangle$$
$$=\langle n,0|ua_ja_jE_pa_{ip}^+a_{ip}ua_ia_i|n,0\rangle+\langle n,0|ua_ja_jE_pa_{ip}^+a_{ip}va_ia_ia_i^+a_i^+|n,0\rangle$$
$$+\langle n,0|ua_ja_jE_pa_{ip}^+a_{ip}ua_j^+a_j^+|n,0\rangle+\langle n,0|ua_ja_jE_pa_{ip}^+a_{ip}va_j^+a_j^+a_i^+a_i^+|n,0\rangle$$
$$+\langle n,0|ua_j^+a_j^+E_pa_{ip}^+a_{ip}ua_ia_i|n,0\rangle+\langle n,0|ua_j^+a_j^+E_pa_{ip}^+a_{ip}va_ia_ia_i^+a_i^+|n,0\rangle$$
$$+\langle n,0|ua_j^+a_j^+E_pa_{ip}^+a_{ip}ua_j^+a_j^+|n,0\rangle+\langle n,0|ua_j^+a_j^+E_pa_{ip}^+a_{ip}va_j^+a_j^+a_i^+a_i^+|n,0\rangle$$
$$+\langle n,0|va_ia_ia_ja_jE_pa_{ip}^+a_{ip}ua_ia_i|n,0\rangle+\langle n,0|va_ia_ia_ja_jE_pa_{ip}^+a_{ip}va_ia_ia_i^+a_i^+|n,0\rangle$$
$$+\langle n,0|va_ia_ia_ja_jE_pa_{ip}^+a_{ip}ua_j^+a_j^+|n,0\rangle+\langle n,0|va_ia_ia_ja_jE_pa_{ip}^+a_{ip}va_j^+a_j^+a_i^+a_i^+|n,0\rangle$$
$$+\langle n,0|va_ia_ia_i^+a_i^+E_pa_{ip}^+a_{ip}ua_ia_i|n,0\rangle+\langle n,0|va_ia_ia_i^+a_i^+E_pa_{ip}^+a_{ip}va_ia_ia_i^+a_i^+|n,0\rangle$$
$$+\langle n,0|va_ia_ia_i^+a_i^+E_pa_{ip}^+a_{ip}ua_j^+a_j^+|n,0\rangle+\langle n,0|va_ia_ia_i^+a_i^+E_pa_{ip}^+a_{ip}va_j^+a_j^+a_i^+a_i^+|n,0\rangle$$

(4.5)

Applying the properties of creation and annihilation operators to the eq. (4.5), we obtain

$$\langle n,0|ua_ja_jE_pa_{ip}^+a_{ip}ua_ia_i|n,0\rangle=u^2E_p\langle n,0|a_ja_ja_{ip}^+a_{ip}a_ia_i|n,0\rangle=0 \qquad (4.6)$$

$$\langle n,0|ua_ja_jE_pa_{ip}^+a_{ip}va_ia_ia_i^+a_i^+|n,0\rangle=uvE_p\langle n,0|a_ja_ja_{ip}^+a_{ip}a_ia_ia_i^+a_i^+|n,0\rangle=0 \qquad (4.7)$$

$$\langle n,0|ua_j a_j E_p a_{ip}^+ a_{ip} ua_j^+ a_j^+ |n,0\rangle = u^2 E_p \langle n,0|a_j a_j a_{ip}^+ a_{ip} a_j^+ a_j^+ |n,0\rangle$$
$$= u^2 E_p (n+1)^{\frac{1}{2}} \langle n,0|a_j a_j a_{ip}^+ a_{ip} a_j^+ |(n+1),0\rangle$$
$$= u^2 E_p (n+1)^{\frac{1}{2}} (n+2)^{\frac{1}{2}} \langle n,0|a_j a_j a_{ip}^+ a_{ip} |(n+2),0\rangle$$
$$= u^2 E_p (n+1)^{\frac{1}{2}} (n+2) \langle n,0|a_j a_j a_{ip}^+ |(n+1),0\rangle$$
$$= u^2 E_p (n+1)^{\frac{1}{2}} (n+2)^{\frac{3}{2}} \langle n,0|a_j a_j |(n+2),0\rangle$$
$$= u^2 E_p (n+1)^{\frac{1}{2}} (n+2)^2 \langle n,0|a_j |(n+1),0\rangle$$
$$= u^2 E_p (n+1)(n+2)^2 \langle n,0|n,0\rangle = u^2 E_p (n+1)(n+2)^2$$

(4.8)

$$\langle n,0|ua_j a_j E_p a_{ip}^+ a_{ip} va_j^+ a_j^+ a_i^+ a_i^+ |n,0\rangle = 0 \quad (4.9)$$

$$\langle n,0|ua_j^+ a_j^+ E_p a_{ip}^+ a_{ip} ua_i a_i |n,0\rangle = u^2 E_p n^{\frac{1}{2}} \langle n,0|a_j^+ a_j^+ a_{ip}^+ a_{ip} a_i |(n-1),0\rangle$$
$$= u^2 E_p n^{\frac{1}{2}} (n-1)^{\frac{1}{2}} \langle n,0|a_j^+ a_j^+ a_{ip}^+ a_{ip} |(n-2),0\rangle$$
$$= u^2 E_p n^{\frac{1}{2}} (n-1)^{\frac{1}{2}} (n-2)^{\frac{1}{2}} \langle n,0|a_j^+ a_j^+ a_{ip}^+ |(n-3),0\rangle$$
$$= u^2 E_p n^{\frac{1}{2}} (n-1)^{\frac{1}{2}} (n-2) \langle n,0|a_j^+ a_j^+ |(n-2),0\rangle$$
$$= u^2 E_p n^{\frac{1}{2}} (n-1)(n-2) \langle n,0|a_j^+ |(n-1),0\rangle = u^2 E_p n(n-1)(n-2) \langle n,0|n,0\rangle$$
$$= u^2 E_p n(n-1)(n-2)$$

(4.10)

$$\langle n,0|ua_j^+ a_j^+ E_p a_{ip}^+ a_{ip} va_i a_i a_i^+ a_i^+ |n,0\rangle = 0 \quad (4.11)$$

$$\langle n,0|ua_j^+ a_j^+ E_p a_{ip}^+ a_{ip} ua_j^+ a_j^+ |n,0\rangle = 0 \quad (4.12)$$

$$\langle n,0|ua_j^+ a_j^+ E_p a_{ip}^+ a_{ip} va_j^+ a_j^+ a_i^+ a_i^+ |n,0\rangle = 0 \quad (4.13)$$

$$\langle n,0|va_i a_i a_j a_j E_p a_{ip}^+ a_{ip} ua_i a_i |n,0\rangle = 0 \quad (4.14)$$

$$\langle n,0|va_i a_i a_j a_j E_p a_{ip}^+ a_{ip} va_i a_i a_i^+ a_i^+ |n,0\rangle = 0 \quad (4.15)$$

$$\langle n,0|va_ia_ia_ja_jE_pa_{ip}^+a_{ip}ua_j^+a_j^+|n,0\rangle=0 \tag{4.16}$$

$$\begin{aligned}
&\langle n,0|a_ia_ia_ja_ja_{ip}^+a_{ip}a_j^+a_j^+a_i^+a_i^+|n,0\rangle\\
&=v^2E_p(n+1)^{\frac{1}{2}}\langle n,0|a_ia_ia_ja_ja_{ip}^+a_{ip}a_j^+a_j^+a_i^+|(n+1),0\rangle\\
&=v^2E_p(n+1)^{\frac{1}{2}}(n+2)^{\frac{1}{2}}\langle n,0|a_ia_ia_ja_ja_{ip}^+a_{ip}a_j^+a_j^+|(n+2),0\rangle\\
&=v^2E_p(n+1)^{\frac{1}{2}}(n+2)^{\frac{1}{2}}(n+3)^{\frac{1}{2}}\langle n,0|a_ia_ia_ja_ja_{ip}^+a_{ip}a_j^+|(n+3),0\rangle\\
&=v^2E_p(n+1)^{\frac{1}{2}}(n+2)^{\frac{1}{2}}(n+3)^{\frac{1}{2}}(n+4)^{\frac{1}{2}}\langle n,0|a_ia_ia_ja_ja_{ip}^+a_{ip}|(n+4),0\rangle\\
&=v^2E_p(n+1)^{\frac{1}{2}}(n+2)^{\frac{1}{2}}(n+3)^{\frac{1}{2}}(n+4)\langle n,0|a_ia_ia_ja_ja_{ip}^+|(n+3),0\rangle\\
&=v^2E_p(n+1)^{\frac{1}{2}}(n+2)^{\frac{1}{2}}(n+3)^{\frac{1}{2}}(n+4)^{\frac{3}{2}}\langle n,0|a_ia_ia_ja_j|(n+4),0\rangle\\
&=v^2E_p(n+1)^{\frac{1}{2}}(n+2)^{\frac{1}{2}}(n+3)^{\frac{1}{2}}(n+4)^2\langle n,0|a_ia_ia_j|(n+3),0\rangle\\
&=v^2E_p(n+1)^{\frac{1}{2}}(n+2)^{\frac{1}{2}}(n+3)(n+4)^2\langle n,0|a_ia_i|(n+2),0\rangle\\
&=v^2E_p(n+1)^{\frac{1}{2}}(n+2)(n+3)(n+4)^2\langle n,0|a_i|(n+1),0\rangle\\
&=v^2E_p(n+1)(n+2)(n+3)(n+4)^2\langle n,0|n,0\rangle\\
&=v^2E_p(n+1)(n+2)(n+3)(n+4)^2
\end{aligned} \tag{4.17}$$

$$\langle n,0|va_ia_ia_i^+a_i^+E_pa_{ip}^+a_{ip}ua_ia_i|n,0\rangle=0 \tag{4.18}$$

$$\begin{aligned}
&\langle n,0|va_ia_ia_i^+a_i^+E_pa_{ip}^+a_{ip}va_ia_ia_i^+a_i^+|n,0\rangle\\
&=v^2E_p(n+1)^{\frac{1}{2}}\langle n,0|a_ia_ia_i^+a_i^+a_{ip}^+a_{ip}a_ia_ia_i^+|(n+1),0\rangle\\
&=v^2E_p(n+1)^{\frac{1}{2}}(n+2)^{\frac{1}{2}}\langle n,0|a_ia_ia_i^+a_i^+a_{ip}^+a_{ip}a_ia_i|(n+2),0\rangle\\
&=v^2E_p(n+1)^{\frac{1}{2}}(n+2)\langle n,0|a_ia_ia_i^+a_i^+a_{ip}^+a_{ip}a_i|(n+1),0\rangle\\
&=v^2E_p(n+1)(n+2)\langle n,0|a_ia_ia_i^+a_i^+a_{ip}^+a_{ip}|n,0\rangle\\
&=v^2E_pn^{\frac{1}{2}}(n+1)(n+2)\langle n,0|a_ia_ia_i^+a_i^+a_{ip}^+|(n-1),0\rangle\\
&=v^2E_pn^{\frac{1}{2}}(n+1)(n+2)\langle n,0|a_ia_ia_i^+a_i^+a_{ip}^+|(n-1),0\rangle\\
&=v^2E_pn(n+1)(n+2)\langle n,0|a_ia_ia_i^+a_i^+|n,0\rangle\\
&=v^2E_pn(n+1)^{\frac{3}{2}}(n+2)\langle n,0|a_ia_ia_i^+|(n+1),0\rangle\\
&=v^2E_pn(n+1)^{\frac{3}{2}}(n+2)^{\frac{3}{2}}\langle n,0|a_ia_i|(n+2),0\rangle\\
&=v^2E_pn(n+1)^{\frac{3}{2}}(n+2)\langle n,0|a_i|(n+1),0\rangle\\
&=v^2E_pn(n+1)(n+2)\langle n,0|n,0\rangle=v^2E_pn(n+1)(n+2)
\end{aligned} \tag{4.19}$$

$$\langle n,0|va_ia_ia_i^+a_i^+E_pa_{ip}^+a_{ip}ua_j^+a_j^+|n,0\rangle=0 \tag{4.20}$$

$$\langle n,0|va_ia_ia_i^+a_i^+E_pa_{ip}^+a_{ip}va_j^+a_j^+a_i^+a_i^+|n,0\rangle=0 \tag{4.21}$$

The sum of sum of eq. (4.8), (4.10), (4.17) and (4.19) gives,

$$\begin{aligned}
&u^2E_p(n+1)(n+2)^2+u^2E_pn(n-1)(n-2)\\
&+v^2E_p(n+1)(n+2)(n+3)(n+4)^2+v^2E_pn(n+1)(n+2)\\
&=\left\{\begin{matrix}u^2(n+1)(n+2)^2+u^2n(n-1)(n-2)\\+v^2(n+1)(n+2)(n+3)(n+4)^2+v^2n(n+1)(n+2)\end{matrix}\right\}E_p
\end{aligned} \tag{4.22}$$

From eq. (4.4), the terms containing E_d were obtained;

$$\langle n,0|(u+va_ia_i)\left(a_ja_j+a_i^+a_i^+\right)\left[E_da_{jd}^+a_{jd}\right]$$
$$(a_ia_i+a_j^+a_j^+)(u+va_i^+a_i^+|n,0\rangle$$
$$=\langle n,0|\left(ua_ja_j+ua_i^+a_i^++va_ia_ia_ja_j+va_ia_ia_i^+a_i^+\right)\left[E_da_{jd}^+a_{jd}\right]$$
$$(a_ia_i+a_j^+a_j^+)(u+va_i^+a_i^+|n,0\rangle$$
$$=\langle n,0|\begin{pmatrix}ua_ja_jE_da_{jd}^+a_{jd}+ua_i^+a_i^+E_da_{jd}^+a_{jd}\\+va_ia_ia_ja_jE_da_{jd}^+a_{jd}+va_ia_ia_i^+a_i^+E_da_{jd}^+a_{jd}\end{pmatrix}$$
$$(ua_ia_i+ua_j^+a_j^++a_ia_iva_i^+a_i^++a_j^+a_j^+va_i^+a_i^+)|n,0\rangle$$
$$=\langle n,0|\begin{pmatrix}ua_ja_jE_da_{jd}^+a_{jd}+ua_i^+a_i^+E_da_{jd}^+a_{jd}\\+va_ia_ia_ja_jE_da_{jd}^+a_{jd}+va_ia_ia_i^+a_i^+E_da_{jd}^+a_{jd}\end{pmatrix}$$
$$(ua_ia_i+ua_j^+a_j^++a_ia_iva_i^+a_i^++a_j^+a_j^+va_i^+a_i^+)|n,0\rangle$$
$$=\langle n,0|ua_ja_jE_da_{jd}^+a_{jd}ua_ia_i|n,0\rangle+\langle n,0|ua_ja_jE_da_{jd}^+a_{jd}ua_j^+a_j^+|n,0\rangle$$
$$+\langle n,0|ua_ja_jE_da_{jd}^+a_{jd}a_ia_iva_i^+a_i^+|n,0\rangle+\langle n,0|ua_ja_jE_da_{jd}^+a_{jd}a_j^+a_j^+va_i^+a_i^+|n,0\rangle$$
$$+\langle n,0|ua_i^+a_i^+E_da_{jd}^+a_{jd}ua_ia_i|n,0\rangle+\langle n,0|ua_i^+a_i^+E_da_{jd}^+a_{jd}ua_j^+a_j^+|n,0\rangle$$
$$+\langle n,0|ua_i^+a_i^+E_da_{jd}^+a_{jd}a_ia_iva_i^+a_i^+|n,0\rangle+\langle n,0|ua_i^+a_i^+E_da_{jd}^+a_{jd}a_j^+a_j^+va_i^+a_i^+|n,0\rangle$$
$$+\langle n,0|va_ia_ia_ja_jE_da_{jd}^+a_{jd}ua_ia_i|n,0\rangle+\langle n,0|va_ia_ia_ja_jE_da_{jd}^+a_{jd}ua_j^+a_j^+|n,0\rangle$$
$$+\langle n,0|va_ia_ia_ja_jE_da_{jd}^+a_{jd}a_ia_iva_i^+a_i^+|n,0\rangle+\langle n,0|va_ia_ia_ja_jE_da_{jd}^+a_{jd}a_j^+a_j^+va_i^+a_i^+|n,0\rangle$$
$$+\langle n,0|va_ia_ia_ja_jE_da_{jd}^+a_{jd}ua_ia_i|n,0\rangle+\langle n,0|va_ia_ia_ja_jE_da_{jd}^+a_{jd}ua_j^+a_j^+|n,0\rangle$$
$$+\langle n,0|va_ia_ia_ja_jE_da_{jd}^+a_{jd}a_ia_iva_i^+a_i^+|n,0\rangle+\langle n,0|va_ia_ia_ja_jE_da_{jd}^+a_{jd}a_j^+a_j^+va_i^+a_i^+|n,0\rangle$$
$$+\langle n,0|va_ia_ia_i^+a_i^+E_da_{jd}^+a_{jd}ua_ia_i|n,0\rangle+\langle n,0|va_ia_ia_i^+a_i^+E_da_{jd}^+a_{jd}ua_j^+a_j^+|n,0\rangle$$
$$+\langle n,0|va_ia_ia_i^+a_i^+E_da_{jd}^+a_{jd}a_ia_iva_i^+a_i^+|n,0\rangle+\langle n,0|va_ia_ia_i^+a_i^+E_da_{jd}^+a_{jd}a_j^+a_j^+va_i^+a_i^+|n,0\rangle$$

(4.23)

Applying the properties of creation and annihilation operators to eq. (4.23), the terms in the equation reduced to:

$$\langle n,0|ua_ja_jE_da_{jd}^+a_{jd}ua_ia_i|n,0\rangle=0 \qquad (4.24)$$

$$\langle n,0|ua_j a_j E_d a_{jd}^+ a_{jd} ua_j^+ a_j^+ |n,0\rangle = u^2 E_d \langle n,0|a_j a_j a_{jd}^+ a_{jd} a_j^+ a_j^+ |n,0\rangle$$
$$= u^2 E_d (n+1)^{\frac{1}{2}} \langle n,0|a_j a_j a_{jd}^+ a_{jd} a_j^+ |(n+1),0\rangle$$
$$= u^2 E_d (n+1)^{\frac{1}{2}} (n+2)^{\frac{1}{2}} \langle n,0|a_j a_j a_{jd}^+ a_{jd} |(n+2),0\rangle$$
$$= u^2 E_d (n+1)^{\frac{1}{2}} (n+2) \langle n,0|a_j a_j a_{jd}^+ |(n+1),0\rangle$$
$$= u^2 E_d (n+1)^{\frac{1}{2}} (n+2)^{\frac{3}{2}} \langle n,0|a_j a_j |(n+2),0\rangle$$
$$= u^2 E_d (n+1)^{\frac{1}{2}} (n+2)^2 \langle n,0|a_j |(n+1),0\rangle$$
$$= u^2 E_d (n+1)(n+2)^2 \langle n,0|n,0\rangle = u^2 E_d (n+1)(n+2)^2$$

(4.25)

$$\langle n,0|ua_j a_j E_d a_{jd}^+ a_{jd} a_i a_i v a_i^+ a_i^+ |n,0\rangle = 0 \tag{4.26}$$

$$\langle n,0|ua_j a_j E_d a_{jd}^+ a_{jd} a_j^+ a_j^+ v a_i^+ a_i^+ |n,0\rangle = 0 \tag{4.27}$$

$$\langle n,0|ua_i^+ a_i^+ E_d a_{jd}^+ a_{jd} ua_i a_i |n,0\rangle = u^2 E_d n^{\frac{1}{2}} \langle n,0|a_i^+ a_i^+ a_{jd}^+ a_{jd} a_i |(n-1),0\rangle$$
$$= u^2 E_d n^{\frac{1}{2}} (n-1)^{\frac{1}{2}} \langle n,0|a_i^+ a_i^+ a_{jd}^+ a_{jd} |(n-2),0\rangle$$
$$= u^2 E_d n^{\frac{1}{2}} (n-1)^{\frac{1}{2}} (n-2)^{\frac{1}{2}} \langle n,0|a_i^+ a_i^+ a_{jd}^+ |(n-3),0\rangle$$
$$= u^2 E_d n^{\frac{1}{2}} (n-1)^{\frac{1}{2}} (n-2) \langle n,0|a_i^+ a_i^+ |(n-2),0\rangle$$
$$= u^2 E_d n^{\frac{1}{2}} (n-1)(n-2) \langle n,0|a_i^+ |(n-1),0\rangle$$
$$= u^2 E_d n(n-1)(n-2) \langle n,0|n,0\rangle = u^2 E_d n(n-1)(n-2)$$

(4.28)

$$\langle n,0|ua_i^+ a_i^+ E_d a_{jd}^+ a_{jd} ua_j^+ a_j^+ |n,0\rangle = 0 \tag{4.29}$$

$$\langle n,0|ua_i^+ a_i^+ E_d a_{jd}^+ a_{jd} a_i a_i v a_i^+ a_i^+ |n,0\rangle = 0 \tag{4.30}$$

$$\langle n,0|ua_i^+ a_i^+ E_d a_{jd}^+ a_{jd} a_j^+ a_j^+ v a_i^+ a_i^+ |n,0\rangle = 0 \tag{4.31}$$

$$\langle n,0|va_i a_i a_j a_j E_d a_{jd}^+ a_{jd} ua_i a_i |n,0\rangle = 0 \tag{4.32}$$

$$\langle n,0|va_ia_ia_ja_jE_da_{jd}^+a_{jd}ua_j^+a_j^+|n,0\rangle=0 \tag{4.33}$$

$$\langle n,0|va_ia_ia_ja_jE_da_{jd}^+a_{jd}a_ia_iva_i^+a_i^+|n,0\rangle=0 \tag{4.34}$$

$$\begin{aligned}
&\langle n,0|va_ia_ia_ja_jE_da_{jd}^+a_{jd}a_j^+a_j^+va_i^+a_i^+|n,0\rangle\\
&=v^2E_d(n+1)^{\frac{1}{2}}\langle n,0|a_ia_ia_ja_ja_{jd}^+a_{jd}a_j^+a_j^+a_i^+|(n+1),0\rangle\\
&=v^2E_d(n+1)^{\frac{1}{2}}(n+2)^{\frac{1}{2}}\langle n,0|a_ia_ia_ja_ja_{jd}^+a_{jd}a_j^+a_j^+|(n+2),0\rangle\\
&=v^2E_d(n+1)^{\frac{1}{2}}(n+2)^{\frac{1}{2}}(n+3)^{\frac{1}{2}}\langle n,0|a_ia_ia_ja_ja_{jd}^+a_{jd}a_j^+|(n+3),0\rangle\\
&=v^2E_d(n+1)^{\frac{1}{2}}(n+2)^{\frac{1}{2}}(n+3)^{\frac{1}{2}}(n+4)^{\frac{1}{2}}\langle n,0|a_ia_ia_ja_ja_{jd}^+a_{jd}|(n+4),0\rangle\\
&=v^2E_d(n+1)^{\frac{1}{2}}(n+2)^{\frac{1}{2}}(n+3)^{\frac{1}{2}}(n+4)\langle n,0|a_ia_ia_ja_ja_{jd}^+|(n+3),0\rangle\\
&=v^2E_d(n+1)^{\frac{1}{2}}(n+2)^{\frac{1}{2}}(n+3)^{\frac{1}{2}}(n+4)^{\frac{3}{2}}\langle n,0|a_ia_ia_ja_j|(n+4),0\rangle\\
&=v^2E_d(n+1)^{\frac{1}{2}}(n+2)^{\frac{1}{2}}(n+3)^{\frac{1}{2}}(n+4)^2\langle n,0|a_ia_ia_j|(n+3),0\rangle\\
&=v^2E_d(n+1)^{\frac{1}{2}}(n+2)^{\frac{1}{2}}(n+3)(n+4)^2\langle n,0|a_ia_i|(n+2),0\rangle\\
&=v^2E_d(n+1)^{\frac{1}{2}}(n+2)(n+3)(n+4)^2\langle n,0|a_i|(n+1),0\rangle\\
&=v^2E_d(n+1)(n+2)(n+3)(n+4)^2\langle n,0|n,0\rangle\\
&=v^2E_d(n+1)(n+2)(n+3)(n+4)^2
\end{aligned} \tag{4.35}$$

$$\langle n,0|va_ia_ia_ja_jE_da_{jd}^+a_{jd}ua_ia_i|n,0\rangle=0 \tag{4.36}$$

$$\langle n,0|va_ia_ia_ja_jE_da_{jd}^+a_{jd}ua_j^+a_j^+|n,0\rangle=0 \tag{4.37}$$

$$\langle n,0|va_ia_ia_ja_jE_da_{jd}^+a_{jd}a_ia_iva_i^+a_i^+|n,0\rangle=0 \tag{4.38}$$

$$\begin{aligned}
&\langle n,0|va_ia_ia_ja_jE_da_{jd}^+a_{jd}a_j^+a_j^+va_i^+a_i^+|n,0\rangle \\
&=v^2E_d(n+1)^{\frac{1}{2}}\langle n,0|a_ia_ia_ja_ja_{jd}^+a_{jd}a_j^+a_j^+a_i^+|(n+1),0\rangle \\
&=v^2E_d(n+1)^{\frac{1}{2}}(n+2)^{\frac{1}{2}}\langle n,0|a_ia_ia_ja_ja_{jd}^+a_{jd}a_j^+a_j^+|(n+2),0\rangle \\
&=v^2E_d(n+1)^{\frac{1}{2}}(n+2)^{\frac{1}{2}}(n+3)^{\frac{1}{2}}\langle n,0|a_ia_ia_ja_ja_{jd}^+a_{jd}a_j^+|(n+3),0\rangle \\
&=v^2E_d(n+1)^{\frac{1}{2}}(n+2)^{\frac{1}{2}}(n+3)^{\frac{1}{2}}(n+4)^{\frac{1}{2}}\langle n,0|a_ia_ia_ja_ja_{jd}^+a_{jd}|(n+4),0\rangle \\
&=v^2E_d(n+1)^{\frac{1}{2}}(n+2)^{\frac{1}{2}}(n+3)^{\frac{1}{2}}(n+4)^{\frac{3}{2}}\langle n,0|a_ia_ia_ja_ja_{jd}^+|(n+3),0\rangle \\
&=v^2E_d(n+1)^{\frac{1}{2}}(n+2)^{\frac{1}{2}}(n+3)^{\frac{1}{2}}(n+4)^2\langle n,0|a_ia_ia_ja_j|(n+4),0\rangle \\
&=v^2E_d(n+1)^{\frac{1}{2}}(n+2)^{\frac{1}{2}}(n+3)^{\frac{1}{2}}(n+4)^{\frac{5}{2}}\langle n,0|a_ia_ia_j|(n+3),0\rangle \\
&=v^2E_d(n+1)^{\frac{1}{2}}(n+2)^{\frac{1}{2}}(n+3)(n+4)^{\frac{5}{2}}\langle n,0|a_ia_i|(n+2),0\rangle \\
&=v^2E_d(n+1)^{\frac{1}{2}}(n+2)(n+3)(n+4)^{\frac{5}{2}}\langle n,0|a_i|(n+1),0\rangle \\
&=v^2E_d(n+1)(n+2)(n+3)(n+4)^{\frac{5}{2}}\langle n,0|n,0\rangle \\
&=v^2E_d(n+1)(n+2)(n+3)(n+4)^{\frac{5}{2}}
\end{aligned} \tag{4.39}$$

$$\langle n,0|va_ia_ia_i^+a_i^+E_da_{jd}^+a_{jd}ua_ia_i|n,0\rangle=0 \tag{4.40}$$

$$\langle n,0|va_ia_ia_i^+a_i^+E_da_{jd}^+a_{jd}ua_j^+a_j^+|n,0\rangle=0 \tag{4.41}$$

$$\begin{aligned}
&\langle n,0|va_ia_ia_i^+a_i^+E_da_{jd}^+a_{jd}a_ia_iva_i^+a_i^+|n,0\rangle \\
&=v^2E_d(n+1)^{\frac{1}{2}}\langle n,0|a_ia_ia_i^+a_i^+a_{jd}^+a_{jd}a_ia_ia_i^+|(n+1),0\rangle \\
&=v^2E_d(n+1)^{\frac{1}{2}}(n+2)^{\frac{1}{2}}\langle n,0|a_ia_ia_i^+a_i^+a_{jd}^+a_{jd}a_ia_ia|(n+2),0\rangle \\
&=v^2E_d(n+1)^{\frac{1}{2}}(n+2)\langle n,0|a_ia_ia_i^+a_i^+a_{jd}^+a_{jd}a_ia_i|(n+1),0\rangle \\
&=v^2E_d(n+1)(n+2)\langle n,0|a_ia_ia_i^+a_i^+a_{jd}^+a_{jd}a_i|n,0\rangle \\
&=v^2E_dn^{\frac{1}{2}}(n+1)(n+2)\langle n,0|a_ia_ia_i^+a_i^+a_{jd}^+a_{jd}|(n-1),0\rangle \\
&=v^2E_d(n-1)^{\frac{1}{2}}n^{\frac{1}{2}}(n+1)(n+2)\langle n,0|a_ia_ia_i^+a_i^+a_{jd}^+|(n-2),0\rangle \\
&=v^2E_d(n-1)n^{\frac{1}{2}}(n+1)(n+2)\langle n,0|a_ia_ia_i^+a_i^+|(n-1),0\rangle \\
&=v^2E_d(n-1)n(n+1)(n+2)\langle n,0|a_ia_ia_i^+|n,0\rangle \\
&=v^2E_d(n-1)n(n+1)^{\frac{3}{2}}(n+2)\langle n,0|a_ia_i|(n+1),0\rangle \\
&=v^2E_d(n-1)n(n+1)^2(n+2)\langle n,0|a_i|(n+1),0\rangle \\
&=v^2E_d(n-1)n(n+1)^{\frac{5}{2}}(n+2)\langle n,0|n,0\rangle \\
&=v^2E_d(n-1)n(n+1)^{\frac{5}{2}}(n+2)
\end{aligned} \tag{4.42}$$

$$\langle n,0|va_ia_ia_i^+a_i^+E_da_{jd}^+a_{jd}a_j^+a_j^+va_i^+a_i^+|n,0\rangle=0 \tag{4.43}$$

The sum of eqs. (4.25), (4.28), (4.35), (4.39) and (4.42) gives,

$$\left\{\begin{aligned}
&u^2(n+1)(n+2)^2+u^2n(n-1)(n-2)+v^2(n+1)(n+2)(n+3)(n+4)^2 \\
&+v^2(n+1)(n+2)(n+3)(n+4)^{\frac{5}{2}}+v^2(n-1)n(n+1)^{\frac{5}{2}}(n+2)
\end{aligned}\right\}E_d \tag{4.44}$$

The terms containing t_{pd} were obtained by expanding the third term in eqn. (4.44) as follows:

$$\langle n,0|\left(u+va_i a_i\right)\left(a_j a_j+a_i^+ a_i^+\right)(t_{pd}a_{ip}^+ a_{jd}+t_{pd}a_{jd}^+ a_{ip})(a_i a_i+a_j^+ a_j^+)(u+va_i^+ a_i^+|n,0\rangle$$

$$=\langle n,0|\left(ua_j a_j+ua_i^+ a_i^++va_i a_i a_j a_j+va_i a_i a_i^+ a_i^+\right)(t_{pd}a_{ip}^+ a_{jd}+t_{pd}a_{jd}^+ a_{ip})(a_i a_i+a_j^+ a_j^+)(u+va_i^+ a_i^+|n,0\rangle$$

$$=\langle n,0|\begin{pmatrix} ua_j a_j t_{pd}a_{ip}^+ a_{jd}+ua_i^+ a_i^+ t_{pd}a_{ip}^+ a_{jd}+va_i a_i a_j a_j t_{pd}a_{ip}^+ a_{jd} \\ +va_i a_i a_i^+ a_i^+ t_{pd}a_{ip}^+ a_{jd}+ua_j a_j t_{pd}a_{jd}^+ a_{ip}+ua_i^+ a_i^+ t_{pd}a_{jd}^+ a_{ip} \\ +va_i a_i a_j a_j t_{pd}a_{jd}^+ a_{ip}+va_i a_i a_i^+ a_i^+ t_{pd}a_{jd}^+ a_{ip} \end{pmatrix}(a_i a_i+a_j^+ a_j^+)(u+va_i^+ a_i^+|n,0\rangle$$

$$=\langle n,0|\begin{pmatrix} ua_j a_j t_{pd}a_{ip}^+ a_{jd}a_i a_i+ua_i^+ a_i^+ t_{pd}a_{ip}^+ a_{jd}a_i a_i+va_i a_i a_j a_j t_{pd}a_{ip}^+ a_{jd}a_i a_i \\ +va_i a_i a_i^+ a_i^+ t_{pd}a_{ip}^+ a_{jd}a_i a_i+ua_j a_j t_{pd}a_{jd}^+ a_{ip}a_i a_i+ua_i^+ a_i^+ t_{pd}a_{jd}^+ a_{ip}a_i a_i \\ +va_i a_i a_j a_j t_{pd}a_{jd}^+ a_{ip}a_i a_i+va_i a_i a_i^+ a_i^+ t_{pd}a_{jd}^+ a_{ip}a_i a_i+ua_j a_j t_{pd}a_{ip}^+ a_{jd}a_j^+ a_j^+ \\ +ua_i^+ a_i^+ t_{pd}a_{ip}^+ a_{jd}a_j^+ a_j^++va_i a_i a_j a_j t_{pd}a_{ip}^+ a_{jd}a_j^+ a_j^++va_i a_i a_i^+ a_i^+ t_{pd}a_{ip}^+ a_{jd}a_j^+ a_j^+ \\ +ua_j a_j t_{pd}a_{jd}^+ a_{ip}a_j^+ a_j^++ua_i^+ a_i^+ t_{pd}a_{jd}^+ a_{ip}a_j^+ a_j^++va_i a_i a_j a_j t_{pd}a_{jd}^+ a_{ip}a_j^+ a_j^+ \\ +va_i a_i a_i^+ a_i^+ t_{pd}a_{jd}^+ a_{ip}a_j^+ a_j^+ \end{pmatrix}(u+va_i^+ a_i^+|n,0\rangle$$

$$=\langle n,0|\begin{pmatrix} ua_j a_j t_{pd}a_{ip}^+ a_{jd}a_i a_i u+ua_i^+ a_i^+ t_{pd}a_{ip}^+ a_{jd}a_i a_i u+va_i a_i a_j a_j t_{pd}a_{ip}^+ a_{jd}a_i a_i u \\ +va_i a_i a_i^+ a_i^+ t_{pd}a_{ip}^+ a_{jd}a_i a_i u+ua_j a_j t_{pd}a_{jd}^+ a_{ip}a_i a_i u+ua_i^+ a_i^+ t_{pd}a_{jd}^+ a_{ip}a_i a_i u \\ +va_i a_i a_j a_j t_{pd}a_{jd}^+ a_{ip}a_i a_i u+va_i a_i a_i^+ a_i^+ t_{pd}a_{jd}^+ a_{ip}a_i a_i u+ua_j a_j t_{pd}a_{ip}^+ a_{jd}a_j^+ a_j^+ u \\ +ua_i^+ a_i^+ t_{pd}a_{ip}^+ a_{jd}a_j^+ a_j^+ u+va_i a_i a_j a_j t_{pd}a_{ip}^+ a_{jd}a_j^+ a_j^+ u+va_i a_i a_i^+ a_i^+ t_{pd}a_{ip}^+ a_{jd}a_j^+ a_j^+ u \\ +ua_j a_j t_{pd}a_{jd}^+ a_{ip}a_j^+ a_j^+ u+ua_i^+ a_i^+ t_{pd}a_{jd}^+ a_{ip}a_j^+ a_j^+ u+va_i a_i a_j a_j t_{pd}a_{jd}^+ a_{ip}a_j^+ a_j^+ u \\ +va_i a_i a_i^+ a_i^+ t_{pd}a_{jd}^+ a_{ip}a_j^+ a_j^+ u+ua_j a_j t_{pd}a_{ip}^+ a_{jd}a_i a_i va_i^+ a_i^++ua_i^+ a_i^+ t_{pd}a_{ip}^+ a_{jd}a_i a_i va_i^+ a_i^+ \\ +va_i a_i a_j a_j t_{pd}a_{ip}^+ a_{jd}a_i a_i va_i^+ a_i^++va_i a_i a_i^+ a_i^+ t_{pd}a_{ip}^+ a_{jd}a_i a_i va_i^+ a_i^++ua_j a_j t_{pd}a_{jd}^+ a_{ip}a_i a_i va_i^+ a_i^+ \\ +ua_i^+ a_i^+ t_{pd}a_{jd}^+ a_{ip}a_i a_i va_i^+ a_i^++va_i a_i a_j a_j t_{pd}a_{jd}^+ a_{ip}a_i a_i va_i^+ a_i^++va_i a_i a_i^+ a_i^+ t_{pd}a_{jd}^+ a_{ip}a_i a_i va_i^+ a_i^+ \\ +ua_j a_j t_{pd}a_{ip}^+ a_{jd}a_j^+ a_j^+ va_i^+ a_i^++ua_i^+ a_i^+ t_{pd}a_{ip}^+ a_{jd}a_j^+ a_j^+ va_i^+ a_i^++va_i a_i a_j a_j t_{pd}a_{ip}^+ a_{jd}a_j^+ a_j^+ va_i^+ a_i^+ \\ +va_i a_i a_i^+ a_i^+ t_{pd}a_{ip}^+ a_{jd}a_j^+ a_j^+ va_i^+ a_i^++ua_j a_j t_{pd}a_{jd}^+ a_{ip}a_j^+ a_j^+ va_i^+ a_i^++ua_i^+ a_i^+ t_{pd}a_{jd}^+ a_{ip}a_j^+ a_j^+ va_i^+ a_i^+ \\ +va_i a_i a_j a_j t_{pd}a_{jd}^+ a_{ip}a_j^+ a_j^+ va_i^+ a_i^++va_i a_i a_i^+ a_i^+ t_{pd}a_{jd}^+ a_{ip}a_j^+ a_j^+ va_i^+ a_i^+ \end{pmatrix}|n,0\rangle$$

(4.45)

Applying the properties of creation and annihilation operators to eq. (4.45), one obtains the following;

$$\langle n,0|ua_j a_j t_{pd}a_{ip}^+ a_{jd}a_i a_i u|n,0\rangle=0 \tag{4.46}$$

$$\langle n,0|ua_i^+a_i^+t_{pd}a_{ip}^+a_{jd}a_ia_iu|n,0\rangle = u^2t_{pd}n^{\frac{1}{2}}\langle n,0|a_i^+a_i^+a_{ip}^+a_{jd}a_i|(n-1),0\rangle$$
$$= u^2t_{pd}n^{\frac{1}{2}}(n-1)^{\frac{1}{2}}\langle n,0|a_i^+a_i^+a_{ip}^+a_{jd}|(n-2),0\rangle$$
$$= u^2t_{pd}n^{\frac{1}{2}}(n-1)^{\frac{1}{2}}(n-2)^{\frac{1}{2}}\langle n,0|a_i^+a_i^+a_{ip}^+|(n-3),0\rangle$$
$$= u^2t_{pd}n^{\frac{1}{2}}(n-1)^{\frac{1}{2}}(n-2)\langle n,0|a_i^+a_i^+|(n-2),0\rangle$$
$$= u^2t_{pd}n^{\frac{1}{2}}(n-1)(n-2)\langle n,0|a_i^+|(n-1),0\rangle$$
$$= u^2t_{pd}n(n-1)(n-2)\langle n,0|n,0\rangle = u^2t_{pd}n(n-1)(n-2)$$

(4.47)

$$\langle n,0|va_ia_ia_ja_jt_{pd}a_{ip}^+a_{jd}a_ia_iu|n,0\rangle = 0 \tag{4.48}$$

$$\langle n,0|va_ia_ia_i^+a_i^+t_{pd}a_{ip}^+a_{jd}a_ia_iu|n,0\rangle = 0 \tag{4.49}$$

$$\langle n,0|ua_ja_jt_{pd}a_{jd}^+a_{ip}a_ia_iu|n,0\rangle = 0 \tag{4.50}$$

$$\langle n,0|ua_i^+a_i^+t_{pd}a_{jd}^+a_{ip}a_ia_iu|n,0\rangle$$
$$= u^2t_{pd}n^{\frac{1}{2}}\langle n,0|a_i^+a_i^+a_{jd}^+a_{ip}a_i|(n-1),0\rangle$$
$$= u^2t_{pd}n^{\frac{1}{2}}(n-1)^{\frac{1}{2}}\langle n,0|a_i^+a_i^+a_{jd}^+a_{ip}|(n-2),0\rangle$$
$$= u^2t_{pd}n^{\frac{1}{2}}(n-1)^{\frac{1}{2}}(n-2)^{\frac{1}{2}}\langle n,0|a_i^+a_i^+a_{jd}^+|(n-3),0\rangle$$
$$= u^2t_{pd}n^{\frac{1}{2}}(n-1)^{\frac{1}{2}}(n-2)\langle n,0|a_i^+a_i^+|(n-2),0\rangle$$
$$= u^2t_{pd}n^{\frac{1}{2}}(n-1)(n-2)\langle n,0|a_i^+|(n-1),0\rangle$$
$$= u^2t_{pd}n(n-1)(n-2)\langle n,0|n,0\rangle = u^2t_{pd}n(n-1)(n-2)$$

(4.51)

$$\langle n,0|va_ia_ia_i^+a_i^+t_{pd}a_{jd}^+a_{ip}a_ia_iu|n,0\rangle = 0 \tag{4.52}$$

$$\begin{aligned}
&\langle n,0|ua_j a_j t_{pd} a_{ip}^+ a_{jd} a_j^+ a_j^+ u|n,0\rangle = u^2 t_{pd} (n+1)^{\frac{1}{2}} \langle n,0|a_j a_j a_{ip}^+ a_{jd} a_j^+ |(n+1),0\rangle \\
&= u^2 t_{pd} (n+1)^{\frac{1}{2}} (n+2)^{\frac{1}{2}} \langle n,0|a_j a_j a_{ip}^+ a_{jd} |(n+2),0\rangle \\
&= u^2 t_{pd} (n+1)^{\frac{1}{2}} (n+2) \langle n,0|a_j a_j a_{ip}^+ |(n+1),0\rangle \\
&= u^2 t_{pd} (n+1)^{\frac{1}{2}} (n+2)^{\frac{3}{2}} \langle n,0|a_j a_j |(n+2),0\rangle \\
&= u^2 t_{pd} (n+1)^{\frac{1}{2}} (n+2)^2 \langle n,0|a_j |(n+1),0\rangle \\
&= u^2 t_{pd} (n+1)(n+2)^2 \langle n,0|n,0\rangle = u^2 t_{pd} (n+1)(n+2)^2
\end{aligned} \tag{4.53}$$

$$\langle n,0|ua_i^+ a_i^+ t_{pd} a_{ip}^+ a_{jd} a_j^+ a_j^+ u|n,0\rangle = 0 \tag{4.54}$$

$$\langle n,0|va_i a_i a_j a_j t_{pd} a_{ip}^+ a_{jd} a_j^+ a_j^+ u|n,0\rangle = 0 \tag{4.55}$$

$$\langle n,0|va_i a_i a_i^+ a_i^+ t_{pd} a_{ip}^+ a_{jd} a_j^+ a_j^+ u|n,0\rangle = 0 \tag{4.56}$$

$$\begin{aligned}
&\langle n,0|ua_j a_j t_{pd} a_{jd}^+ a_{ip} a_j^+ a_j^+ u|n,0\rangle \\
&= u^2 t_{pd} (n+1)^{\frac{1}{2}} \langle n,0|a_j a_j a_{jd}^+ a_{ip} a_j^+ |(n+1),0\rangle \\
&= u^2 t_{pd} (n+1)^{\frac{1}{2}} (n+2)^{\frac{1}{2}} \langle n,0|a_j a_j a_{jd}^+ a_{ip} |(n+2),0\rangle \\
&= u^2 t_{pd} (n+1)^{\frac{1}{2}} (n+2) \langle n,0|a_j a_j a_{jd}^+ |(n+1),0\rangle \\
&= u^2 t_{pd} (n+1)^{\frac{1}{2}} (n+2)^{\frac{3}{2}} \langle n,0|a_j a_j |(n+2),0\rangle \\
&= u^2 t_{pd} (n+1)^{\frac{1}{2}} (n+2)^2 \langle n,0|a_j |(n+1),0\rangle \\
&= u^2 t_{pd} (n+1)(n+2)^2 \langle n,0|n,0\rangle = u^2 t_{pd} (n+1)(n+2)^2
\end{aligned} \tag{4.57}$$

$$\langle n,0|ua_i^+ a_i^+ t_{pd} a_{jd}^+ a_{ip} a_j^+ a_j^+ u|n,0\rangle = 0 \tag{4.58}$$

$$\langle n,0|va_i a_i a_j a_j t_{pd} a_{jd}^+ a_{ip} a_j^+ a_j^+ u|n,0\rangle = 0 \tag{4.59}$$

$$\langle n,0|va_i a_i a_i^+ a_i^+ t_{pd} a_{jd}^+ a_{ip} a_j^+ a_j^+ u|n,0\rangle = 0 \tag{4.60}$$

$$\langle n,0|ua_j a_j t_{pd} a_{ip}^+ a_{jd} a_i a_i v a_i^+ a_i^+ |n,0\rangle = 0 \tag{4.61}$$

$$\langle n,0|ua_i^+a_i^+t_{pd}a_{ip}^+a_{jd}a_ia_iva_i^+a_i^+|n,0\rangle=0 \tag{4.62}$$

$$\langle n,0|va_ia_ia_ja_jt_{pd}a_{ip}^+a_{jd}a_ia_iva_i^+a_i^+|n,0\rangle=0 \tag{4.63}$$

$$\begin{aligned}
&\langle n,0|va_ia_ia_i^+a_i^+t_{pd}a_{ip}^+a_{jd}a_ia_iva_i^+a_i^+|n,0\rangle\\
&=uvt_{pd}(n+1)^{\frac{1}{2}}\langle n,0|a_ia_ia_i^+a_i^+a_{ip}^+a_{jd}a_ia_ia_i^+|(n+1),0\rangle\\
&=uvt_{pd}(n+1)^{\frac{1}{2}}(n+2)^{\frac{1}{2}}\langle n,0|a_ia_ia_i^+a_i^+a_{ip}^+a_{jd}a_ia_i|(n+2),0\rangle\\
&=uvt_{pd}(n+1)^{\frac{1}{2}}(n+2)\langle n,0|a_ia_ia_i^+a_i^+a_{ip}^+a_{jd}a_i|(n+1),0\rangle\\
&=uvt_{pd}(n+1)(n+2)\langle n,0|a_ia_ia_i^+a_i^+a_{ip}^+a_{jd}|n,0\rangle\\
&=uvt_{pd}n^{\frac{1}{2}}(n+1)(n+2)\langle n,0|a_ia_ia_i^+a_i^+a_{ip}^+|(n-1),0\rangle\\
&=uvt_{pd}n(n+1)(n+2)\langle n,0|a_ia_ia_i^+a_i^+|n,0\rangle\\
&=uvt_{pd}n(n+1)^{\frac{3}{2}}(n+2)\langle n,0|a_ia_ia_i^+|(n+1),0\rangle\\
&=uvt_{pd}n(n+1)^{\frac{3}{2}}(n+2)^{\frac{3}{2}}\langle n,0|a_ia_i|(n+2),0\rangle\\
&=uvt_{pd}n(n+1)^{\frac{3}{2}}(n+2)^2\langle n,0|a_i|(n+1),0\rangle\\
&=uvt_{pd}n(n+1)^2(n+2)^2\langle n,0|n,0\rangle=uvt_{pd}n(n+1)^2(n+2)^2
\end{aligned} \tag{4.64}$$

$$\langle n,0|ua_ja_jt_{pd}a_{jd}^+a_{ip}a_ia_iva_i^+a_i^+|n,0\rangle=0 \tag{4.65}$$

$$\langle n,0|ua_i^+a_i^+t_{pd}a_{jd}^+a_{ip}a_ia_iva_i^+a_i^+|n,0\rangle=0 \tag{4.66}$$

$$\langle n,0|va_ia_ia_ja_jt_{pd}a_{jd}^+a_{ip}a_ia_iva_i^+a_i^+|n,0\rangle=0 \tag{4.67}$$

$$\begin{aligned}
&\langle n,0|va_i a_i a_i^+ a_i^+ t_{pd} a_{jd}^+ a_{ip} a_i a_i v a_i^+ a_i^+ |n,0\rangle \\
&= v^2 t_{pd} (n+1)^{\frac{1}{2}} \langle n,0|a_i a_i a_i^+ a_i^+ a_{jd}^+ a_{ip} a_i a_i a_i^+ |(n+1),0\rangle \\
&= v^2 t_{pd} (n+1)^{\frac{1}{2}} (n+2)^{\frac{1}{2}} \langle n,0|a_i a_i a_i^+ a_i^+ a_{jd}^+ a_{ip} a_i a_i |(n+2),0\rangle \\
&= v^2 t_{pd} (n+1)^{\frac{1}{2}} (n+2) \langle n,0|a_i a_i a_i^+ a_i^+ a_{jd}^+ a_{ip} a_i |(n+1),0\rangle \\
&= v^2 t_{pd} (n+1)(n+2) \langle n,0|a_i a_i a_i^+ a_i^+ a_{jd}^+ a_{ip} |n,0\rangle \\
&= v^2 t_{pd} n^{\frac{1}{2}} (n+1)(n+2) \langle n,0|a_i a_i a_i^+ a_i^+ a_{jd}^+ |(n-1),0\rangle \\
&= v^2 t_{pd} n (n+1)^{\frac{3}{2}} (n+2) \langle n,0|a_i a_i a_i^+ a_i^+ |n,0\rangle \\
&= v^2 t_{pd} n (n+1)^2 (n+2) \langle n,0|a_i a_i a_i^+ |(n+1),0\rangle \\
&= v^2 t_{pd} n (n+1)^2 (n+2)^{\frac{3}{2}} \langle n,0|a_i a_i |(n+2),0\rangle \\
&= v^2 t_{pd} n (n+1)^2 (n+2)^2 \langle n,0|a_i |(n+1),0\rangle \\
&= v^2 t_{pd} n (n+1)^{\frac{5}{2}} (n+2)^2 \langle n,0|n,0\rangle = v^2 t_{pd} n (n+1)^{\frac{5}{2}} (n+2)^2
\end{aligned} \tag{4.68}$$

$$\langle n,0|ua_j a_j t_{pd} a_{ip}^+ a_{jd} a_j^+ a_j^+ v a_i^+ a_i^+ |n,0\rangle = 0 \tag{4.69}$$

$$\langle n,0|ua_i^+ a_i^+ t_{pd} a_{ip}^+ a_{jd} a_j^+ a_j^+ v a_i^+ a_i^+ |n,0\rangle = 0 \tag{4.70}$$

$$
\begin{aligned}
&\langle n,0|va_ia_ia_ja_jt_{pd}a_{ip}^{+}a_{jd}a_j^{+}a_j^{+}va_i^{+}a_i^{+}|n,0\rangle \\
&=v^{\frac{1}{2}}t_{pd}(n+1)^{\frac{1}{2}}\langle n,0|a_ia_ia_ja_ja_{ip}^{+}a_{jd}a_j^{+}a_j^{+}a_i^{+}|(n+1),0\rangle \\
&=v^{\frac{1}{2}}t_{pd}(n+1)^{\frac{1}{2}}(n+2)^{\frac{1}{2}}\langle n,0|a_ia_ia_ja_ja_{ip}^{+}a_{jd}a_j^{+}a_j^{+}|(n+2),0\rangle \\
&=v^{\frac{1}{2}}t_{pd}(n+1)^{\frac{1}{2}}(n+2)^{\frac{1}{2}}(n+3)^{\frac{1}{2}}\langle n,0|a_ia_ia_ja_ja_{ip}^{+}a_{jd}a_j^{+}|(n+3),0\rangle \\
&=v^{\frac{1}{2}}t_{pd}(n+1)^{\frac{1}{2}}(n+2)^{\frac{1}{2}}(n+3)^{\frac{1}{2}}(n+4)^{\frac{1}{2}}\langle n,0|a_ia_ia_ja_ja_{ip}^{+}a_{jd}|(n+4),0\rangle \\
&=v^{\frac{1}{2}}t_{pd}(n+1)^{\frac{1}{2}}(n+2)^{\frac{1}{2}}(n+3)^{\frac{1}{2}}(n+4)\langle n,0|a_ia_ia_ja_ja_{ip}^{+}|(n+3),0\rangle \\
&=v^{\frac{1}{2}}t_{pd}(n+1)^{\frac{1}{2}}(n+2)^{\frac{1}{2}}(n+3)^{\frac{1}{2}}(n+4)^{\frac{3}{2}}\langle n,0|a_ia_ia_ja_j|(n+4),0\rangle \\
&=v^{\frac{1}{2}}t_{pd}(n+1)^{\frac{1}{2}}(n+2)^{\frac{1}{2}}(n+3)^{\frac{1}{2}}(n+4)^{2}\langle n,0|a_ia_ia_j|(n+3),0\rangle \\
&=v^{\frac{1}{2}}t_{pd}(n+1)^{\frac{1}{2}}(n+2)^{\frac{1}{2}}(n+3)(n+4)^{2}\langle n,0|a_ia_i|(n+2),0\rangle \\
&=v^{\frac{1}{2}}t_{pd}(n+1)^{\frac{1}{2}}(n+2)(n+3)(n+4)^{2}\langle n,0|a_i|(n+1),0\rangle \\
&=v^{\frac{1}{2}}t_{pd}(n+1)(n+2)(n+3)(n+4)^{2}\langle n,0|n,0\rangle \\
&=v^{\frac{1}{2}}t_{pd}(n+1)(n+2)(n+3)(n+4)^{2}
\end{aligned}
\tag{4.71}
$$

$$\langle n,0|va_ia_ia_i^{+}a_i^{+}t_{pd}a_{ip}^{+}a_{jd}a_j^{+}a_j^{+}va_i^{+}a_i^{+}|n,0\rangle=0 \tag{4.72}$$

$$\langle n,0|ua_ja_jt_{pd}a_{jd}^{+}a_{ip}a_j^{+}a_j^{+}va_i^{+}a_i^{+}|n,0\rangle=0 \tag{4.73}$$

$$\langle n,0|ua_i^{+}a_i^{+}t_{pd}a_{jd}^{+}a_{ip}a_j^{+}a_j^{+}va_i^{+}a_i^{+}|n,0\rangle=0 \tag{4.74}$$

$$
\begin{aligned}
&\langle n,0|va_i a_i a_j a_j t_{pd} a_{jd}^+ a_{ip} a_j^+ a_j^+ va_i^+ a_i^+ |n,0\rangle \\
&= v^2 t_{pd} (n+1)^{\frac{1}{2}} \langle n,0|a_i a_i a_j a_j a_{jd}^+ a_{ip} a_j^+ a_j^+ a_i^+ |(n+1),0\rangle \\
&= v^2 t_{pd} (n+1)^{\frac{1}{2}} (n+2)^{\frac{1}{2}} \langle n,0|a_i a_i a_j a_j a_{jd}^+ a_{ip} a_j^+ a_j^+ |(n+2),0\rangle \\
&= v^2 t_{pd} (n+1)^{\frac{1}{2}} (n+2)^{\frac{1}{2}} (n+3)^{\frac{1}{2}} \langle n,0|a_i a_i a_j a_j a_{jd}^+ a_{ip} a_j^+ |(n+3),0\rangle \\
&= v^2 t_{pd} (n+1)^{\frac{1}{2}} (n+2)^{\frac{1}{2}} (n+3)^{\frac{1}{2}} (n+4)^{\frac{1}{2}} \langle n,0|a_i a_i a_j a_j a_{jd}^+ a_{ip} |(n+4),0\rangle \\
&= v^2 t_{pd} (n+1)^{\frac{1}{2}} (n+2)^{\frac{1}{2}} (n+3)^{\frac{1}{2}} (n+4) \langle n,0|a_i a_i a_j a_j a_{jd}^+ |(n+3),0\rangle \\
&= v^2 t_{pd} (n+1)^{\frac{1}{2}} (n+2)^{\frac{1}{2}} (n+3)^{\frac{1}{2}} (n+4)^{\frac{3}{2}} \langle n,0|a_i a_i a_j a_j |(n+4),0\rangle \\
&= v^2 t_{pd} (n+1)^{\frac{1}{2}} (n+2)^{\frac{1}{2}} (n+3)^{\frac{1}{2}} (n+4)^2 \langle n,0|a_i a_i a_j |(n+3),0\rangle \\
&= v^2 t_{pd} (n+1)^{\frac{1}{2}} (n+2)^{\frac{1}{2}} (n+3)(n+4)^2 \langle n,0|a_i a_i |(n+2),0\rangle \\
&= v^2 t_{pd} (n+1)^{\frac{1}{2}} (n+2)(n+3)(n+4)^2 \langle n,0|a_i |(n+1),0\rangle \\
&= v^2 t_{pd} (n+1)(n+2)(n+3)(n+4)^2 \langle n,0|n,0\rangle \\
&= v^2 t_{pd} (n+1)(n+2)(n+3)(n+4)^2
\end{aligned}
\tag{4.75}
$$

$$
\langle n,0|va_i a_i a_i^+ a_i^+ t_{pd} a_{jd}^+ a_{ip} a_j^+ a_j^+ va_i^+ a_i^+ |n,0\rangle = 0 \tag{4.76}
$$

The sum of eq. (4.47), (4.51), (4.53), (4.57), (4.64), (4.68), (4.71) and (4.75) gives

$$
\left\{
\begin{aligned}
&u^2 t_{pd} n(n-1)(n-2) + u^2 t_{pd} n(n-1)(n-2) \\
&+u^2 (n+1)(n+2)^2 + u^2 (n+1)(n+2)^2 \\
&+uvn(n+1)^2 (n+2)^2 + v^2 n(n+1)^{\frac{5}{2}} (n+2)^2 \\
&+v^{\frac{1}{2}} (n+1)(n+2)(n+3)(n+4)^2 \\
&+v^2 (n+1)(n+2)(n+3)(n+4)^2
\end{aligned}
\right\} t_{pd}
\tag{4.77}
$$

From eq. (4.4), the terms in u_d were determined as follows;

$$\begin{aligned}
&\langle n,0|\left(u+va_ia_i\right)\left(a_ja_j+a_i^+a_i^+\right)(u_da_{jd}^+a_{jd}^+a_{ip}a_{ip})(a_ia_i+a_j^+a_j^+)(u+va_i^+a_i^+)|n,0\rangle \\
&=\langle n,0|\left\{\begin{matrix}\left(ua_ja_j+ua_i^+a_i^++va_ia_ia_ja_j+va_ia_ia_i^+a_i^+\right)\\(u_da_{jd}^+a_{jd}^+a_{ip}a_{ip})(a_ia_i+a_j^+a_j^+)(u+va_i^+a_i^+)\end{matrix}\right\}|n,0\rangle \\
&=\langle n,0|\left\{\begin{matrix}\left(\begin{matrix}ua_ja_ju_da_{jd}^+a_{jd}^+a_{ip}a_{ip}+ua_i^+a_i^+u_da_{jd}^+a_{jd}^+a_{ip}a_{ip}\\+va_ia_ia_ja_ju_da_{jd}^+a_{jd}^+a_{ip}a_{ip}+va_ia_ia_i^+a_i^+u_da_{jd}^+a_{jd}^+a_{ip}a_{ip}\end{matrix}\right)\\(u_da_{jd}^+a_{jd}^+a_{ip}a_{ip})(a_ia_i+a_j^+a_j^+)(u+va_i^+a_i^+)\end{matrix}\right\}|n,0\rangle \\
&=\langle n,0|\left\{\begin{matrix}\left(\begin{matrix}ua_ja_ju_da_{jd}^+a_{jd}^+a_{ip}a_{ip}+ua_i^+a_i^+u_da_{jd}^+a_{jd}^+a_{ip}a_{ip}\\+va_ia_ia_ja_ju_da_{jd}^+a_{jd}^+a_{ip}a_{ip}+va_ia_ia_i^+a_i^+u_da_{jd}^+a_{jd}^+a_{ip}a_{ip}\end{matrix}\right)\\(a_ia_iu+a_j^+a_j^+u+a_ia_iva_i^+a_i^++a_j^+a_j^+va_i^+a_i^+)\end{matrix}\right\}|n,0\rangle \\
&=\langle n,0|\left\{\begin{matrix}ua_ja_ju_da_{jd}^+a_{jd}^+a_{ip}a_{ip}a_ia_iu+ua_i^+a_i^+u_da_{jd}^+a_{jd}^+a_{ip}a_{ip}a_ia_iu\\+va_ia_ia_ja_ju_da_{jd}^+a_{jd}^+a_{ip}a_{ip}a_ia_iu+va_ia_ia_i^+a_i^+u_da_{jd}^+a_{jd}^+a_{ip}a_{ip}a_ia_iu\\+ua_ja_ju_da_{jd}^+a_{jd}^+a_{ip}a_{ip}a_j^+a_j^+u+ua_i^+a_i^+u_da_{jd}^+a_{jd}^+a_{ip}a_{ip}a_j^+a_j^+u\\+va_ia_ia_ja_ju_da_{jd}^+a_{jd}^+a_{ip}a_{ip}a_j^+a_j^+u+va_ia_ia_i^+a_i^+u_da_{jd}^+a_{jd}^+a_{ip}a_{ip}a_j^+a_j^+u\\+ua_ja_ju_da_{jd}^+a_{jd}^+a_{ip}a_{ip}a_ia_iva_i^+a_i^++ua_i^+a_i^+u_da_{jd}^+a_{jd}^+a_{ip}a_{ip}a_ia_iva_i^+a_i^+\\+va_ia_ia_ja_ju_da_{jd}^+a_{jd}^+a_{ip}a_{ip}a_ia_iva_i^+a_i^++va_ia_ia_i^+a_i^+u_da_{jd}^+a_{jd}^+a_{ip}a_{ip}a_ia_iva_i^+a_i^+\\+ua_ja_ju_da_{jd}^+a_{jd}^+a_{ip}a_{ip}a_j^+a_j^+va_i^+a_i^++ua_i^+a_i^+u_da_{jd}^+a_{jd}^+a_{ip}a_{ip}a_j^+a_j^+va_i^+a_i^+\\+va_ia_ia_ja_ju_da_{jd}^+a_{jd}^+a_{ip}a_{ip}a_j^+a_j^+va_i^+a_i^++va_ia_ia_i^+a_i^+u_da_{jd}^+a_{jd}^+a_{ip}a_{ip}a_j^+a_j^+va_i^+a_i^+\end{matrix}\right\}|n,0\rangle
\end{aligned} \tag{4.78}$$

Applying properties of creation and annihilation operators to eq. (4.78), one obtains the following;

$$\langle n,0|ua_ja_ju_da_{jd}^+a_{jd}^+a_{ip}a_{ip}a_ia_iu|n,0\rangle=0 \tag{4.79}$$

$$\begin{aligned}
&\langle n,0|ua_i^+a_i^+u_da_{jd}^+a_{jd}^+a_{ip}a_{ip}a_ia_iu|n,0\rangle\\
&=u^{\frac{1}{2}}u_dn^{\frac{1}{2}}\langle n,0|a_i^+a_i^+a_{jd}^+a_{jd}^+a_{ip}a_{ip}a_i|(n-1),0\rangle\\
&=u^{\frac{1}{2}}u_dn^{\frac{1}{2}}\langle n,0|a_i^+a_i^+a_{jd}^+a_{jd}^+a_{ip}a_{ip}a_i|(n-1),0\rangle\\
&=u^{\frac{1}{2}}u_dn^{\frac{1}{2}}(n-1)^{\frac{1}{2}}\langle n,0|a_i^+a_i^+a_{jd}^+a_{jd}^+a_{ip}a_{ip}|(n-2),0\rangle\\
&=u^{\frac{1}{2}}u_dn^{\frac{1}{2}}(n-1)^{\frac{1}{2}}(n-2)^{\frac{1}{2}}\langle n,0|a_i^+a_i^+a_{jd}^+a_{jd}^+a_{ip}|(n-3),0\rangle\\
&=u^{\frac{1}{2}}u_dn^{\frac{1}{2}}(n-1)^{\frac{1}{2}}(n-2)^{\frac{1}{2}}(n-3)^{\frac{1}{2}}\langle n,0|a_i^+a_i^+a_{jd}^+a_{jd}^+|(n-4),0\rangle\\
&=u^{\frac{1}{2}}u_dn^{\frac{1}{2}}(n-1)^{\frac{1}{2}}(n-2)^{\frac{1}{2}}(n-3)\langle n,0|a_i^+a_i^+a_{jd}^+|(n-3),0\rangle\\
&=u^{\frac{1}{2}}u_dn^{\frac{1}{2}}(n-1)^{\frac{1}{2}}(n-2)(n-3)\langle n,0|a_i^+a_i^+|(n-2),0\rangle\\
&=u^{\frac{1}{2}}u_dn^{\frac{1}{2}}(n-1)(n-2)(n-3)\langle n,0|a_i^+|(n-1),0\rangle\\
&=u^{\frac{1}{2}}u_dn(n-1)(n-2)(n-3)\langle n,0|n,0\rangle=u^{\frac{1}{2}}u_dn(n-1)(n-2)(n-3)
\end{aligned} \tag{4.80}$$

$$\langle n,0|va_ia_ia_ja_ju_da_{jd}^+a_{jd}^+a_{ip}a_{ip}a_ia_iu|n,0\rangle=0 \tag{4.81}$$

$$\langle n,0|va_ia_ia_i^+a_i^+u_da_{jd}^+a_{jd}^+a_{ip}a_{ip}a_ia_iu|n,0\rangle=0 \tag{4.82}$$

$$\begin{aligned}
&\langle n,0|ua_ja_ju_da_{jd}^+a_{jd}^+a_{ip}a_{ip}a_j^+a_j^+u|n,0\rangle\\
&=u^2u_d(n+1)^{\frac{1}{2}}\langle n,0|a_ja_ja_{jd}^+a_{jd}^+a_{ip}a_{ip}a_j^+|(n+1),0\rangle\\
&=u^2u_d(n+1)^{\frac{1}{2}}(n+2)^{\frac{1}{2}}\langle n,0|a_ja_ja_{jd}^+a_{jd}^+a_{ip}a_{ip}|(n+2),0\rangle\\
&=u^2u_d(n+1)^{\frac{1}{2}}(n+2)\langle n,0|a_ja_ja_{jd}^+a_{jd}^+a_{ip}|(n+1),0\rangle\\
&=u^2u_d(n+1)(n+2)\langle n,0|a_ja_ja_{jd}^+a_{jd}^+|n,0\rangle\\
&=u^2u_d(n+1)^{\frac{3}{2}}(n+2)\langle n,0|a_ja_ja_{jd}^+|(n+1),0\rangle=u^2u_d(n+1)^{\frac{3}{2}}(n+2)^{\frac{3}{2}}\langle n,0|a_ja_j|(n+2),0\rangle\\
&=u^2u_d(n+1)^{\frac{3}{2}}(n+2)^2\langle n,0|a_j|(n+1),0\rangle=u^2u_d(n+1)^2(n+2)^2\langle n,0|n,0\rangle=u^2u_d(n+1)^2(n+2)^2
\end{aligned} \tag{4.83}$$

$$\langle n,0|ua_i^+a_i^+u_da_{jd}^+a_{jd}^+a_{ip}a_{ip}a_j^+a_j^+u|n,0\rangle=0 \tag{4.84}$$

$$\langle n,0|va_ia_ia_ja_ju_da_{jd}^+a_{jd}^+a_{ip}a_{ip}a_j^+a_j^+u|n,0\rangle=0 \tag{4.85}$$

$$\langle n,0|va_ia_ia_i^+a_i^+u_da_{jd}^+a_{jd}^+a_{ip}a_{ip}a_j^+a_j^+u|n,0\rangle=0 \tag{4.86}$$

$$\langle n,0|ua_ja_ju_da_{jd}^+a_{jd}^+a_{ip}a_{ip}a_ia_iva_i^+a_i^+|n,0\rangle=0 \tag{4.87}$$

$$\langle n,0|ua_i^+a_i^+u_da_{jd}^+a_{jd}^+a_{ip}a_{ip}a_ia_iva_i^+a_i^+|n,0\rangle=0 \tag{4.88}$$

$$\langle n,0|va_ia_ia_ja_ju_da_{jd}^+a_{jd}^+a_{ip}a_{ip}a_ia_iva_i^+a_i^+|n,0\rangle=0 \tag{4.89}$$

$$\begin{aligned}
&\langle n,0|va_ia_ia_i^+a_i^+u_da_{jd}^+a_{jd}^+a_{ip}a_{ip}a_ia_iva_i^+a_i^+|n,0\rangle\\
&=v^2u_d(n+1)^{\frac{1}{2}}\langle n,0|a_ia_ia_i^+a_i^+a_{jd}^+a_{jd}^+a_{ip}a_{ip}a_ia_ia_i^+|(n+1),0\rangle\\
&=v^2u_d(n+1)^{\frac{1}{2}}(n+2)^{\frac{1}{2}}\langle n,0|a_ia_ia_i^+a_i^+a_{jd}^+a_{jd}^+a_{ip}a_{ip}a_ia_i|(n+2),0\rangle\\
&=v^2u_d(n+1)^{\frac{1}{2}}(n+2)\langle n,0|a_ia_ia_i^+a_i^+a_{jd}^+a_{jd}^+a_{ip}a_{ip}a_i|(n+1),0\rangle\\
&=v^2u_d(n+1)(n+2)\langle n,0|a_ia_ia_i^+a_i^+a_{jd}^+a_{jd}^+a_{ip}a_{ip}|n,0\rangle\\
&=v^2u_dn^{\frac{1}{2}}(n+1)(n+2)\langle n,0|a_ia_ia_i^+a_i^+a_{jd}^+a_{jd}^+a_{ip}|(n-1),0\rangle\\
&=v^2u_d(n-1)^{\frac{1}{2}}n^{\frac{1}{2}}(n+1)(n+2)\langle n,0|a_ia_ia_i^+a_i^+a_{jd}^+a_{jd}^+|(n-2),0\rangle\\
&=v^2u_d(n-2)^{\frac{1}{2}}(n-1)n^{\frac{1}{2}}(n+1)(n+2)\langle n,0|a_ia_ia_i^+a_i^+a_{jd}^+|(n-1),0\rangle\\
&=v^2u_d(n-2)(n-1)n(n+1)(n+2)\langle n,0|a_ia_ia_i^+a_i^+|n,0\rangle\\
&=v^2u_d(n-2)(n-1)n(n+1)^{\frac{3}{2}}(n+2)\langle n,0|a_ia_ia_i^+|(n+1),0\rangle\\
&=v^2u_d(n-2)(n-1)n(n+1)^{\frac{3}{2}}(n+2)^{\frac{3}{2}}\langle n,0|a_ia_i|(n+2),0\rangle\\
&=v^2u_d(n-2)(n-1)n(n+1)^2(n+2)^{\frac{3}{2}}\langle n,0|a_i|(n+1),0\rangle\\
&=v^2u_d(n-2)(n-1)n(n+1)^{\frac{5}{2}}(n+2)^{\frac{3}{2}}\langle n,0|n,0\rangle\\
&=v^2u_d(n-2)(n-1)n(n+1)^{\frac{5}{2}}(n+2)^{\frac{3}{2}}
\end{aligned} \tag{4.90}$$

$$\langle n,0|ua_ja_ju_da_{jd}^+a_{jd}^+a_{ip}a_{ip}a_j^+a_j^+va_i^+a_i^+|n,0\rangle=0 \tag{4.91}$$

$$\langle n,0|ua_i^+a_i^+u_da_{jd}^+a_{jd}^+a_{ip}a_{ip}a_j^+a_j^+va_i^+a_i^+|n,0\rangle=0 \tag{4.92}$$

$$\begin{aligned}
&\langle n,0|va_ia_ia_ja_ju_da_{jd}^+a_{jd}^+a_{ip}a_{ip}a_j^+a_j^+va_i^+a_i^+|n,0\rangle\\
&=v^2u_d(n+1)^{\frac{1}{2}}\langle n,0|a_ia_ia_ja_ja_{jd}^+a_{jd}^+a_{ip}a_{ip}a_j^+a_j^+a_i^+|(n+1),0\rangle\\
&=v^2u_d(n+1)^{\frac{1}{2}}(n+2)^{\frac{1}{2}}\langle n,0|a_ia_ia_ja_ja_{jd}^+a_{jd}^+a_{ip}a_{ip}a_j^+a_j^+|(n+2),0\rangle\\
&=v^2u_d(n+1)^{\frac{1}{2}}(n+2)^{\frac{1}{2}}(n+3)^{\frac{1}{2}}\langle n,0|a_ia_ia_ja_ja_{jd}^+a_{jd}^+a_{ip}a_{ip}a_j^+|(n+3),0\rangle\\
&=v^2u_d(n+1)^{\frac{1}{2}}(n+2)^{\frac{1}{2}}(n+3)^{\frac{1}{2}}(n+4)^{\frac{1}{2}}\langle n,0|a_ia_ia_ja_ja_{jd}^+a_{jd}^+a_{ip}a_{ip}|(n+4),0\rangle\\
&=v^2u_d(n+1)^{\frac{1}{2}}(n+2)^{\frac{1}{2}}(n+3)^{\frac{1}{2}}(n+4)\langle n,0|a_ia_ia_ja_ja_{jd}^+a_{jd}^+a_{ip}|(n+3),0\rangle\\
&=v^2u_d(n+1)^{\frac{1}{2}}(n+2)^{\frac{1}{2}}(n+3)(n+4)\langle n,0|a_ia_ia_ja_ja_{jd}^+a_{jd}^+|(n+2),0\rangle\\
&=v^2u_d(n+1)^{\frac{1}{2}}(n+2)^{\frac{1}{2}}(n+3)^{\frac{3}{2}}(n+4)\langle n,0|a_ia_ia_ja_ja_{jd}^+|(n+3),0\rangle\\
&=v^2u_d(n+1)^{\frac{1}{2}}(n+2)^{\frac{1}{2}}(n+3)^{\frac{3}{2}}(n+4)^{\frac{3}{2}}\langle n,0|a_ia_ia_ja_j|(n+4),0\rangle\\
&=v^2u_d(n+1)^{\frac{1}{2}}(n+2)^{\frac{1}{2}}(n+3)^{\frac{3}{2}}(n+4)^2\langle n,0|a_ia_ia_j|(n+3),0\rangle\\
&=v^2u_d(n+1)^{\frac{1}{2}}(n+2)^{\frac{1}{2}}(n+3)^2(n+4)^2\langle n,0|a_ia_i|(n+2),0\rangle\\
&=v^2u_d(n+1)^{\frac{1}{2}}(n+2)(n+3)^2(n+4)^2\langle n,0|a_i|(n+1),0\rangle\\
&=v^2u_d(n+1)(n+2)(n+3)^2(n+4)^2\langle n,0|n,0\rangle\\
&=v^2u_d(n+1)(n+2)(n+3)^2(n+4)^2
\end{aligned} \tag{4.93}$$

$$\langle n,0|va_ia_ia_i^+a_i^+u_da_{jd}^+a_{jd}^+a_{ip}a_{ip}a_j^+a_j^+va_i^+a_i^+|n,0\rangle=0 \tag{4.94}$$

The sum of eq. (4.80), (4.83), (4.90) and (4.93), gives

$$\left\{\begin{aligned}
&u^{\frac{1}{2}}u_dn(n-1)(n-2)(n-3)+u^2u_d(n+1)^2(n+2)^2\\
&+v^2u_d(n-2)(n-1)n(n+1)^{\frac{5}{2}}(n+2)^{\frac{3}{2}}+v^2u_d(n+1)(n+2)(n+3)^2(n+4)^2
\end{aligned}\right\}u_d \tag{4.95}$$

From eq. (4.4), the terms in g_{ep} were determined as follows;

$$\begin{aligned}
&\langle n,0|(u+va_ia_i)\left(a_ja_j+a_i^+a_i^+\right)(g_{ep}a_{k\sigma}^+a_{k+X,\sigma}+g_{ep}a_{k+X,\sigma}^+a_{k\sigma})\\
&(a_ia_i+a_j^+a_j^+)(u+va_i^+a_i^+\,|n,0\rangle\\
&=\langle n,0|\left(ua_ja_j+va_ia_ia_ja_j+ua_i^+a_i^++va_ia_ia_i^+a_i^+\right)(g_{ep}a_{k\sigma}^+a_{k+X,\sigma}+g_{ep}a_{k+X,\sigma}^+a_{k\sigma})\\
&(a_ia_i+a_j^+a_j^+)(u+va_i^+a_i^+\,|n,0\rangle\\
&=\langle n,0|\begin{pmatrix}
ua_ja_jg_{ep}a_{k\sigma}^+a_{k+X,\sigma}a_ia_iu+va_ia_ia_ja_jg_{ep}a_{k\sigma}^+a_{k+X,\sigma}a_ia_iu\\
+ua_i^+a_i^+g_{ep}a_{k\sigma}^+a_{k+X,\sigma}a_ia_iu+va_ia_ia_i^+a_i^+g_{ep}a_{k\sigma}^+a_{k+X,\sigma}a_ia_iu\\
+ua_ja_jg_{ep}a_{k+X,\sigma}^+a_{k\sigma}a_ia_iu+va_ia_ia_ja_jg_{ep}a_{k+X,\sigma}^+a_{k\sigma}a_ia_iu\\
+ua_i^+a_i^+g_{ep}a_{k+X,\sigma}^+a_{k\sigma}a_ia_iu+va_ia_ia_i^+a_i^+g_{ep}a_{k+X,\sigma}^+a_{k\sigma}a_ia_iu\\
ua_ja_jg_{ep}a_{k\sigma}^+a_{k+X,\sigma}a_j^+a_j^+u+va_ia_ia_ja_jg_{ep}a_{k\sigma}^+a_{k+X,\sigma}a_j^+a_j^+u\\
+ua_i^+a_i^+g_{ep}a_{k\sigma}^+a_{k+X,\sigma}a_j^+a_j^+u+va_ia_ia_i^+a_i^+g_{ep}a_{k\sigma}^+a_{k+X,\sigma}a_j^+a_j^+u\\
+ua_ja_jg_{ep}a_{k+X,\sigma}^+a_{k\sigma}a_j^+a_j^+u+va_ia_ia_ja_jg_{ep}a_{k+X,\sigma}^+a_{k\sigma}a_j^+a_j^+u\\
+ua_i^+a_i^+g_{ep}a_{k+X,\sigma}^+a_{k\sigma}a_j^+a_j^+u+va_ia_ia_i^+a_i^+g_{ep}a_{k+X,\sigma}^+a_{k\sigma}a_j^+a_j^+u\\
ua_ja_jg_{ep}a_{k\sigma}^+a_{k+X,\sigma}a_ia_iva_i^+a_i^++va_ia_ia_ja_jg_{ep}a_{k\sigma}^+a_{k+X,\sigma}a_ia_iva_i^+a_i^+\\
+ua_i^+a_i^+g_{ep}a_{k\sigma}^+a_{k+X,\sigma}a_ia_iva_i^+a_i^++va_ia_ia_i^+a_i^+g_{ep}a_{k\sigma}^+a_{k+X,\sigma}a_ia_iva_i^+a_i^+\\
+ua_ja_jg_{ep}a_{k+X,\sigma}^+a_{k\sigma}a_ia_iva_i^+a_i^++va_ia_ia_ja_jg_{ep}a_{k+X,\sigma}^+a_{k\sigma}a_ia_iva_i^+a_i^+\\
+ua_i^+a_i^+g_{ep}a_{k+X,\sigma}^+a_{k\sigma}a_ia_iva_i^+a_i^++va_ia_ia_i^+a_i^+g_{ep}a_{k+X,\sigma}^+a_{k\sigma}a_ia_iva_i^+a_i^+\\
ua_ja_jg_{ep}a_{k\sigma}^+a_{k+X,\sigma}a_j^+a_j^+va_i^+a_i^++va_ia_ia_ja_jg_{ep}a_{k\sigma}^+a_{k+X,\sigma}a_j^+a_j^+va_i^+a_i^+\\
+ua_i^+a_i^+g_{ep}a_{k\sigma}^+a_{k+X,\sigma}a_j^+a_j^+va_i^+a_i^++va_ia_ia_i^+a_i^+g_{ep}a_{k\sigma}^+a_{k+X,\sigma}a_j^+a_j^+va_i^+a_i^+\\
+ua_ja_jg_{ep}a_{k+X,\sigma}^+a_{k\sigma}a_j^+a_j^+va_i^+a_i^++va_ia_ia_ja_jg_{ep}a_{k+X,\sigma}^+a_{k\sigma}a_j^+a_j^+va_i^+a_i^+\\
+ua_i^+a_i^+g_{ep}a_{k+X,\sigma}^+a_{k\sigma}a_j^+a_j^+va_i^+a_i^++va_ia_ia_i^+a_i^+g_{ep}a_{k+X,\sigma}^+a_{k\sigma}a_j^+a_j^+va_i^+a_i^+
\end{pmatrix}|n,0\rangle
\end{aligned}$$

(4.96)

Applying the properties of creation and annihilation operators to eq. (4.96), one obtains;

$$\langle n,0|ua_ja_jg_{ep}a_{k\sigma}^+a_{k+X,\sigma}a_ia_iu|n,0\rangle=0 \tag{4.97}$$

$$\langle n,0|va_ia_ia_ja_jg_{ep}a_{k\sigma}^+a_{k+X,\sigma}a_ia_iu|n,0\rangle=0 \tag{4.98}$$

$$\begin{aligned}
&\langle n,0|ua_i^+a_i^+g_{ep}a_{k\sigma}^+a_{k+X,\sigma}a_ia_iu|n,0\rangle \\
&=u^2g_{ep}n^{\frac{1}{2}}\langle n,0|a_i^+a_i^+a_{k\sigma}^+a_{k+X,\sigma}a_i|(n-1),0\rangle \\
&=u^2g_{ep}n^{\frac{1}{2}}(n-1)^{\frac{1}{2}}\langle n,0|a_i^+a_i^+a_{k\sigma}^+a_{k+X,\sigma}|(n-2),0\rangle \\
&=u^2g_{ep}n^{\frac{1}{2}}(n-1)^{\frac{1}{2}}(n-2)^{\frac{1}{2}}\langle n,0|a_i^+a_i^+a_{k\sigma}^+|(n-3),0\rangle \\
&=u^2g_{ep}n^{\frac{1}{2}}(n-1)^{\frac{1}{2}}(n-2)\langle n,0|a_i^+a_i^+|(n-2),0\rangle \\
&=u^2g_{ep}n^{\frac{1}{2}}(n-1)(n-2)\langle n,0|a_i^+|(n-1),0\rangle \\
&=u^2g_{ep}n(n-1)(n-2)\langle n,0|n,0\rangle=u^2g_{ep}n(n-1)(n-2)
\end{aligned} \tag{4.99}$$

$$\langle n,0|va_ia_ia_i^+a_i^+g_{ep}a_{k\sigma}^+a_{k+X,\sigma}a_ia_iu|n,0\rangle=0 \tag{4.100}$$

$$\langle n,0|ua_ja_jg_{ep}a_{k+X,\sigma}^+a_{k\sigma}a_ia_iu|n,0\rangle=0 \tag{4.101}$$

$$\langle n,0|va_ia_ia_ja_jg_{ep}a_{k+X,\sigma}^+a_{k\sigma}a_ia_iu|n,0\rangle=0 \tag{4.102}$$

$$\begin{aligned}
&\langle n,0|ua_i^+a_i^+g_{ep}a_{k+X,\sigma}^+a_{k\sigma}a_ia_iu|n,0\rangle \\
&=u^2g_{ep}n^{\frac{1}{2}}\langle n,0|a_i^+a_i^+a_{k+X,\sigma}^+a_{k\sigma}a_i|(n-1),0\rangle \\
&=u^2g_{ep}n^{\frac{1}{2}}(n-1)^{\frac{1}{2}}\langle n,0|a_i^+a_i^+a_{k+X,\sigma}^+a_{k\sigma}|(n-2),0\rangle \\
&=u^2g_{ep}n^{\frac{1}{2}}(n-1)^{\frac{1}{2}}(n-2)^{\frac{1}{2}}\langle n,0|a_i^+a_i^+a_{k+X,\sigma}^+|(n-3),0\rangle \\
&=u^2g_{ep}n^{\frac{1}{2}}(n-1)^{\frac{1}{2}}(n-2)\langle n,0|a_i^+a_i^+|(n-2),0\rangle \\
&=u^2g_{ep}n^{\frac{1}{2}}(n-1)(n-2)\langle n,0|a_i^+|(n-1),0\rangle \\
&=u^2g_{ep}n(n-1)(n-2)\langle n,0|n,0\rangle=u^2g_{ep}n(n-1)(n-2)
\end{aligned} \tag{4.103}$$

$$\langle n,0|va_ia_ia_i^+a_i^+g_{ep}a_{k+X,\sigma}^+a_{k\sigma}a_ia_iu|n,0\rangle=0 \tag{4.104}$$

$$\begin{aligned}
&\langle n,0|ua_j a_j g_{ep} a^+_{k\sigma} a_{k+X,\sigma} a^+_j a^+_j u|n,0\rangle \\
&= u^2 g_{ep} (n+1)^{\frac{1}{2}} \langle n,0|a_j a_j a^+_{k\sigma} a_{k+X,\sigma} a^+_j|(n+1),0\rangle \\
&= u^2 g_{ep} (n+1)^{\frac{1}{2}} (n+2)^{\frac{1}{2}} \langle n,0|a_j a_j a^+_{k\sigma} a_{k+X,\sigma}|(n+2),0\rangle \\
&= u^2 g_{ep} (n+1)^{\frac{1}{2}} (n+2) \langle n,0|a_j a_j a^+_{k\sigma}|(n+1),0\rangle \\
&= u^2 g_{ep} (n+1)^{\frac{1}{2}} (n+2)^{\frac{3}{2}} \langle n,0|a_j a_j|(n+2),0\rangle \\
&= u^2 g_{ep} (n+1)^{\frac{1}{2}} (n+2)^2 \langle n,0|a_j|(n+1),0\rangle \\
&= u^2 g_{ep} (n+1)(n+2)^2 \langle n,0|n,0\rangle = u^2 g_{ep} (n+1)(n+2)^2
\end{aligned} \tag{4.105}$$

$$\langle n,0|va_i a_i a_j a_j g_{ep} a^+_{k\sigma} a_{k+X,\sigma} a^+_j a^+_j u|n,0\rangle = 0 \tag{4.106}$$

$$\langle n,0|ua^+_i a^+_i g_{ep} a^+_{k\sigma} a_{k+X,\sigma} a^+_j a^+_j u|n,0\rangle = 0 \tag{4.107}$$

$$\langle n,0|va_i a_i a^+_i a^+_i g_{ep} a^+_{k\sigma} a_{k+X,\sigma} a^+_j a^+_j u|n,0\rangle = 0 \tag{4.108}$$

$$\begin{aligned}
&\langle n,0|ua_j a_j g_{ep} a^+_{k+X,\sigma} a_{k\sigma} a^+_j a^+_j u|n,0\rangle = \\
&= u^2 g_{ep} (n+1)^{\frac{1}{2}} \langle n,0|a_j a_j a^+_{k+X,\sigma} a_{k\sigma} a^+_j|(n+1),0\rangle \\
&= u^2 g_{ep} (n+1)^{\frac{1}{2}} (n+2)^{\frac{1}{2}} \langle n,0|a_j a_j a^+_{k+X,\sigma} a_{k\sigma}|(n+2),0\rangle \\
&= u^2 g_{ep} (n+1)^{\frac{1}{2}} (n+2) \langle n,0|a_j a_j a^+_{k+X,\sigma}|(n+1),0\rangle \\
&= u^2 g_{ep} (n+1)^{\frac{1}{2}} (n+2)^{\frac{3}{2}} \langle n,0|a_j a_j|(n+2),0\rangle \\
&= u^2 g_{ep} (n+1)^{\frac{1}{2}} (n+2)^2 \langle n,0|a_j|(n+1),0\rangle \\
&= u^2 g_{ep} (n+1)(n+2)^2 \langle n,0|n,0\rangle = u^2 g_{ep} (n+1)(n+2)^2
\end{aligned} \tag{4.109}$$

$$\langle n,0|va_i a_i a_j a_j g_{ep} a^+_{k+X,\sigma} a_{k\sigma} a^+_j a^+_j u|n,0\rangle = 0 \tag{4.110}$$

$$\langle n,0|ua^+_i a^+_i g_{ep} a^+_{k+X,\sigma} a_{k\sigma} a^+_j a^+_j u|n,0\rangle = 0 \tag{4.111}$$

$$\langle n,0|va_i a_i a^+_i a^+_i g_{ep} a^+_{k+X,\sigma} a_{k\sigma} a^+_j a^+_j u|n,0\rangle \tag{4.112}$$

$$\left\langle n,0\left|ua_j a_j g_{ep} a_{k\sigma}^{+} a_{k+X,\sigma} a_i a_i v a_i^{+} a_i^{+}\right|n,0\right\rangle = 0 \tag{4.113}$$

$$\left\langle n,0\left|va_i a_i a_j a_j g_{ep} a_{k\sigma}^{+} a_{k+X,\sigma} a_i a_i v a_i^{+} a_i^{+}\right|n,0\right\rangle = 0 \tag{4.114}$$

$$\left\langle n,0\left|ua_i^{+} a_i^{+} g_{ep} a_{k\sigma}^{+} a_{k+X,\sigma} a_i a_i v a_i^{+} a_i^{+}\right|n,0\right\rangle = 0 \tag{4.115}$$

$$\begin{aligned}
&\left\langle n,0\left|va_i a_i a_i^{+} a_i^{+} g_{ep} a_{k\sigma}^{+} a_{k+X,\sigma} a_i a_i v a_i^{+} a_i^{+}\right|n,0\right\rangle \\
&= v^2 g_{ep} (n+1)^{\frac{1}{2}} \left\langle n,0\left|a_i a_i a_i^{+} a_i^{+} a_{k\sigma}^{+} a_{k+X,\sigma} a_i a_i a_i^{+}\right|(n+1),0\right\rangle \\
&= v^2 g_{ep} (n+1)^{\frac{1}{2}} (n+2)^{\frac{1}{2}} \left\langle n,0\left|a_i a_i a_i^{+} a_i^{+} a_{k\sigma}^{+} a_{k+X,\sigma} a_i a_i\right|(n+2),0\right\rangle \\
&= v^2 g_{ep} (n+1)^{\frac{1}{2}} (n+2) \left\langle n,0\left|a_i a_i a_i^{+} a_i^{+} a_{k\sigma}^{+} a_{k+X,\sigma} a_i\right|(n+1),0\right\rangle \\
&= v^2 g_{ep} (n+1)(n+2) \left\langle n,0\left|a_i a_i a_i^{+} a_i^{+} a_{k\sigma}^{+} a_{k+X,\sigma}\right|n,0\right\rangle \\
&= v^2 g_{ep} n^{\frac{1}{2}} (n+1)(n+2) \left\langle n,0\left|a_i a_i a_i^{+} a_i^{+} a_{k\sigma}^{+}\right|(n-1),0\right\rangle \\
&= v^2 g_{ep} n(n+1)(n+2) \left\langle n,0\left|a_i a_i a_i^{+} a_i^{+}\right|n,0\right\rangle \\
&= v^2 g_{ep} n(n+1)^{\frac{3}{2}} (n+2) \left\langle n,0\left|a_i a_i a_i^{+}\right|(n+1),0\right\rangle \\
&= v^2 g_{ep} n(n+1)^{\frac{3}{2}} (n+2)^{\frac{3}{2}} \left\langle n,0\left|a_i a_i\right|(n+2),0\right\rangle \\
&= v^2 g_{ep} n(n+1)^{\frac{3}{2}} (n+2)^{2} \left\langle n,0\left|a_i\right|(n+1),0\right\rangle \\
&= v^2 g_{ep} n(n+1)^{\frac{3}{2}} (n+2)^{2} \left\langle n,0\middle|n,0\right\rangle = v^2 g_{ep} n(n+1)^{\frac{3}{2}} (n+2)^{2}
\end{aligned} \tag{4.116}$$

$$\left\langle n,0\left|ua_j a_j g_{ep} a_{k+X,\sigma}^{+} a_{k\sigma} a_i a_i v a_i^{+} a_i^{+}\right|n,0\right\rangle = 0 \tag{4.117}$$

$$\left\langle n,0\left|va_i a_i a_j a_j g_{ep} a_{k+X,\sigma}^{+} a_{k\sigma} a_i a_i v a_i^{+} a_i^{+}\right|n,0\right\rangle = 0 \tag{4.118}$$

$$\left\langle n,0\left|ua_i^{+} a_i^{+} g_{ep} a_{k+X,\sigma}^{+} a_{k\sigma} a_i a_i v a_i^{+} a_i^{+}\right|n,0\right\rangle = 0 \tag{4.119}$$

$$\begin{aligned}
&\langle n,0|va_i a_i a_i^+ a_i^+ g_{ep} a_{k+X,\sigma}^+ a_{k\sigma} a_i a_i v a_i^+ a_i^+ |n,0\rangle \\
&= v^2 g_{ep} (n+1)^{\frac{1}{2}} \langle n,0|a_i a_i a_i^+ a_i^+ a_{k+X,\sigma}^+ a_{k\sigma} a_i a_i a_i^+ |(n+1),0\rangle \\
&= v^2 g_{ep} (n+1)^{\frac{1}{2}} (n+2)^{\frac{1}{2}} \langle n,0|a_i a_i a_i^+ a_i^+ a_{k+X,\sigma}^+ a_{k\sigma} a_i a_i |(n+2),0\rangle \\
&= v^2 g_{ep} (n+1)^{\frac{1}{2}} (n+2) \langle n,0|a_i a_i a_i^+ a_i^+ a_{k+X,\sigma}^+ a_{k\sigma} a_i |(n+1),0\rangle \\
&= v^2 g_{ep} (n+1)(n+2) \langle n,0|a_i a_i a_i^+ a_i^+ a_{k+X,\sigma}^+ a_{k\sigma} |n,0\rangle \\
&= v^2 g_{ep} n^{\frac{1}{2}} (n+1)(n+2) \langle n,0|a_i a_i a_i^+ a_i^+ a_{k+X,\sigma}^+ |(n-1),0\rangle \\
&= v^2 g_{ep} n(n+1)(n+2) \langle n,0|a_i a_i a_i^+ a_i^+ |n,0\rangle \\
&= v^2 g_{ep} n(n+1)^{\frac{3}{2}} (n+2) \langle n,0|a_i a_i a_i^+ |(n+1),0\rangle \\
&= v^2 g_{ep} n(n+1)^{\frac{3}{2}} (n+2)^{\frac{3}{2}} \langle n,0|a_i a_i |(n+2),0\rangle \\
&= v^2 g_{ep} n(n+1)^{\frac{3}{2}} (n+2)^2 \langle n,0|a_i |(n+1),0\rangle \\
&= v^2 g_{ep} n(n+1)^2 (n+2)^2 \langle n,0|n,0\rangle = v^2 g_{ep} n(n+1)^2 (n+2)^2
\end{aligned} \tag{4.120}$$

$$\langle n,0|ua_j a_j g_{ep} a_{k\sigma}^+ a_{k+X,\sigma} a_j^+ a_j^+ v a_i^+ a_i^+ |n,0\rangle = 0 \tag{4.121}$$

$$
\begin{aligned}
&\left\langle n,0\left|va_i a_i a_j a_j g_{ep} a^+_{k\sigma} a_{k+X,\sigma} a^+_j a^+_j v a^+_i a^+_i\right|n,0\right\rangle \\
&= v^2 g_{ep} (n+1)^{\frac{1}{2}} \left\langle n,0\left|a_i a_i a_j a_j a^+_{k\sigma} a_{k+X,\sigma} a^+_j a^+_j a^+_i\right|(n+1),0\right\rangle \\
&= v^2 g_{ep} (n+1)^{\frac{1}{2}} (n+2)^{\frac{1}{2}} \left\langle n,0\left|a_i a_i a_j a_j a^+_{k\sigma} a_{k+X,\sigma} a^+_j a^+_j\right|(n+2),0\right\rangle \\
&= v^2 g_{ep} (n+1)^{\frac{1}{2}} (n+2)^{\frac{1}{2}} (n+3)^{\frac{1}{2}} \left\langle n,0\left|a_i a_i a_j a_j a^+_{k\sigma} a_{k+X,\sigma} a^+_j\right|(n+3),0\right\rangle \\
&= v^2 g_{ep} (n+1)^{\frac{1}{2}} (n+2)^{\frac{1}{2}} (n+3)^{\frac{1}{2}} (n+4)^{\frac{1}{2}} \left\langle n,0\left|a_i a_i a_j a_j a^+_{k\sigma} a_{k+X,\sigma}\right|(n+4),0\right\rangle \\
&= v^2 g_{ep} (n+1)^{\frac{1}{2}} (n+2)^{\frac{1}{2}} (n+3)^{\frac{1}{2}} (n+4) \left\langle n,0\left|a_i a_i a_j a_j a^+_{k\sigma}\right|(n+3),0\right\rangle \\
&= v^2 g_{ep} (n+1)^{\frac{1}{2}} (n+2)^{\frac{1}{2}} (n+3)^{\frac{1}{2}} (n+4)^{\frac{3}{2}} \left\langle n,0\left|a_i a_i a_j a_j\right|(n+4),0\right\rangle \\
&= v^2 g_{ep} (n+1)^{\frac{1}{2}} (n+2)^{\frac{1}{2}} (n+3)^{\frac{1}{2}} (n+4)^2 \left\langle n,0\left|a_i a_i a_j\right|(n+3),0\right\rangle \\
&= v^2 g_{ep} (n+1)^{\frac{1}{2}} (n+2)^{\frac{1}{2}} (n+3)(n+4)^2 \left\langle n,0\left|a_i a_i\right|(n+2),0\right\rangle \\
&= v^2 g_{ep} (n+1)^{\frac{1}{2}} (n+2)(n+3)(n+4)^2 \left\langle n,0\left|a_i\right|(n+1),0\right\rangle \\
&= v^2 g_{ep} (n+1)(n+2)(n+3)(n+4)^2 \left\langle n,0\middle|n,0\right\rangle \\
&= v^2 g_{ep} (n+1)(n+2)(n+3)(n+4)^2
\end{aligned}
\tag{4.122}
$$

$$
\left\langle n,0\left|ua^+_i a^+_i g_{ep} a^+_{k\sigma} a_{k+X,\sigma} a^+_j a^+_j v a^+_i a^+_i\right|n,0\right\rangle = 0 \tag{4.123}
$$

$$
\left\langle n,0\left|va_i a_i a^+_i a^+_i g_{ep} a^+_{k\sigma} a_{k+X,\sigma} a^+_j a^+_j v a^+_i a^+_i\right|n,0\right\rangle = 0 \tag{4.124}
$$

$$
\left\langle n,0\left|ua_j a_j g_{ep} a^+_{k+X,\sigma} a_{k\sigma} a^+_j a^+_j v a^+_i a^+_i\right|n,0\right\rangle = 0 \tag{4.125}
$$

$$
\begin{aligned}
&\left\langle n,0\left|va_i a_i a_j a_j g_{ep} a^+_{k+X,\sigma} a_{k\sigma} a^+_j a^+_j v a^+_i a^+_i\right|n,0\right\rangle \\
&= v^2 g_{ep}(n+1)^{\frac{1}{2}}\left\langle n,0\left|a_i a_i a_j a_j a^+_{k+X,\sigma} a_{k\sigma} a^+_j a^+_j a^+_i\right|(n+1),0\right\rangle \\
&= v^2 g_{ep}(n+1)^{\frac{1}{2}}(n+2)^{\frac{1}{2}}\left\langle n,0\left|a_i a_i a_j a_j a^+_{k+X,\sigma} a_{k\sigma} a^+_j a^+_j\right|(n+2),0\right\rangle \\
&= v^2 g_{ep}(n+1)^{\frac{1}{2}}(n+2)^{\frac{1}{2}}(n+3)^{\frac{1}{2}}\left\langle n,0\left|a_i a_i a_j a_j a^+_{k+X,\sigma} a_{k\sigma} a^+_j\right|(n+3),0\right\rangle \\
&= v^2 g_{ep}(n+1)^{\frac{1}{2}}(n+2)^{\frac{1}{2}}(n+3)^{\frac{1}{2}}(n+4)^{\frac{1}{2}}\left\langle n,0\left|a_i a_i a_j a_j a^+_{k+X,\sigma} a_{k\sigma}\right|(n+4),0\right\rangle \\
&= v^2 g_{ep}(n+1)^{\frac{1}{2}}(n+2)^{\frac{1}{2}}(n+3)^{\frac{1}{2}}(n+4)\left\langle n,0\left|a_i a_i a_j a_j a^+_{k+X,\sigma}\right|(n+3),0\right\rangle \\
&= v^2 g_{ep}(n+1)^{\frac{1}{2}}(n+2)^{\frac{1}{2}}(n+3)^{\frac{1}{2}}(n+4)^{\frac{3}{2}}\left\langle n,0\left|a_i a_i a_j a_j\right|(n+4),0\right\rangle \\
&= v^2 g_{ep}(n+1)^{\frac{1}{2}}(n+2)^{\frac{1}{2}}(n+3)^{\frac{1}{2}}(n+4)^2\left\langle n,0\left|a_i a_i a_j\right|(n+3),0\right\rangle \\
&= v^2 g_{ep}(n+1)^{\frac{1}{2}}(n+2)^{\frac{1}{2}}(n+3)(n+4)^2\left\langle n,0\left|a_i a_i\right|(n+2),0\right\rangle \\
&= v^2 g_{ep}(n+1)^{\frac{1}{2}}(n+2)(n+3)(n+4)^2\left\langle n,0\left|a_i\right|(n+1),0\right\rangle \\
&= v^2 g_{ep}(n+1)(n+2)(n+3)(n+4)^2\left\langle n,0\middle|n,0\right\rangle \\
&= v^2 g_{ep}(n+1)(n+2)(n+3)(n+4)^2
\end{aligned}
\tag{4.126}
$$

$$
\left\langle n,0\left|ua^+_i a^+_i g_{ep} a^+_{k+X,\sigma} a_{k\sigma} a^+_j a^+_j v a^+_i a^+_i\right|n,0\right\rangle = 0 \tag{4.127}
$$

$$
\left\langle n,0\left|va_i a_i a^+_i a^+_i g_{ep} a^+_{k+X,\sigma} a_{k\sigma} a^+_j a^+_j v a^+_i a^+_i\right|n,0\right\rangle = 0 \tag{4.128}
$$

The sum of eq. (4.99), (4.103), (4.105), (4.109), (4.116), (4.120), (4.122) and (4.126) gives;

$$
\left\{\begin{array}{l}
u^2 n(n-1)(n-2) + u^2 n(n-1)(n-2) + u^2(n+1)(n+2)^2 \\
+u^2(n+1)(n+2)^2 + v^2 n(n+1)^{\frac{3}{2}}(n+2)^2 + v^2 n(n+1)^2(n+2)^2 \\
+v^2(n+1)(n+2)(n+3)(n+4)^2 + v^2(n+1)(n+2)(n+3)(n+4)^2
\end{array}\right\} g_{ep}
\tag{4.129}
$$

The sum of eqs. (4.22), (4.44), (4.77), (4.95), and (4.129) gives the expectation value of the H_{epc} as

$$
\begin{aligned}
E_n = & \left\{ \begin{matrix} u^2(n+1)(n+2)^2 + u^2 n(n-1)(n-2) \\ +v^2(n+1)(n+2)(n+3)(n+4)^2 + v^2 n(n+1)(n+2) \end{matrix} \right\} E_p \\
& + \left\{ \begin{matrix} u^2(n+1)(n+2)^2 + u^2 n(n-1)(n-2) + v^2(n+1)(n+2)(n+3)(n+4)^2 \\ +v^2(n+1)(n+2)(n+3)(n+4)^{\frac{5}{2}} + v^2(n-1)n(n+1)^{\frac{5}{2}}(n+2) \end{matrix} \right\} E_d \\
& + \left\{ \begin{matrix} u^2 t_{pd} n(n-1)(n-2) + u^2 t_{pd} n(n-1)(n-2) \\ +u^2(n+1)(n+2)^2 + u^2(n+1)(n+2)^2 \\ +uvn(n+1)^2(n+2)^2 + v^2 n(n+1)^{\frac{5}{2}}(n+2)^2 \\ +v^{\frac{1}{2}}(n+1)(n+2)(n+3)(n+4)^2 \\ +v^2(n+1)(n+2)(n+3)(n+4)^2 \end{matrix} \right\} t_{pd} \\
& + \left\{ \begin{matrix} u^{\frac{1}{2}} n(n-1)(n-2)(n-3) + u^2(n+1)^2(n+2)^2 \\ +v^2(n-2)(n-1)n(n+1)^{\frac{5}{2}}(n+2)^{\frac{3}{2}} + v^2(n+1)(n+2)(n+3)^2(n+4)^2 \end{matrix} \right\} u_d \\
& + \left\{ \begin{matrix} u^2 n(n-1)(n-2) + u^2 n(n-1)(n-2) + u^2(n+1)(n+2)^2 \\ +u^2(n+1)(n+2)^2 + v^2 n(n+1)^{\frac{3}{2}}(n+2)^2 + v^2 n(n+1)^2(n+2)^2 \\ +v^2(n+1)(n+2)(n+3)(n+4)^2 + v^2(n+1)(n+2)(n+3)(n+4)^2 \end{matrix} \right\} g_{ep}
\end{aligned}
$$

(4.130)

For n =1, when the system is in its lowest energy state (superconducting state) and substituting $u = v = \frac{1}{\sqrt{2}}$ (from second quantization formalism) in eq. (4.130) one gets;

$$
\begin{aligned}
E_1 = & \left\{\frac{1}{2}(2)(3)(4)(5)^2 + \frac{1}{2}(2)(3)\right\}E_p \\
& + \left\{\frac{1}{2}(2)(3)^2 + \frac{1}{2}(2)(3)(4)(5)^2 + \frac{1}{2}(2)(3)(4)(5)^{\frac{5}{2}}\right\}E_d \\
& + \left\{\begin{array}{l}\frac{1}{2}(2)(3)^2 + \frac{1}{2}(2)(3)^2 + \frac{1}{2}(2)^2(3)^2 + \frac{1}{2}(2)^{\frac{5}{2}}(3)^2 \\ + \frac{1}{2}(2)(3)(4)(5)^2 + \frac{1}{2}(2)(3)(4)(5)^2\end{array}\right\}t_{pd} \\
& + \left\{\frac{1}{2}(2)(3)(4)^2(5)^2\right\}u_d \\
& + \left\{\begin{array}{l}\frac{1}{2}(2)(3)^2 + \frac{1}{2}(2)(3)^2 + \frac{1}{2}(2)^{\frac{3}{2}}(3)^2 + \frac{1}{2}(2)^2(3)^2 \\ + \frac{1}{2}(2)(3)(4)(5)^2 + \frac{1}{2}(2)(3)(4)(5)^2\end{array}\right\}g_{ep}
\end{aligned}
\tag{4.131}
$$

Eq. (4.131) simplifies to

$$E_1 = 312E_p + 980E_d + 888t_{pd} + 800u_d + 720g_{ep} \tag{4.132}$$

Eq. (4.132) is the expectation value of the electron – phonon and Coulomb interactions Hamiltonian.

4.3 Effects of electron – phonon and Coulomb interactions on the transition temperature of high – T_c cuprate superconductors.

At the temperature of interest, it is necessary to consider the difference between the states in which the hopping electron is on one site and then when it is on another site of similar symmetry or different symmetry. The difference in energy of the two sites gives the probability amplitude Green's function which according to quantum treatment of lattice vibrations, is equivalent to the thermal activation factor exp ($-E_1/kT$). Thus, the values of energy at ground state multiplied by the thermal activation factor gives

$$E = E_1 e^{-\frac{E_1}{kT}} \tag{4.133}$$

where *k* is Boltzmann's constant.

The specific heat, C_v, of the system is obtained from the first derivative of eq. (4.133) with respect to absolute temperature and is written as,

$$C_v = \frac{\partial E}{\partial T} = E_1 \frac{\partial}{\partial T}\left(e^{-\frac{E_1}{kT}}\right) = \frac{E_1}{kT^2} e^{-\frac{E_1}{kT}} \tag{4.134}$$

To obtain the equation relating entropy, *S*, and absolute temperature *T*, one may start with the equation

$$dS = \frac{dQ}{T} = \frac{C_v dT}{T} \tag{4.135}$$

Taking integrals on both sides of eq. (4.135), one obtains,

$$\int dS = \int \frac{C_v dT}{T} \tag{4.136}$$

Substituting for C_v from eq. (4.134) in eq. (4.136), one obtains,

$$\int dS = \int \frac{E_1}{kT^2} e^{-\frac{E_1}{kT}} \frac{dT}{T} \tag{4.137}$$

From eq. (4.137), one obtains,

$$S = \frac{E_1}{k} \int \frac{1}{T^2} e^{-\frac{E_1}{kT}} \frac{dT}{T} = \frac{E_1}{k} \int \frac{1}{T^3} e^{-\frac{E_1}{kT}} dT \tag{4.138}$$

To obtain an exact calculation of the integral in eq. (4.138), we let

$$u = -\frac{E_1}{kT} \tag{4.139}$$

From eq. (4.139), one obtains,

$$du = \frac{E_1}{kT^2} dT \tag{4.140}$$

From eq. (4.140), one obtains,

$$dT = \frac{kT^2}{E_1} du \tag{4.141}$$

Substituting value of u and dT from eqs. (4.139) and (4.141) in eq. (4.138), one obtains,

$$S = \frac{E_1}{k} \int \frac{1}{T^3} e^u \frac{kT^2}{E_1} du = \int \frac{e^u}{T} du \tag{4.142}$$

Substituting for $T = -\frac{E_1}{ku}$ in eq. (4.142), one obtains,

$$S = \int \frac{-e^u}{E_1 / ku} du = -\frac{k}{E_1} \int u e^u du \tag{4.143}$$

Applying integration by parts to eq. (4.143), one obtains,

$$S = \frac{e^{-\frac{E_1}{kT}}}{T} + \frac{k}{E} e^{-\frac{E_1}{kT}} + C \tag{4.144}$$

where C is a constant of integration.

As T tends to zero, S = 0 and hence, C = 0. Therefore eq. (4.144) becomes.

$$S = \frac{e^{-\frac{E_1}{kT}}}{T} + \frac{k}{E} e^{-\frac{E_1}{kT}} = e^{-\frac{E_1}{kT}} \left(\frac{1}{T} + \frac{k}{E} \right) \tag{4.145}$$

The effects of electron – phonon and Coulomb interactions on the Tc of cuprate superconductors was investigated in terms of Cv and S using ens (4.134) and (4.145) respectively.

4.4 Effect of Various Parameters on Transition Temperature and Specific Heat

4.4.1 Effect of t_{pd} and g_{ep} on C_v and T_c(For E_p = 3.5 x 10^{-6} eV and u_d = 2.5 x 10^{-6}eV) for YBaCuO.

Eqn. (4.134) was used to investigate the effects of t_{pd} and g_{ep} on C_v. The values of the other parameters in eq. (4.132) were kept constant at E_p = 3.5 x 10^{-6} eV, E_d = 2.0 x 10^{-6} eV and u_d = 2.5 x 10^{-6} eV. Four equations relating specific heat and absolute temperature were obtained from eq. (4.134) as follows;

i) Substituting in eq. (4.134) for E_p = 3.5 x 10^{-6} eV, E_d = 2.0 x 10^{-6} eV , t_{pd} = 0 eV, u_d = 2.5 x 10^{-6} eV g_{ep} = 0 eV and k = 8.6 x 10^{-5} eV/K, one obtains the equation;

$$C_v = \frac{58}{T^2} e^{-\frac{58}{T}} \tag{4.146}$$

ii) Substituting in eq. (4.134) for E_p = 3.5 x 10^{-6} eV, E_d = 2.0 x 10^{-6} eV , t_{pd} = 0 eV, u_d = 2.5 x 10^{-6} eV , g_{ep} = 2.0 x 10^{-6} eV and k = 8.6 x 10^{-5} eV/K ,one obtains the equation;

$$C_v = \frac{76}{T^2} e^{-\frac{76}{T}} \tag{4.147}$$

iii) Substituting in eq. (4.134) for E_p = 3.5 x 10^{-6} eV, E_d = 2.0 x 10^{-6} eV , t_{pd} = 1.6 x 10^{-6} eV, u_d = 2.5 x 10^{-6} eV , g_{ep} = 0 eV, and k = 8.6 x 10^{-5} eV/K ,one obtains the equation;

$$C_v = \frac{74}{T^2} e^{-\frac{74}{T}} \tag{4.148}$$

iv) Substituting in eq. (4.134) for E_p = 3.5 x 10^{-6} eV, E_d = 2.0 x 10^{-6} eV ,

t_{pd} = 1.6 x 10^{-6} eV, u_d = 2.5 x 10^{-6} eV , g_{ep} = 2.0 x 10^{-6} eV and k = 8.6 x 10^{-5} eV/K, one obtains the equation;

$$C_v = \frac{92}{T^2} e^{-\frac{92}{T}} \tag{4.149}$$

Using equations (4.146), (4.147), (4.148) and (4.149) values of C_v at different T were calculated and tabulated in Table 1 in appendix C.

Fig. 4.1, shows a plot of C_v against T for the data in Table 1, for different combinations of t_{pd} and g_{ep}.

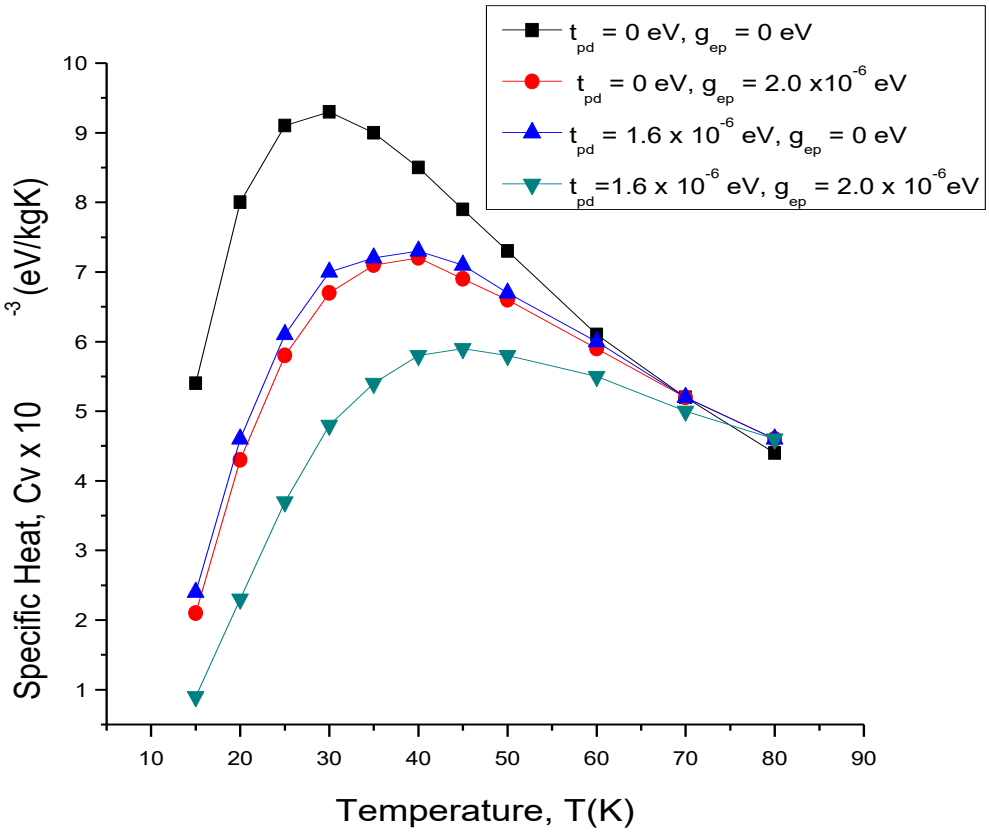

Figure 4.1: Variation of Specific Heat with temperature for YBaCuO

From Figure (4.1) , one notices that C_v increases with absolute temperature and attains a peak value and thereafter, decreases with further increase in absolute temperature.

The peak values of C_v are 9.3 x 10^{-3} eV/kgK, 7.2 X 10^{-3} eV/kgK, 7.3 x 10^{-3} eV/kgK and 7.2 X 10^{-3} eV/kgK for the control parameters t_{pd} and g_{ep} which occur at 30 K, 40 K, 40 K and 45 K respectively.

These results show that as t_{pd} and g_{ep} are increased, the peak value of C_v reduce but T_c increases.

4.4.2 Effect of t_{pd} and g_{ep} on C_v and T_c(For E_p = 5.5 x 10^{-6} eV and u_d = 5.5 x 10^{-6}eV) for YBaCuO.

Eqn. (4.134) was used to investigate the effects of t_{pd} and g_{ep} on C_v. The values of the other parameters in eq. (4.132) were changed to new values and kept constant at E_p = 5.5 x 10^{-6} eV, E_d = 2.0 x 10^{-6} eV and u_d = 5.5 x 10^{-6} eV. Four equations relating specific heat and absolute temperature were obtained from eq. (4.134) as follows;

i) Substituting in eq. (4.134) for E_p = 5.5 x 10^{-6} eV, E_d = 2.0 x 10^{-6} eV , t_{pd} = 0 eV, u_d = 5.5 x 10^{-6} eV g_{ep} = 0 eV and k = 8.6 x 10^{-5} eV/K, one obtains the equation;

$$C_v = \frac{93}{T^2} e^{-\frac{93}{T}} \tag{4.150}$$

ii) Substituting in eq. (4.134) for E_p = 5.5 x 10^{-6} eV, E_d = 2.0 x 10^{-6} eV , t_{pd} = 0 eV, u_d = 5.5 x 10^{-6} eV , g_{ep} = 2.0 x 10^{-6} eV and k = 8.6 x 10^{-5} eV/K, one obtains the equation;

$$C_v = \frac{110}{T^2} e^{-\frac{110}{T}} \tag{4.151}$$

iii) Substituting in eq. (4.134) for E_p = 5.5 x 10^{-6} eV, E_d = 2.0 x 10^{-6} eV , t_{pd} = 1.6 x 10^{-6} eV, u_d = 5.5 x 10^{-6} eV , g_{ep} = 0 eV and k = 8.6 x 10^{-5} eV/K, one obtains the equation;

$$C_v = \frac{109}{T^2} e^{-\frac{109}{T}} \tag{4.152}$$

iv) Substituting in eq. (4.134) for E_p = 5.5 x 10^{-6} eV, E_d = 2.0 x 10^{-6} eV ,

t_{pd} = 1.6 x 10^{-6} eV, u_d = 5.5 x 10^{-6} eV , g_{ep} = 2.0 x 10^{-6} eV and k = 8.6 x 10^{-5} eV/K, one obtains the equation;

$$C_v = \frac{127}{T^2} e^{-\frac{127}{T}} \tag{4.153}$$

Using equations (4.150), (4.151), (4.152) and (4.153) values of C_v against T were calculated and recorded in Table 2, appendix C.

Figure (4.2) shows the variation of Cv with T .

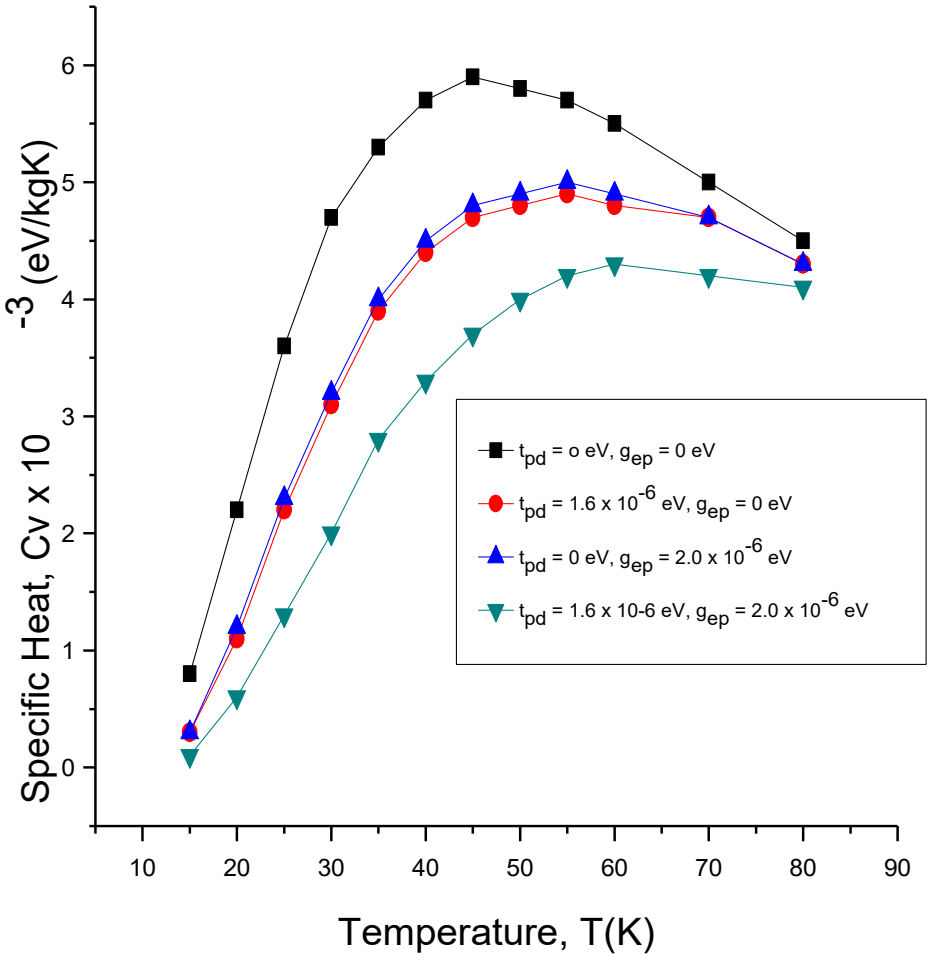

Figure 4.2: Variation of Specific heat with absolute temperature for YBaCuO

From Figure (4.2) above, C_V increases with absolute temperature and attains a peak value and thereafter, decreases with further increase in absolute temperature. The peak values of C_Vs are 5.9 x 10^{-3} eV/kgK, 4.9 x 10^{-3} eV/kgK, 5.0 x 10^{-3} eV/kgK and 4.3 x 10^{-3}eV/kgK which occur at 45 K, 55 K, 55 K and 60 K respectively. These transiton temperatures are higher than the value obtained in section 4.5.1. These results show that as t_{pd} and g_{ep} are increased, the peak value of C_v decreases but T_c increases.

4.4.3 Effect of t_{pd} and g_{ep} on C_v and T_c (For E_p = 7.5 x 10^{-6} eV and u_d = 6.5 x 10^{-6} eV) for YBaCuO.

Eqn. (4.134) was used to investigate the effects of t_{pd} and g_{ep} on C_v. The values of the other parameters in eq. (4.132) were again increased further and kept constant at E_p = 7.5 x 10^{-6} eV, E_d = 2.0 x 10^{-6} eV and u_d = 6.5 x 10^{-6} eV. Four equations relating specific heat and absolute temperature were obtained from eq. (4.134) as follows;

i) Substituting in eq. (4.134) for E_p = 7.5 x 10^{-6} eV, E_d = 2.0 x 10^{-6} eV , t_{pd} = 0 eV, u_d = 6.5 x 10^{-6} eV , g_{ep} = 0 eV and k = 8.6 x 10^{-5} eV/K, one obtains the equation;

$$C_v = \frac{109}{T^2} e^{-\frac{109}{T}} \tag{4.154}$$

ii) Substituting in eq. (4.134) for E_p = 7.5 x 10^{-6} eV, E_d = 2.0 x 10^{-6} eV , t_{pd} = 0 eV, u_d = 6.5 x 10^{-6} eV and g_{ep} = 2.0 x 10^{-6} eV, one obtains the equation;

$$C_v = \frac{122}{T^2} e^{-\frac{122}{T}} \tag{4.155}$$

iii) Substituting in eq. (4.134) for E_p = 7.5 x 10^{-6} eV, E_d = 2.0 x 10^{-6} eV , t_{pd} = 1.6 x 10^{-6} eV, u_d = 6.5 x 10^{-6} eV and g_{ep} = 0 eV, one obtains the equation;

$$C_v = \frac{126}{T^2} e^{-\frac{126}{T}} \tag{4.156}$$

iv) Substituting in eq. (4.134) for E_p = 7.5 x 10^{-6} eV, E_d = 2.0 x 10^{-6} eV , t_{pd} = 1.6 x 10^{-6} eV, u_d = 6.5 x 10^{-6} eV and g_{ep} = 2.0 x 10^{-6} eV, one obtains the equation;

$$C_v = \frac{143}{T^2} e^{-\frac{143}{T}} \tag{4.157}$$

Using equations (4.154), (4.155), (4.156) and (4.157) numerical values of C_v against T were calculated and recorded in table 3 in appendix C.

From Table 3 in appendix III, graphs of numerical values of C_v against T were drawn as shown in Figure (4.3)

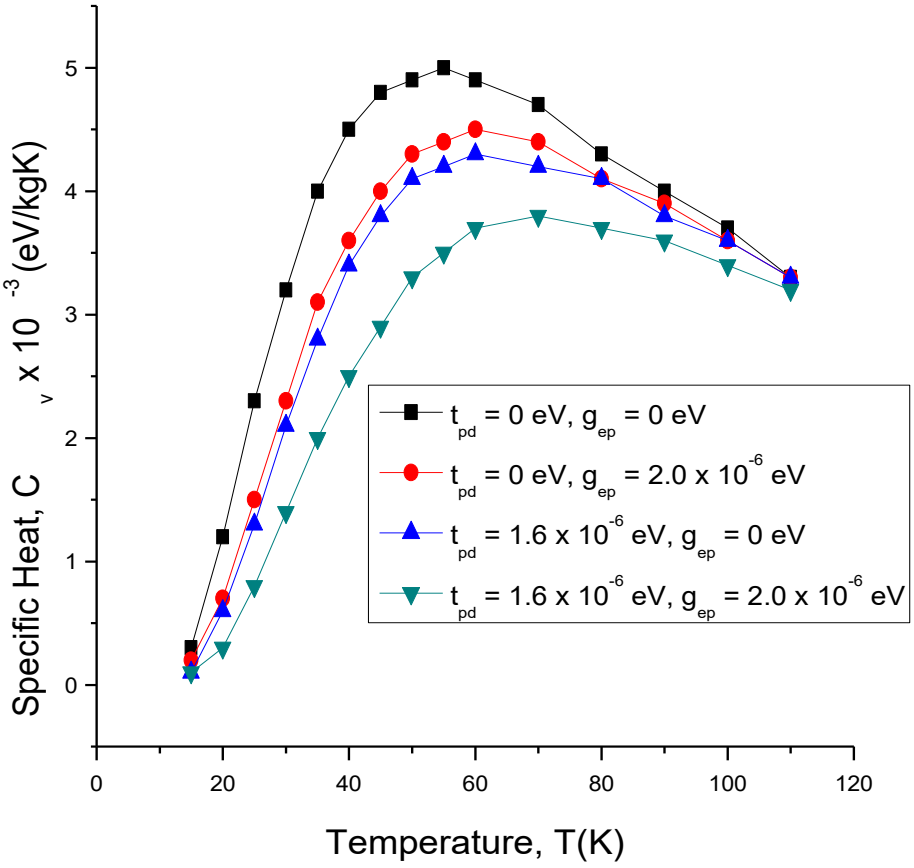

Figure 4.3: Variation of Specific Heat with absolute Temperature (For E_p = 7.5 x 10^{-6} eV and u_d = 6.5 x 10^{-6} eV) for YBaCuO

From Figure 4.3 above, one notices that C_v increases with absolute temperature and attains a peak value and thereafter, decreases with further increase in absolute temperature. The maximum values of C_{vs} are 5.0 x 10^{-3} eV/kgK, 4.5 x 10^{-3} eV/kgK and 3.8 x 10^{-3} eV/kgK occurring at 55 K, 60 K, 60 K and 70 K respectively.

The values of C_v are lower as compared to the values obtained in section 4.5.2 However, the values of T_c obtained are higher.

These results show that T_c increase with increase in the values of the various parameters but C_v decrease.

4.5 Effects of Various Parameters on Transition Temperature and Entropy

Numerical values of entropy against absolute temperature were calculated using eq. (4.145) with t_{pd} and g_{ep} as controlled parameters. The calculations were done for t_{pd} = 0 eV , t_{pd} = 1.6 x 10^{-6} eV, g_{ep} = 0 eV and g_{ep} = 2.0 x 10^{-6} eV. The other values were fixed at E_p = 3.5 x 10^{-6} eV, E_d= 2.0 x 10^{-6} eV, u_d = 2.5 x 10^{-6} eV. From the values, graphs of entropy against temperature were drawn.

4.5.1 Effect of t_{pd} and g_{ep} on S and T_c (For E_p = 3.5 x 10^{-6} eV and u_d = 2.5 x 10^{-6} eV) for YBaCuO.

Eqn. (4.145) was used to investigate the effects of t_{pd} and g_{ep} on S. The values of the other parameters in eq. (4.132) were kept constant at E_p = 3.5 x 10^{-6} eV, E_d = 2.0 x 10^{-6} eV and u_d = 2.5 x 10^{-6} eV. Four equations relating entropy and absolute temperature were obtained from eq. (4.145) as follows;

i) Substituting in eq. (3.167) for E_p = 3.5 x 10^{-6} eV, E_d = 2.0 x 10^{-6} eV , t_{pd} = 0 eV, u_d = 2.5 x 10^{-6} eV and g_{ep} = 0 eV, one obtains the equation;

$$S = \left(\frac{1}{T} + 0.017\right) e^{-\frac{58}{T}} \tag{4.158}$$

ii) Substituting in eq. (4.145) for E_p = 3.5 x 10^{-6} eV, E_d = 2.0 x 10^{-6} eV , t_{pd} = 0 eV, u_d = 2.5 x 10^{-6} eV and g_{ep} = 2.0 x 10^{-6} eV, one obtains the equation;

$$S = \left(\frac{1}{T} + 0.013\right) e^{-\frac{76}{T}} \tag{4.159}$$

iii) Substituting in eq. (4.145) for E_p = 3.5 x 10^{-6} eV, E_d = 2.0 x 10^{-6} eV , t_{pd} = 1.6 x 10^{-6} eV, u_d = 2.5 x 10^{-6} eV and g_{ep} = 0 eV, one obtains the equation;

$$S = \left(\frac{1}{T} + 0.014\right) e^{-\frac{74}{T}} \tag{4.160}$$

iv) Substituting in eq. (4.145) for E_p = 3.5 x 10^{-6} eV, E_d = 2.0 x 10^{-6} eV , t_{pd} = 1.6 x 10^{-6} eV, u_d = 2.5 x 10^{-6} eV and g_{ep} = 2.0 x 10^{-6} eV, one obtains the equation;

$$S = \left(\frac{1}{T} + 0.011\right) e^{-\frac{92}{T}} \tag{4.161}$$

Using equations (4.158), (4.159), (4.160) and (4.161), numerical values of S against T were calculated and recorded in Table 4 in appendix C.

From Table 4 in appendix III, graphs of values of S against T were drawn as shown in Figure (4.4)

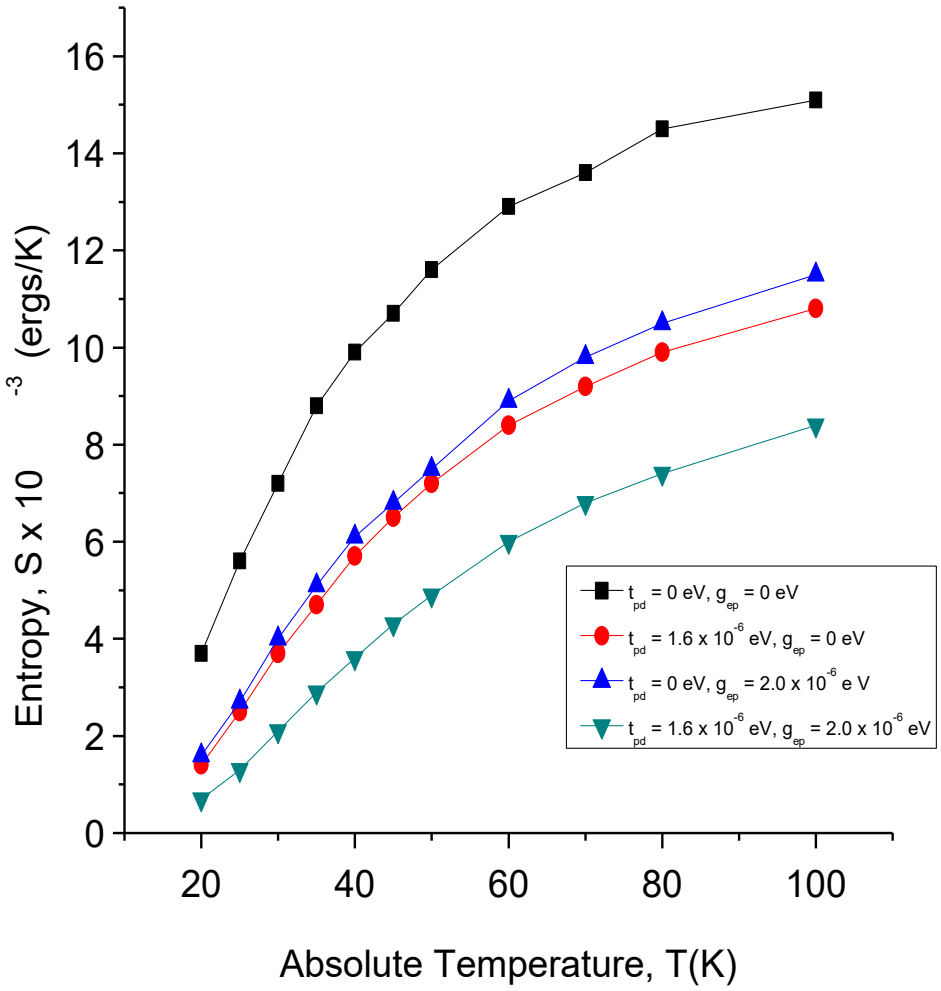

Figure 4.4: Variation of Entropy with absolute Temperature for YBaCuO

From Figure (4.4) above, *S* increases with absolute temperature. The increase is large for lower values of absolute temperature as compared to higher values of absolute temperature. The graphs above change from linear to non – linear at temperatures of 35 K, 40 K, 40 K and 50 K respectively. These occur at entropy of 9.0 x 10^{-3} ergs/K, 5.0 X 10^{-3} ergs / K, 4.3 X 10^{-3} ergs/ K and 4.0 x 10^{-3} ergs/K respectively.

These results show that as t_{pd} and g_{ep} are increased, the value of S reduce. However, the transition temperature increase with increase in values of t_{pd} and g_{ep}.

4.5.2. Effect of t_{pd} and g_{ep} on S and T_c (For $E_p = 5.5 \times 10^{-6}$eV and $u_d = 5.5 \times 10^{-6}$ eV) for YBaCuO.

Eqn. (4.145) was used to investigate the effects of t_{pd} and g_{ep} on S. The values of the other parameters in eq. (4.132) were increased and kept constant at $E_p = 5.5 \times 10^{-6}$ eV, $E_d = 2.0 \times 10^{-6}$ eV and $u_d = 5.5 \times 10^{-6}$ eV. Four equations relating entropy and absolute temperature were obtained from eq. (4.145) as follows;

i) Substituting in eq. (4.145) for $E_p = 5.5 \times 10^{-6}$ eV, $E_d = 2.0 \times 10^{-6}$ eV , $t_{pd} = 0$ eV, $u_d = 5.5 \times 10^{-6}$ eV $g_{ep} = 0$ eV and $k = 8.6 \times 10^{-5}$ eV/K one obtains the equation;

$$S = \left(\frac{1}{T} + 0.011\right) e^{-\frac{93}{T}} \tag{4.162}$$

ii) Substituting in eq. (4.145) for $E_p = 5.5 \times 10^{-6}$ eV, $E_d = 2.0 \times 10^{-6}$ eV , $t_{pd} = 0$ eV, $u_d = 5.5 \times 10^{-6}$ eV , $g_{ep} = 2.0 \times 10^{-6}$ eV and $k = 8.6 \times 10^{-5}$ eV/K, one obtains the equation;

$$S = \left(\frac{1}{T} + 0.0091\right) e^{-\frac{110}{T}} \tag{4.163}$$

iii) Substituting in eq. (4.145) for $E_p = 5.5 \times 10^{-6}$ eV, $E_d = 2.0 \times 10^{-6}$ eV , $t_{pd} = 1.6 \times 10^{-6}$ eV, $u_d = 5.5 \times 10^{-6}$ eV , $g_{ep} = 0$ eV, and $k = 8.6 \times 10^{-5}$ eV, one obtains the equation;

$$S = \left(\frac{1}{T} + 0.0092 \right) e^{-\frac{109}{T}} \tag{4.164}$$

iv) Substituting in eq. (4.145) for E_p = 5.5 x 10^{-6} eV, E_d = 2.0 x 10^{-6} eV , t_{pd} = 1.6 x 10^{-6} eV, u_d = 5.5 x 10^{-6} eV, g_{ep} = 2.0 x 10^{-6} eV,and k = 8.6 x 10^{-5} eV, one obtains the equation;

$$S = \left(\frac{1}{T} + 0.0079 \right) e^{-\frac{127}{T}} \tag{4.165}$$

Using equations (4.162), (4.163), (4.164) and (4.165), numerical values of S against T were calculated and recorded in Table 5 in appendix C.

From Table 5 in appendix C, graphs of numerical values of S against T were drawn as shown in Figure (4.5).

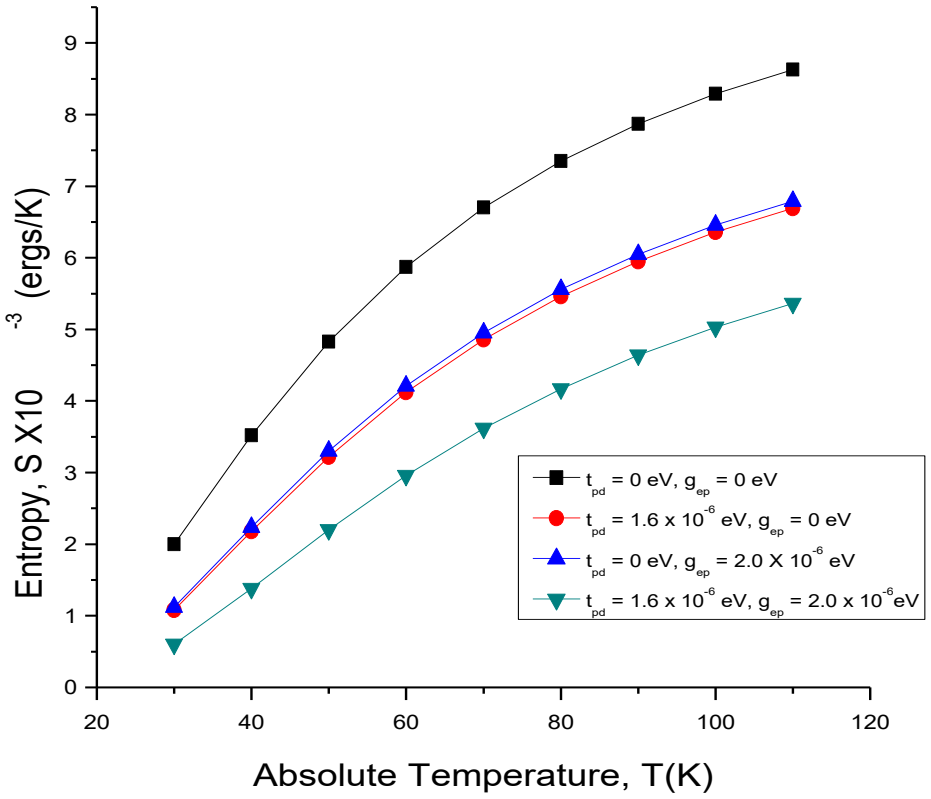

Figure 4.5: Variation of entropy with absolute temperature for YBaCuO

From Figure (4.5) above, S increases with absolute temperature.

The graphs change from linear to non linear at temperatures of 45 K, 60 K, 60 K and 70 K respectively. This occur at entropy of 4.8 x 10^{-3} ergs/K, 4.3 x 10^{-3} ergs/K, 4.2 X 10^{-3} ergs/ K and 3.5 x 10^{-3} ergs/K respectively.

These results show that as t_{pd} and g_{ep} are increased, the values of S reduce but values of T_c increase.

4.5.3 Effect of t_{pd} and g_{ep} on S and T_c (For $E_p = 7.5 \times 10^{-6}$ eV and $u_d = 6.5 \times 10^{-6}$ eV) for YBaCuO.

Eqn. (4.145) was used to investigate the effects of t_{pd} and g_{ep} on C_v. The values of the other parameters were kept constant at $E_p = 7.5 \times 10^{-6}$ eV, $E_d = 2.0 \times 10^{-6}$ eV and $u_d = 6.5 \times 10^{-6}$ eV. Four equations relating specific heat and absolute temperature were obtained from eq. (4.145) as follows;

i) Substituting in eq. (4.145) for $E_p = 7.5 \times 10^{-6}$ eV, $E_d = 2.0 \times 10^{-6}$ eV , $t_{pd} = 0$ eV, $u_d = 6.5 \times 10^{-6}$ eV , $g_{ep} = 0$ eV and $k = 8.6 \times 10^{-6}$ eV, one obtains the equation;

$$S = \left(\frac{1}{T} + 0.0092\right) e^{-\frac{109}{T}} \tag{4.166}$$

ii) Substituting in eq. (4.145) for $E_p = 7.5 \times 10^{-6}$ eV, $E_d = 2.0 \times 10^{-6}$ eV , $t_{pd} = 0$ eV, $u_d = 6.5 \times 10^{-6}$ eV , $g_{ep} = 2.0 \times 10^{-6}$ eV and $k = 8.6 \times 10^{-5}$ eV, one obtains the equation;

$$S = \left(\frac{1}{T} + 0.0079\right) e^{-\frac{126}{T}} \tag{4.167}$$

iii) Substituting in eq. (4.145) for $E_p = 7.5 \times 10^{-6}$ eV, $E_d = 2.0 \times 10^{-6}$ eV , $t_{pd} = 1.6 \times 10^{-6}$ eV, $u_d = 6.5 \times 10^{-6}$ eV , $g_{ep} = 0$ eV, and $k = 8.6 \times 10^{-6}$ eV,one obtains the equation;

$$S = \left(\frac{1}{T} + 0.0082\right) e^{-\frac{122}{T}} \tag{4.168}$$

iv) Substituting in eq. (4.145) for E_p = 7.5 x 10^{-6} eV, E_d = 2.0 x 10^{-6} eV , t_{pd} = 1.6 x 10^{-6} eV, u_d = 6.5 x 10^{-6} eV , g_{ep} = 2.0 x 10^{-6} eV, k = 8.6 x 10^{-6} eV one obtains the equation;

$$S = \left(\frac{1}{T} + 0.0070\right) e^{-\frac{143}{T}} \qquad (4.169)$$

Using equations (4.166), (4.167), (4.168) and (4.169) numerical values of S against T were calculated and recorded in Table 6, appendix C.

From Table 6 in appendix C, graphs of numerical values of S against T were drawn as shown in Figure (4.6).

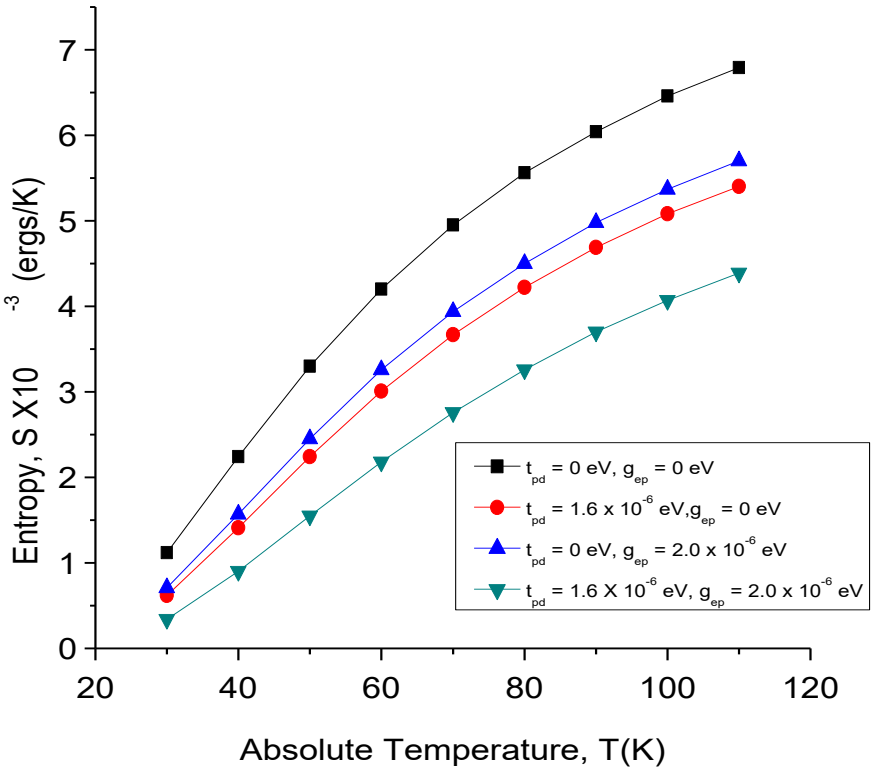

Figure 4.6: Variation of Entropy with absolute Temperature for YBaCuO

From Figure (4.6) above, S increases with absolute temperature. The graphs change from linear to non linear at temperatures of 70 K, 80 K, 80 K and 90 K with corresponding values of entropy of 4.2 x 10^{-3} ergs/K, 3.8 X 10^{-3} ergs/K, 3.5 X 10^{-3} ergs/K and 3.0 x 10^{-3} ergs/K respectively.

These values of S are lower compared with values obtained in section 4.5, but the values of T_c are higher.

These results show that as t_{pd} and g_{ep} are increased, the value of S reduce but values of T_c increase.

CHAPTER FIVE

CONCLUSIONS AND RECOMMENDATIONS

5.1 Conclusions

The combined effects of electron – phonon and Coulomb interactions on the transition temperature of high - T_c cuprate superconductors were investigated by deriving the electron – phonon and Coulomb interaction Hamiltonian using the frozen phonon method. The expectation value of the derived electron – phonon and Coulomb interaction Hamiltonian was calculated using second quantization and many body techniques.

The effects of E_p, E_d, t_{pd}, u_d and g_{ep} on T_c were determined from the results of specific heat against absolute temperature and graphs of entropy against absolute temperature. From the study, it was found out that

(i) the electron Phonon and Coulomb interaction Hamiltonian is

$$H_{epc} = g_{ep}\sum_{k,\sigma}(\alpha^{+}_{k,\sigma}\alpha_{k+X,\sigma} + \alpha^{+}_{k+X,\sigma}\alpha_{k,\sigma}) + E_p\sum_{i}a^{+}_{ip}a_{ip} + E_d\sum_{j}a^{+}_{jd}a_{jd} + t_{pd}\sum_{ij}(a^{+}_{ip}a_{jd} + a^{+}_{jd}a_{ip}) + u_d\sum_{ji}a^{+}_{jd}a^{+}_{jd}a_{ip}a_{ip}$$

(ii) the expectation value of the electron – phonon and Coulomb interaction Hamiltonian is given by

$$E_1 = 303E_p + 980E_d + 888t_{pd} + 800u_d + 720g_{ep}$$

(iii) increase in E_p, E_d, t_{pd}, u_d and g_{ep} in cuprate superconductors leads increase in transition temperature from 30 K to 90 K.

It can therefore be concluded that the role of long range electron – phonon and Coulomb interactions is to increase the transition temperature of cuprate superconductors.

5.2 Recommendations

In future,

i) electron – dipole and dipole – dipole interactions effects on superconductivity may be investigated

ii) internal electric and magnetic fields effects on superconductivity may be studied

iii) effects of internal electric and magnetic fields on onsite energy of copper (E_d) and onsite energy of oxygen (E_p) in cuprate superconductors may be investigated

REFERENCES

Alexandrov, A. S., & Mott, N. F. (1995).*Polarons & bipolarons* (p. 191). Singapore: World Scientific.

Alexandrov, A. S., Zhao, G. M., Keller, H., Lorenz, B., Wang, Y. S., & Chu, C. W. (2001).Evidence for polaronic Fermi liquid in manganites.*Physical Review B*, *64*(14), 140404.

Alexandrov, A. S., & Kornilovitch, P. E. (2002).The Fröhlich-Coulomb model of high-temperature superconductivity and charge segregation in the cuprates.*Journal of Physics: Condensed Matter*, *14*(21), 5337.

Alexandrov, A. S. (2003). *Theory of superconductivity: from weak to strong coupling*. CRC Press.

Alexandrov, A. S. (2007). Bose–Einstein condensation of strongly correlated electrons and phonons in cuprate superconductors. *Journal of Physics: Condensed Matter*, *19*(12), 125216.

Anderson, P. W., Lee, P. A., Randeria, M., Rice, T. M., Trivedi, N., & Zhang, F. C. (2004). The physics behind high-temperature superconducting cuprates: the'plain vanilla'version of RVB. *Journal of Physics: Condensed Matter*, *16*(24), R755.

Anisimov, V. I., Zaanen, J., & Andersen, O. K. (1991). Band theory and Mott insulators: Hubbard U instead of Stoner I. *Physical Review B*, *44*(3), 943.

Anisimov, V. I., Korotin, M. A., Mylnikova, A. S., Kozhevnikov, A. V., Korotin, D. M., & Lorenzana, J. (2004). Computation of stripes in cuprates within the LDA+ U method.*Physical Review B*, *70*(17), 172501.

Armitage, N. P., Ronning, F., Lu, D. H., Kim, C., Damascelli, A., Shen, K. M., ...& Tokura, Y. (2002). Doping dependence of an n-type cuprate superconductor investigated by angle-resolved photoemission spectroscopy. *Physical review letters*, *88*(25), 257001.

Auerbach, A. (2012). *Interacting electrons and quantum magnetism*.Springer Science & Business Media.

Bardeen, J., Cooper, L. N., & Schrieffer, J. R. (1957).Theory of superconductivity.*Physical Review*, *108*(5), 1175.

Bazak, J. D. (2013). Explorations of a Pi-Striped, d-Wave Superconductor.

Bednorz, J. G., & Müller, K. A. (1986).Possible high Tc superconductivity in the Ba− La− Cu− O system.*ZeitschriftfürPhysik B Condensed Matter*, *64*(2), 189-193.

Bohnen, K. P., Heid, R., & Krauss, M. (2003).Phonon dispersion and electron-phonon interaction for YBa2Cu3O7 from first-principles calculations.*EPL (Europhysics Letters)*, *64*(1), 104.

Borisenko, S. V., Kordyuk, A. A., Koitzsch, A., Kim, T. K., Nenkov, K. A., Knupfer, M.& Berger, H. (2004). Circular dichroism in angle-resolved photoemission spectra of under-and overdoped Pb-Bi2212.*Physical review letters*, *92*(20), 207001.

Bozovic, I., Kim, J. H., Harris Jr, J. S., Eom, C. B., Phillips, J. M., & Cheung, J. T. (1994). Reflectance and Raman spectra of metallic oxides, LaSrCuO and CaSrRuO: resemblance to superconducting cuprates. *Physical review letters*, *73*(10), 1436.

Calandra, M., & Mauri, F. (2007). Electron-phonon coupling and electron self-energy in electron-doped graphene: Calculation of angular-resolved photoemission spectra. *Physical Review B*, *76*(20), 205411.

Campuzano, J. C., Norman, M. R., & Randeria, M. (2004).Photoemission in the High-T c Superconductors.In *The Physics of Superconductors* (pp. 167-273).Springer Berlin Heidelberg.

Carbone, F., Gedik, N., Lorenzana, J., & Zewail, A. H. (2010).Real-time observation of cuprates structural dynamics by ultrafast electron crystallography.*Advances in Condensed Matter Physics*, *2010*.

Chen, X. J., Struzhkin, V. V., Wu, Z., Lin, H. Q., Hemley, R. J., & Mao, H. K. (2007). Unified picture of the oxygen isotope effect in cuprate superconductors.*Proceedings of the National Academy of Sciences*, *104*(10), 3732-3735.

Chuang, Y. D., Gromko, A. D., Fedorov, A. V., Aiura, Y., Oka, K., Ando, Y., ... & Dessau, D. S. (2004). Bilayer splitting and coherence effects in optimal and underdoped Bi 2 Sr 2 CaCu 2 O 8+ δ. *Physical Review B*, *69*(9), 094515.

Clarke, D. G., Strong, S. P., & Anderson, P. W. (1995). Conductivity between Luttinger Liquids in the Confinement Regime and c-axis Conductivity in the Cuprate Superconductors.*Physical review letters*, *74*(22), 4499.

Coleman, P. (2007). Heavy fermions: Electrons at the edge of magnetism. *Handbook of magnetism and advanced magnetic materials*.

Comanac, A., de'Medici, L., Capone, M., & Millis, A. J. (2008).Optical conductivity and the correlation strength of high-temperature copper-oxide superconductors.*Nature Physics*, *4*(4), 287-290.

Cuk, T., Lu, D. H., Zhou, X. J., Shen, Z. X., Devereaux, T. P., & Nagaosa, N. (2005).A review of electron–phonon coupling seen in the high-Tc superconductors by angle-resolved photoemission studies (ARPES).*physica status solidi (b)*, *242*(1), 11-29.

Dagotto, E., Nazarenko, A., & Boninsegni, M. (1994).Flat quasiparticle dispersion in the 2D t-J model.*Physical review letters*, *73*(5), 728.

Dagotto, E. (1994). Correlated electrons in high-temperature superconductors. *Reviews of Modern Physics*, *66*(3), 763.

Dal Conte, S., Giannetti, C. L. A. U. D. I. O., Coslovich, G., Cilento, F., Bossini, D., Abebaw, T.& Parmigiani, F. (2012).Disentangling the electronic and phononic glue in a high-Tc superconductor.*Science*, *335*(6076), 1600-1603.

Ding, H., Engelbrecht, J. R., Wang, Z., Campuzano, J. C., Wang, S. C., Yang, H. B.& Hinks, D. G. (2001). Coherent quasiparticle weight and its connection to high-Tc superconductivity from angle-resolved photoemission.*Physical review letters*, *87*(22), 227001.

Dubroka, A., Rössle, M., Kim, K. W., Malik, V. K., Munzar, D., Basov, D. N.,& Bernhard, C. (2011). Evidence of a Precursor Superconducting Phase at Temperatures as High as 180 K in R Ba 2 Cu 3 O 7− δ (R= Y, Gd, Eu) Superconducting Crystals from Infrared Spectroscopy. *Physical review letters*, *106*(4), 047006.

Emery, V. J. (1987).Theory of high-Tc superconductivity in oxides.*Physical review letters*, *58*(26), 2794.

Flores-Livas, J. A., Debord, R., Botti, S., San Miguel, A., Pailhès, S., & Marques, M. A. (2011). Superconductivity in layered binary silicides: A density functional theory study. *Physical Review B, 84*(18), 184503.

Fong, H. F., Keimer, B., Anderson, P. W., Reznik, D., Doğan, F., & Aksay, I. A. (1995).Phonon and Magnetic Neutron Scattering at 41 meV in YB a 2 C u 3 O 7.*Physical review letters*, *75*(2), 316.

Fu, C. L., & Freeman, A. J. (1988).Multilayer reconstruction and vibrational properties of W (001).*Physical Review B*, *37*(5), 2685.

Gabovich, A. M., Voitenko, A. I., Annett, J. F., & Ausloos, M. (2001).Charge-and spin-density-wave superconductors.*Superconductor Science and Technology*, *14*(4), R1.

Gadermaier, C., Alexandrov, A. S., Kabanov, V. V., Kusar, P., Mertelj, T., Yao, X., ...& Mihailovic, D. (2010). Electron-phonon coupling in high-temperature cuprate superconductors determined from electron relaxation rates. *Physical review letters*, *105*(25), 257001.

Graf, J. (2008). *Kinks in the angle resolved photoemission and inelastic x-ray spectra of high temperature superconductors* (Doctoral dissertation, Swiss Federal Institute of Technology).

Graf, J., d'Astuto, M., Jozwiak, C., Garcia, D. R., Saini, N. L., Krisch, M., ...& Lanzara, A. (2008). Bond stretching phonon softening and kinks in the angle-resolved photoemission spectra of optimally doped Bi 2 Sr 1.6 La 0.4 Cu 2 O 6+ δ superconductors. *Physical Review Letters*, *100*(22), 227002.

Gulácsi, M., & Chan, R. (2001). High-temperature superconductivity: The attractive Up regime. *Journal of superconductivity*, *14*(6), 651-658.

Gunnarsson, O., & Rösch, O. (2008). Interplay between electron–phonon and Coulomb interactions in cuprates. *Journal of Physics: Condensed Matter*, *20*(4), 043201.

Gweon, G. H., Sasagawa, T., Zhou, S. Y., Graf, J., Takagi, H., Lee, D. H., &Lanzara, A. (2004).An unusual isotope effect in a high-transition-temperature superconductor.*Nature*, *430*(6996), 187-190.

Haugan, T., Barnes, P. N., Wheeler, R., Meisenkothen, F., & Sumption, M. (2004).Addition of nanoparticle dispersions to enhance flux pinning of the YBa2Cu3O7-x superconductor.*Nature*, *430*(7002), 867-870.

Hardy, T. M., Hague, J. P., Samson, J. H., & Alexandrov, A. S. (2009). Superconductivity in a Hubbard-Fröhlich model and in cuprates. *Physical Review B*, *79*(21), 212501.

Hohenberg, P., & Kohn, W. (1964).Inhomogeneous electron gas.*Physical review*, *136*(3B), B864.

Horsch, P., & Khaliullin, G. (2005).Doping dependence of density response and bond-stretching phonons in cuprates.*Physica B: Condensed Matter*, *359*, 620-622.

Hwang, J., Timusk, T., &Gu, G. D. (2004). High-transition-temperature superconductivity in the absence of the magnetic-resonance mode.*Nature*, *427*(6976), 714-717.

Ino, A., Kim, C., Mizokawa, T., Shen, Z. X., Fujimori, A., Takaba, M., ...& Uchida, S. (1999). Fermi Surface and Band Dispersion in La 2-x Sr x CuO 4.*Journal of the Physical Society of Japan*, *68*(5), 1496-1499.

Ioffe, L. B., & Wiegmann, P. B. (1990).Linear temperature dependence of resistivity as evidence of gauge interaction.*Physical review letters*, *65*(5), 653.

Johnston, S., Vernay, F., Moritz, B., Shen, Z. X., Nagaosa, N., Zaanen, J., & Devereaux, T. P. (2010).Systematic study of electron-phonon coupling to oxygen modes across the cuprates.*Physical Review B*, *82*(6), 064513.

Kaminski, A., Rosenkranz, S., Fretwell, H. M., Campuzano, J. C., Li, Z., Raffy, H., ...& Höchst, H. (2002). Spontaneous breaking of time-reversal symmetry in the pseudogap state of a high-Tc superconductor.*Nature*, *416*(6881), 610-613.

Kaldis, E., Liarokapis, E., & Müller, K. A. (Eds.). (2012). *High-Tc superconductivity 1996: ten years after the discovery* (Vol. 343). Springer Science & Business Media.

Khanna, K. M., & Kirui, M. S. K. (2002).Anharmonic apical oxygen vibration in high T~ c superconductors.*Indian Journal of Pure and Applied Physics*, *40*(12), 887-916.

Kim, J. H., Levin, K., Wentzcovitch, R., & Auerbach, A. (1991).Electron-phonon interactions in the high-temperature superconductors.*Physical Review B*, *44*(10), 5148.

Kim, Y. J., Hill, J. P., Komiya, S., Ando, Y., Casa, D., Gog, T., & Venkataraman, C. T. (2004).Doping dependence of charge-transfer excitations in La 2− x Sr x CuO 4.*Physical Review B*, *70*(9), 094524.

Kiryukhin, V., Kim, Y. J., Thomas, K. J., Chou, F. C., Erwin, R. W., Huang, Q., ... &Birgeneau, R. J. (2001). Magnetic properties of the S= 1 2 quasi-one-dimensional antiferromagnetCaCu 2 O 3. *Physical Review B*, *63*(14), 144418.

Klemm, R. A. (2012). *Layered Superconductors* (Vol. 153).Oxford University Press.

Klumper, A., Schadschneider, A., & Zittartz, J. (1991).Equivalence and solution of anisotropic spin-1 models and generalized tJ fermion models in one dimension.*Journal of Physics A: Mathematical and General*, *24*(16), L955.

Kohn, W., & Luttinger, J. M. (1965).New mechanism for superconductivity.*Physical Review Letters*, *15*(12), 524.

Kohn, W., & Sham, L. J. (1965).Self-consistent equations including exchange and correlation effects.*Physical Review*, *140*(4A), A1133.

Kordyuk, A. A., Borisenko, S. V., Knupfer, M., & Fink, J. (2003).Measuring the gap in angle-resolved photoemission experiments on cuprates.*Physical Review B*, *67*(6), 064504.

Kordyuk, A. A., Zabolotnyy, V. B., Evtushinsky, D. V., Kim, T. K., Morozov, I. V., Kulić, M. L., ... & Borisenko, S. V. (2011). Angle-resolved photoemission spectroscopy of superconducting LiFeAs: Evidence for strong electron-phonon coupling. *Physical Review B*, *83*(13), 134513.

Lanzara, A., Bogdanov, P. V., Zhou, X. J., Kellar, S. A., Feng, D. L., Lu, E. D., ... & Shen, Z. X. (2001). Evidence for ubiquitous strong electron–phonon coupling in high-temperature superconductors.*Nature*, *412*(6846), 510-514.

Laughlin, R. B. (1988). Superconducting ground state of noninteracting particles obeying fractional statistics. *Physical review letters*, *60*(25), 2677.

Lee, P. A., Nagaosa, N., & Wen, X. G. (2006). Doping a Mott insulator: Physics of high-temperature superconductivity. *Reviews of modern physics*, *78*(1), 17.

Le Tacon, M., Sacuto, A., Georges, A., Kotliar, G., Gallais, Y., Colson, D., & Forget, A. (2006). Two energy scales and two distinct quasiparticle dynamics in the superconducting state of underdoped cuprates. *Nature Physics*, *2*(8), 537-543.

Leggett, A. J. (1996). Interlayer tunneling models of cuprate superconductivity: Implications of a recent experiment. *Science*, *274*(5287), 587.

Li, Y., Balédent, V., Yu, G., Barišić, N., Hradil, K., Mole, R. A., ...& Greven, M. (2010). Hidden magnetic excitation in the pseudogap phase of a high-Tc superconductor.*Nature*, *468*(7321), 283-285.

Lorenz, B., Perner, O., Eckert, J., & Chu, C. W. (2006).Superconducting properties of nanocrystalline MgB2. *Superconductor Science and Technology*, *19*(9), 912.

Lu, D., Vishik, I. M., Yi, M., Chen, Y., Moore, R. G., & Shen, Z. X. (2012). Angle-resolved photoemission studies of quantum materials. *Annu. Rev. Condens. Matter Phys.*, *3*(1), 129-167.

Macridin, A., Moritz, B., Jarrell, M., & Maier, T. (2012).Suppression of superconductivity in the Hubbard model by buckling and breathing phonons.*Journal of Physics: Condensed Matter*, *24*(47), 475603.

Maekawa, S. (2012).High Temperature Superconductors as. In *Physics and Chemistry of Transition Metal Oxides: Proceedings of the 20th Taniguchi Symposium, Kashikojima, Japan, May 25–29, 1998* (Vol. 125, p. 136). Springer Science & Business Media.

Mandal, S., Cohen, R. E., & Haule, K. (2014).Strong pressure-dependent electron-phonon coupling in FeSe.*Physical Review B*, *89*(22), 220502.

Matsui, H., Terashima, K., Sato, T., Takahashi, T., Fujita, M., & Yamada, K. (2005). Direct Observation of a Nonmonotonic d x 2− y 2-Wave Superconducting Gap in the Electron-Doped High-Tc Superconductor Pr 0.89 LaCe 0.11 CuO 4. *Physical review letters*, *95*(1), 017003.

McMahan, A. K., Martin, R. M., & Satpathy, S. (1988). Calculated effective Hamiltonian for La 2 Cu O 4 and solution in the impurity Anderson approximation.*Physical Review B*, *38*(10), 6650.

Mc Queen, R. _.J., Petrov, Y., Egami, T., Yethiraj, M., Shirane, G., & Endoh, Y. (1999). Anomalous dispersion of LO phonons in La 1.85 Sr 0.15 CuO 4 at low temperatures. *Physical Review Letters*, *82*(3), 628.

Meissner, W., &Ochsenfeld, R. (1933).Einneuereffektbeieintritt der supraleitfähigkeit.*Naturwissenschaften*, *21*(44), 787-788.

Mishchenko, A. S. (2009). Electron-phonon coupling in underdoped high-temperature superconductors. *Physics-Uspekhi*, *52*(12), 1193-1212.

Mott, N. (1990). On metal-insulator transitions.*Journal of Solid State Chemistry*, *88*(1), 5-7.

Newns, D. M., Pattnaik, P. C., Rasolt, M., & Papaconstantopoulos, D. A. (1988).Theory of high-Tc superconductors within a realistic Anderson lattice model.*Physical Review B*, *38*(10), 7033.

Nyawere, P. O., & Khanna, K. M. (2011).Specific heat jump and transition temperature T_C for La2− xBaxCuO4.*Indian Journal of Pure & Applied Physics*, *49*, 627-632.

Ohkawa, F. J. (2007). Origin and roles of a strong electron-phonon interaction in cuprate oxide superconductors.*Physical Review B*, *75*(6), 064503.

Onnes, H. K. (1911). The superconductivity of mercury.*Comm. Phys. Lab. Univ. Leiden*, *122*, 124.

Pasupathy, A. N., Pushp, A., Gomes, K. K., Parker, C. V., Wen, J., Xu, Z., ... & Yazdani, A. (2008). Electronic origin of the inhomogeneous pairing interaction in the high-Tc superconductor Bi2Sr2CaCu2O8+ δ. *Science*, *320*(5873), 196-201.

Pavarini, E., Dasgupta, I., Saha-Dasgupta, T., Jepsen, O., & Andersen, O. K. (2001).Band-structure trend in hole-doped cuprates and correlation with Tc max.*Physical Review Letters*, *87*(4), 047003.

Pickett, W. E. (1989). Electronic structure of the high-temperature oxide superconductors.*Reviews of Modern Physics*, *61*(2), 433.

Pilgram, S., Rice, T. M., &Sigrist, M. (2006).Role of inelastic tunneling through the insulating barrier in scanning-tunneling-microscope experiments on cuprate superconductors.*Physical review letters*, *97*(11), 117003.

Pintschovius, L., & Braden, M. (1999).Anomalous dispersion of LO phonons in La 1.85 Sr 0.15 CuO 4.*Physical Review B*, *60*(22), R15039.

Pintschovius, L. (2005). Electron–phonon coupling effects explored by inelastic neutron scattering.*physica status solidi (b)*, *242*(1), 30-50.

Plakida, N. (2010). *High-Temperature Cuprate Superconductors: Experiment, Theory, and Applications* (Vol. 166). Springer Science & Business Media.

Reizer, M. Y. (1989). Effective electron-electron interaction in metals and superconductors.*Physical Review B*, *39*(3), 1602.

Reznik, D., Pintschovius, L., Ito, M., Iikubo, S., Sato, M., Goka, H., ...& Tranquada, J. M. (2006). Electron–phonon coupling reflecting dynamic charge inhomogeneity in copper oxide superconductors.*Nature*, *440*(7088), 1170-1173.

Reznik, D., Sangiovanni, G., Gunnarsson, O., &Devereaux, T. P. (2008).Photoemission kinks and phonons in cuprates.*Nature*, *455*(7213), E6-E7.

Rösch, O., & Gunnarsson, O. (2004).Electron-phonon interaction in the t− J model.*Physical review letters*, *92*(14), 146403.

Sanchez, A., & Navau, C. (2001).Magnetic properties of finite superconducting cylinders. I. Uniform applied field. *Physical Review B*, *64*(21), 214506.

Sato, T., Kamiyama, T., Naitoh, Y., Takahashi, T., Chong, I., Terashima, T., & Takano, M. (2001). Fermi surface and superconducting gap in superstructure-free Bi 1.80 Pb 0.38 Sr 2.01 CuO 6− δ. *Physical Review B*, *63*(13), 132502.

Savrasov, S. Y., & Andersen, O. K. (1996).Linear-Response Calculation of the Electron-Phonon Coupling in Doped CaCu O 2.*Physical review letters*, *77*(21), 4430.

Schabel, M. C., Park, C. H., Matsuura, A., Shen, Z. X., Bonn, D. A., Liang, R., & Hardy, W. N. (1998). Angle-resolved photoemission on untwinned YBa 2 Cu 3 O 6.95. I. Electronic structure and dispersion relations of surface and bulk bands. *Physical Review B*, *57*(10), 6090.

Sénéchal, D., Perez, D., & Plouffe, D. (2002). Cluster perturbation theory for Hubbard models. *Physical Review B*, *66*(7), 075129.

Sentef, M., Kemper, A. F., Moritz, B., Freericks, J. K., Shen, Z. X., & Devereaux, T. P. (2013).Examining electron-boson coupling using time-resolved spectroscopy.*Physical Review X*, *3*(4), 041033.

Shen, K. M., Ronning, F., Meevasana, W., Lu, D. H., Ingle, N. J. C., Baumberger, F., ...& Shen, Z. X. (2007). Angle-resolved photoemission studies of lattice polaron formation in the cuprate Ca 2 Cu O 2 Cl 2. *Physical Review B*, *75*(7), 075115.

Sherman, E. Y., & Ambrosch-Draxl, C. (2000). Multiband electron-phonon coupling in the cuprates: Raman scattering and charge fluctuations. *Physical Review B*, *62*(14), 9713.

Sherrington, D., & Von Molnar, S. (1975). Polaronic effects on interconfigurational fluctuation lifetimes in intermediate valence systems. *Solid State Communications*, *16*(12), 1347-1350.

Sirker, J., & Klümper, A. (2002).Thermodynamics and crossover phenomena in the correlation lengths of the one-dimensional t-J model.*Physical Review B*, *66*(24), 245102.

Succi, S. (2001). *The lattice Boltzmann equation: for fluid dynamics and beyond*. Oxford university press.

Tohyama, T., & Maekawa, S. (2000).Angle-resolved photoemission in high Tc cuprates from theoretical viewpoints.*Superconductor Science and Technology*, *13*(4), R17.

Uchida, S. I. (2015). Copper Oxide Superconductors.In *High Temperature Superconductivity* (pp. 23-59).Springer Japan.

Varma, C. M., Littlewood, P. B., Schmitt-Rink, S., Abrahams, E., &Ruckenstein, A. E. (1989). Phenomenology of the normal state of Cu-O high-temperature superconductors.*Physical Review Letters*, *63*(18), 1996.

Von Stetten, E. C., Berko, S., Li, X. S., Lee, R. R., Brynestad, J., Singh, D., ...& Cohen, R. E. (1988). High Sensitivity of Positrons to Oxygen Vacancies and to Copper-Oxygen Chain Disorder in Y Ba 2 Cu 3 O 7− x. *Physical review letters*, *60*(21), 2198.

Wagner, J., Hanke, W., & Scalapino, D. J. (1991).Optical, magnetic, and single-particle excitations in the multiband Hubbard model for cuprate superconductors.*Physical Review B*, *43*(13), 10517.

Wolf, E. L. (2011). *Principles of electron tunneling spectroscopy*.Oxford University Press.

Xiang, Y. Y., Wang, F., Wang, D., Wang, Q. H., & Lee, D. H. (2012).High-temperature superconductivity at the FeSe/SrTiO 3 interface.*Physical Review B*, *86*(13), 134508.

Yildirim, T. (2013). Ferroelectric soft phonons, charge density wave instability, and strong electron-phonon coupling in BiS 2 layered superconductors: A first-principles study. *Physical Review B*, *87*(2), 020506.

Yokoya, T., Kiss, T., Chainani, A., Shin, S., Nohara, M., & Takagi, H. (2001). Fermi surface sheet-dependent superconductivity in 2H-NbSe2.*Science*, *294*(5551), 2518-2520.

Yokoya, T., Baba, T., Tsuda, S., Kiss, T., Chainani, A., Shin, S., ...& Oguchi, T. (2006). Anisotropic s-wave superconductors studied by angle-resolved photoemission spectroscopy.*Journal of Physics and Chemistry of Solids*, *67*(1), 277-281.

Yoshida, T., Zhou, X. J., Lu, D. H., Komiya, S., Ando, Y., Eisaki, H., ...& Fujimori, A. (2007). Low-energy electronic structure of the high-Tc cuprates La2− xSrxCuO4 studied by angle-resolved photoemission spectroscopy.*Journal of Physics: Condensed Matter*, *19*(12), 125209.

Yu, G., Li, Y., Motoyama, E. M., Zhao, X., Barišić, N., Cho, Y., ...& Greven, M. (2010). Magnetic resonance in the model high-temperature superconductor HgBa 2 CuO 4+ δ. *Physical Review B*, *81*(6), 064518.

Zhang, F. C., & Rice, T. M. (1988).Effective Hamiltonian for the superconducting Cu oxides.*Physical Review B*, *37*(7), 3759.

Zhang, G., Lu, X., Zhang, T., Qu, J., Wang, W., Li, X., & Yu, S. (2006).Microstructure and superconductivity of highly ordered YBa2Cu3O7− δ nanowire arrays.*Nanotechnology*, *17*(16), 4252.

Zhou, X. J., Cuk, T., Devereaux, T., Nagaosa, N., & Shen, Z. X. (2006).Angle-resolved photoemission spectroscopy on electronic structure and electron-phonon coupling in cuprate superconductors.*arXiv preprint cond-mat/0604284*.

Zhou, X. J., Cuk, T., Devereaux, T., Nagaosa, N., & Shen, Z. X. (2007). Angle-Resolved Photoemission Spectroscopy on Electronic Structure and electron–Phonon Coupling in Cuprate Superconductors. In *Handbook of High-Temperature Superconductivity* (pp. 87-144).Springer New York.

APPENDICES

Appendix I: One Dimensional Electron – Phonon Transition Matrix Elements

In this section, we focus on a simplified one – dimensional (copper – oxygen chain) model for the purpose of obtaining insight into the electron – phonon interaction in the copper oxides. We consider only phonon modes that are most relevant to transport properties. For instance, the zone edge (**q=X**) phonon modes, identical to the Periels distortion, interact strongly with electrons by way of doubling the unit cell, (i,e., by Brilluoin zone folding). Therefore, phonon modes with this wave vector are important for transport. The zone center ($q=\Gamma$) modes, on the other hand, are more relevant for Raman scattering and less important for transport measurements. There are six **X** modes in one dimension, two of which are longitudinal (the oxygen and copper breathing modes), the remaining four are twofold – degenerate transverse modes.

To calculate the renormalized band – structure and the quasiparticle states in the infinite U_d limit, we may apply a slave boson formalism to a distorted (**X** mode) lattice. Within this approach, we extend the Anderson lattice Hamiltonain (Levin, et al., 1991)

$$H_{FP}^{1d} = \sum_{i,\sigma}\left[\sum_{n}\varepsilon_{d,n}^{0} d_{in\sigma}^{+} d_{in\sigma} + \sum_{m}\varepsilon_{p,m} C_{im\sigma}^{+} C_{im\sigma} + \sum_{<nm>} V_{n,m}\left(d_{in\sigma}^{+} e_{in} C_{im\sigma} + C_{im\sigma}^{+} e_{in}^{+} d_{in\sigma}\right)\right] \qquad (A1)$$

where the indices n and m = 1, 2 denote two positions for copper and oxygen orbitals, respectively, and <nm> denotes the pairs of nearest – neighbor copper – oxygen orbitals. The operators e_{in}^{+} and $d_{in\sigma}^{+}$ create Cu^{3+} and Cu^{2+} states, respectively, whereas C_{im}^{+} creates an electron at the mth oxygen site. Here, each phonon mode is characterized by the relative displacements of copper and oxygen ions. The quasiparticle operator $\Phi_{k,\sigma}$ of

the Hamiltonian can be expressed as a linear combination of copper and oxygen orbitals at different sites. We may write this in terms of a unitary matrix U

$$\Phi_{k,\sigma} = \begin{bmatrix} \alpha_{k,\sigma} \\ \alpha_{k+Q,\sigma} \\ \beta_{k,\sigma} \\ \beta_{k+Q,\sigma} \end{bmatrix} = \frac{1}{\sqrt{2}} \begin{bmatrix} \sin\theta_k & \sin\theta_{k+Q} & i\cos\theta_{k+Q} & \cos\theta_k \\ \sin\theta_k & -\sin\theta_{k+Q} & -i\cos\theta_{k+Q} & \cos\theta_k \\ \cos\theta_k & i\cos\theta_{k+Q} & \sin\theta_{k+Q} & -\sin\theta_k \\ \cos\theta_k & -i\cos\theta_{k+Q} & -\sin\theta_{k+Q} & -\sin\theta_k \end{bmatrix} \begin{bmatrix} d_{1,k,\sigma} \\ d_{2,k,\sigma} \\ C_{1,k,\sigma} \\ C_{2,k,\sigma} \end{bmatrix} \qquad (A2)$$

where Q = π/a denotes the wave vector for a frozen phonon mode. Here, α and β destroy quasiparticles in the antibonding and bonding bands, respectively.

Although the states at k_{BZ} are degenerate as a consequence of BZ folding, this degeneracy is lifted by ionic displacements because a distortion changes the renormalized parameters ε_d and r_n. The electron – phonon Hamiltonian, therefore, is given by Equation (3.9) with the distortion matrix

$$\overline{M}_D = U.M_D.U^+ \qquad (A3)$$

And

$$M_D = \begin{bmatrix} \varepsilon_{d,1} - \varepsilon_d & 0 & (r_1 e^{ik.\delta R} - r_0)e^{-ik} & (r_1 e^{-ik.\delta R} - r_0)e^{ik} \\ 0 & \varepsilon_{d,2} - \varepsilon_d & (r_2 e^{ik.\delta R} - r_0)e^{ik} & (r_2 e^{-ik.\delta R} - r_0)e^{-ik} \\ (r_1 e^{-ik.\delta R} - r_0)e^{ik} & (r_2 e^{ik.\delta R} - r_0)e^{-ik} & \varepsilon_{p,1} - \varepsilon_p & 0 \\ (r_1 e^{ik.\delta R} - r_0)e^{-ik} & (r_2 e^{ik.\delta R} - r_0)e^{ik} & 0 & \varepsilon_{p,2} - \varepsilon_p \end{bmatrix} \qquad (A4)$$

where δR is the displacement vector for either copper or oxygen ions and $k = ka/2$. The renormalized copper level and effective hybridization are $\varepsilon_{d,n} = \varepsilon^0_{d,n} + \lambda_n$ and

$r_n = e_n V(R \pm \delta R)$. There are two contributions to the matrix $\mathbf{M_D}$ which ultimately lead to electron – phonon scattering processes: one is the shift in Bloch waves by a lattice distortion and other is the change in electronic potential brought about by band renormalizations. The latter contribution is simplified as follows. We assume that the bare energy levels for copper sites are identical. The results do not change significantly even when this restriction is relaxed. As a consequence of screening, the energy level difference, $\varepsilon_{d,1}^0 - \varepsilon_{d,2}^0$, between the copper sites is mostly cancelled by the quantity $\lambda_1 - \lambda_2$ because Coulomb renormalizations tend to minimize the effects of an external perturbation by acting as a restoring force. Similarly, we extend this approximation to the oxygen sites

In order to evaluate Eq. (3.13), we need to account for the variational response functions in Eq. (3.17). We distinguish these functions by their origin. For instance, the hybridization screening response is brought about by either copper or oxygen motion which changes the copper – oxygen overlap integral. The variational response of copper, $S_{Cu} = V(\delta e_0 / \delta R)_{Cu}$ is small compared to that of oxygen, $S_O = V(\delta e_0 / \delta R)_O$. Although the x dependence of the response function S_{Cu} and S_O is different for x>0.12 $(e_0 > 0.1)$, both functions are proportional to e_0 for x < 0.12 (i.e., $S_{Cu} \propto e_0$ and $S_O \propto e_0$). On the other hand, the energy - level screening response, $S_\lambda = (\delta\lambda_0 / \delta R)$, is a direct consequence of charge transfer on the copper sites usually mediaited by an oxygen mode. S_λ varies as powers of e_0^2 for x < 0.12.

The oxygen breathing mode generates charge transfer between copper atoms. When two oxygen atoms are displaced 180^0 out of phase with one another, different local

environments are created for copper site. These inequivalent copper environments lead to a slight accumulation of charge on one site and depletion on the other. As a result, a static copper charge – density wave with wave vector X is formed, but the amplitude of this wave changes as a function of doping concentration. Because the charge fluctuation is strongly suppressed as half is approached, the amplitude is larger in the metallic regime than near the insulating regime. The electron – phonon transition matrix element for this mode, therefore, depends strongly on concentration. The oxygen breating mode corresponds to the following parameterization:

$$V_{1,1} = V_{1,2} \neq V_{2,1} = V_{1,2},\ e_1 = e_2 \quad \text{and} \quad \lambda_1 \neq \lambda_2 \tag{A5}$$

We write the matrix element for oxygen breathing mode near half – filling $(r_0 \to 0)$ as

$$g_{X,0} \approx \frac{1}{2} S_\lambda + \frac{8 r_0}{\varepsilon_d - \varepsilon p} (7 r_0 - S_0) \tag{A6}$$

The concentration dependence of the matrix element in Eq. (A6) comes from band renormalization (r_0 and λ_0). Therefore, we can easily deduce, based on counting powers of e_0, that Eq. (A6) varies as e_0^2 near the metal – insulator transition.

In the copper breathing mode, two copper ions are displaced in opposite directions. As a result, this motion leads to a formation of static oxygen CDW. The copper breathing mode corresponds to the parameterization

$$V_{1,1} = V_{2,1} \neq V_{1,2} = V_{2,2},\ e_1 = e_2 \quad \textit{and} \quad \lambda_1 = \lambda_2 \tag{A7}$$

Because only the oxygen environment is changed, the variational parameters associated with copper sites are identical. Although this copper mode is identical to that of an oxygen mode in many ways, it is translated by a copper – oxygen bond length. This transition leads to the following phase changes in Bloch waves:

$$M_{13} = M_{31}^{*} = (r_1 e^{ik.\delta R} - r)e^{ik} \rightarrow (r_2 e^{-ik.\delta R} - r_0)e^{-ik} \quad \text{(A8)}$$

$$M_{24} = M_{42}^{*} = (r_2 e^{-ik.\delta R} - r_0)e^{-ik} \rightarrow (r_1 e^{ik.\delta R} - r_0)e^{-ik} \quad \text{(A9)}$$

With this changes, the electron – phonon matrix element near the metal – insulator transition is expressed as

$$g_{X,Cu} \approx \frac{4r_0^2}{\varepsilon_d - \varepsilon_p}(2\bar{k}\cos 2\bar{k} - 7\sin 2\bar{k}) \quad \text{(A10)}$$

Although the matrix element for copper does not have contributions from the variational responses, its concentration dependence is similar to that of the oxygen breathing mode due to band renormalization effects.

Because the copper –oxygen overlap integral is almost unchanged when ions are displaced perpendicularly, the transverse motion of either copper or oxygen ions have smaller matrix elements than for the copper breathing mode. To lowest order, the variation in hybridization depends quadratically on the displacement. In linear response theory, both of these motions lead to almost equivalent electronic responses. This corresponds to

$$V_{1,1} = V_{1,2} = V_{2,1} = V_{2,2} \approx V, e_1 = e_2 \text{ and } \lambda_1 = \lambda_2 \quad \text{(A11)}$$

The matrix element for these modes near the metal – insulator transition is

$$g_{X,T} \approx \frac{4r_0^4}{(\varepsilon_d - \varepsilon_p)^2} k_2 \sin 4\bar{k} \quad \text{(A12)}$$

Here, the z axis is the direction perpendicular to the chain. As might be expected, there are no contribution dependence of the transition matrix element, therefore, is entirely from renormalized band structure. Furthermore, we can easily see that the x dependence

of the matrix element is negligible because of the lack of a distortion – induced electronic response.

Appendix II: Two Dimensions Electron – Phonon Transition Matrix Elements

As in one dimension, we consider the scattering processes between states $\alpha_{k,\sigma}$ and $\alpha_{k+Q,\sigma}$, and express these quasiparticle states explicitly in terms of a linear combination of $3d_{x^2-y^2}$, $2p_x$ and $2p_y$, orbitals

$$\alpha_{k,\sigma} = A^{+}(D_{1,k,\sigma} - D_{2,k,\sigma}) + B_x^{+} C_{x_1,k,\sigma} + B_x^{+*} C_{x_2,k,\sigma} + B_y^{+} C_{y_1,k,\sigma} + B_y^{+*} C_{y_2,k,\sigma} \qquad \text{(B1)}$$

and

$$\alpha_{k+Q,\sigma} = A^{-}(D_{1,k,\sigma} - D_{2,k,\sigma}) + B_x^{-} C_{x_1,k,\sigma} + B_x^{-*} C_{x_2,k,\sigma} + B_x^{-} C_{x_1,k,\sigma} + B_x^{-*} C_{x_2,k,\sigma} \qquad \text{(B2)}$$

Here, the coherence factors $A^{\pm}$ and $B_{\eta}^{\pm}$ measure the copper and oxygen contribution to a quasiparticle state. An asterisk $(*)$ denotes the complex conjugate, and the superscripts (+ and -) are used to indicate the elements of the first and second row in the unitary matrix.

In order to derive Eqns (3.14) and (3.15), we determine the overlap integrals V and t as a function of the separation distance and orientation. First, we change the amplitude of the static displacement of either the copper or oxygen ions and then calculate e_n and λ_n from the mean – field equations for H_{FP}^{2d} at each E_F. Finally, we extract $\delta e_0 / \delta R$ and $\delta \lambda_0 / \delta R$ by comparing e_n and λ_n to e_0 and λ_0 as a function of the displacement. Each phonon response leads to a different response. We therefore consider each X mode separately.

Because d and p orbitals are highly directional, the overlap integrals depend strongly on the relative orientation of these orbitals. This is illustrated in the orientation dependence of oxygen – oxygen overlap integral

$$t(p_x, p_y) = \bar{l}\bar{m} V_{pp\sigma} - \bar{l}\bar{m} V_{pp\pi} \qquad \text{(B3)}$$

and the copper – oxygen hybridization

$$V(p_x, d_{x^2-y^2}) = \frac{\sqrt{3}}{2}\bar{l}(\bar{l}^2 - \bar{m}^2)V_{pd\sigma} + \bar{l}(\bar{l} - \bar{l}^2 + \bar{m}^2)V_{pd\pi} \quad \text{(B4)}$$

$$V(p_y, d_{x^2-y^2}) = \frac{\sqrt{3}}{2}\bar{m}(\bar{l}^2 - \bar{m}^2)V_{pd\sigma} \quad \text{(B5)}$$

Here, the relative orientation of two overlapping orbitals are denoted by $\bar{l}, \bar{m}$, and $\bar{n}$ where $d = \bar{l}\hat{x} + \bar{m}\hat{y} + \bar{n}\hat{z}$. The overlap integral between orbitals $d_{x^2-y^2}$ and $p_{x,y}$, and between p_x and p_y also depends strongly on the separation distance

$$V_{pd\sigma(\pi)} = \zeta_{pd\sigma(\pi)} \frac{1}{m} \frac{r_d^{3/2}}{d^{1/2}} \quad \text{(B6)}$$

$$V_{pp\sigma(\pi)} = \zeta_{pp\sigma(\pi)} \frac{1}{m} \frac{1}{d^2} \quad \text{(B7)}$$

Where ζ is a constant which is determined by the types of bonds between the two orbitals.although the hybridization integrals (*V* and *t*) have both σ and π bond contributions, these details are not necessary for the purpose of our calculation. When the distortion is small, we can reexpress the changes in hybridization in terms of the undistorted values *V* and *t*. We calculate the changes in the copper – oxygen as well as the oxygen – oxygen overlap to lowest order in displacement by expanding Eqs. B3, B4 and B5.

Expressing the antibonding state in terms of coherence factors $A^{\pm}$ and $B^{\pm}$, which depend on dopant concentration, we examine the x dependence of the matrix element for each X phonon by evaluating Eq. 3.13. When the antibonding band is half full, the states near E_F are copperlike with no oxygen mixture i.e., $A^{\pm} = 1$ and $B^{\pm} = 0$. When holes are added to this band, however, the copperlike states near E_F become somewhat

oxygenlike.This implies $B_\eta^\pm$ increases while $A^\pm$ decreases by the same amount. Since $A^\pm$ and $B^\pm$ are elements of a unitary matrix, we can easily see concentration dependence of the matrix elements by counting the number of $B_\eta^{\pm}{}'s$.

The frequency of the planer mode, calculated by the LDA approach, range from 6 to 60 meV and the phonon density is a maximum at roughly 20 meV. However, the actual measured value differs somewhat from this because screening effects are not fully accounted for in LDA calculations. The copper mode is equivalent to a one dimensional breathing mode which creates a different local environment for oxygen sites for $2p_x$ and $2p_y$ orbital sites, while maintaining identical copper sites. Therefore, this mode generates a static oxygen CDW by transferring charge from one oxygen site to another. We write the matrix element for this mode as

$$g_{X,M_1} = 4\sum_\eta \left[\sqrt{2}S_{Cu} I_{\alpha,\eta}^{+} + ir_0\left[k_x^{'} I_{b,\eta}^{-} - \frac{7}{\sqrt{2}\ V} I_{c,\eta}^{+}\right]\right] \qquad \text{(B8)}$$

We express the various orbital contributions to the matrix element in terms of coherence factors $A^\pm$ and $B^\pm$

$$I_{a,\eta}^{\pm} = A^{-} B_\eta^{+'} \cos\bar{k}_\eta \pm A^{+} B_\eta^{-''} \sin\bar{k}_\eta, \qquad \text{(B9)}$$

$$I_{b,\eta}^{\pm} = A^{-} B_\eta^{+''} \sin\bar{k}_\eta \pm A^{+} B_\eta^{-'} \cos\bar{k}_\eta, \qquad \text{(B10)}$$

$$I_{c,\eta}^{\pm} = A^{-} B_\eta^{+''} \cos\bar{k}_\eta \pm A^{+} B_\eta^{-'} \sin\bar{k}_\eta, \qquad \text{(B11)}$$

$$I_{d,\eta}^{\pm} = A^{-} B_\eta^{+'} \sin\bar{k}_\eta \pm A^{+} B_\eta^{-''} \cos\bar{k}_\eta \qquad \text{(B12)}$$

Although the $A^\pm$'s are real, the $B_\eta^\pm$'s are complex. Hence, we separate $B^\pm$ in terms of real and imaginary components $B_\eta^\pm = B_\eta^{\pm'} + iB_\eta^{\pm'}$. We use the notation

$$\bar{k}_x = \frac{1}{\sqrt{2}}(\bar{k}_x' - \bar{k}_y'),\ \bar{k}_y = \frac{1}{\sqrt{2}}(\bar{k}_x' + \bar{k}_y') \tag{B13}$$

to simplify the expression. A single prime on k_η denotes the momentum in the reduced BZ corresponding to a distorted lattice having a frozen **X** phonon. By counting the powers of e_0, we see that the x – dependence of this matrix element varies as e_0^2 as half – filling is approached.

Although the oxygen quadrupolar mode appears to transfer charge between copper sites, all copper sites remain identical. Furthermore, all oxygen sites remain equivalent as well. The energy of this mode is 100 meV and the density of the states is very low. The matrix element for this mode is given by

$$g_{X,M_2} = 4\left(\sum_\eta (S_0 I_{a,\eta}^+ - 7r_0 I_{b,\eta}^+) - r_0(\bar{k}_x I_{c,x}^- - \bar{k}_y I_{c,y}^-) + \sqrt{2}t(E^- \bar{k}_x' \cos\bar{k}_y' - E^+ \cos\bar{k}_x')\right) \tag{B14}$$

Appendix III: Data for Specific Heat and Entropy against absolute Temperature.

Table C1: Data for Specific Heat against temperature (E_p = 3.5 x 10^{-6} eV and u_d = 2.5 x 10^{-6} eV) for YBaCuO.

Temperature, T(K)	Specific Heat, C_v x 10^{-3}(eV/kgK)			
	$t_{pd} = 0.0\,eV$ $g_{ep} = 0.0\,eV$	$t_{pd} = 0.0\,eV$ $g_{ep} = 2.0\times10^{-6}\,eV$	$t_{pd} = 1.6\times10^{-6}\,eV$ $g_{ep} = 0.0\,eV$	$t_{pd} = 1.6\times10^{-6}\,eV$ $g_{ep} = 2.0\times10^{-6}\,eV$
15	5.4	2.1	2.4	0.9
20	8.0	4.3	4.6	2.3
25	9.1	5.8	6.1	3.7
30	9.3	6.7	7.0	4.8
35	9.0	7.1	7.2	5.4
40	8.5	7.2	7.3	5.8
45	7.9	6.9	7.1	5.9
50	7.3	6.6	6.7	5.8
60	6.1	5.9	6.0	5.5
70	5.2	5.2	5.2	5.0
80	4.4	4.6	4.6	4.6

Table C2: Data for specific heat against absolute temperature (E_p = 5.5 x 10^{-6} eV and u_d = 5.5 x 10^{-6} eV) for YBaCuO.

Temperature, T(K)	Specific Heat, C_v x 10^{-3}(eV/kgK)			
	$t_{pd} = 0.0eV$ $g_{ep} = 0.0eV$	$t_{pd} = 0.0eV$ $g_{ep} = 2.0\times10^{-6}eV$	$t_{pd} = 1.6\times10^{-6}eV$ $g_{ep} = 0.0eV$	$t_{pd} = 1.6\times10^{-6}eV$ $g_{ep} = 2.0\times10^{-6}eV$
15	0.8	0.3	0.3	0.1
20	2.2	1.1	1.2	0.6
25	3.6	2.2	2.3	1.3
30	4.7	3.1	3.2	2.0
35	5.3	3.9	4.0	2.8
40	5.7	4.4	4.5	3.3
45	5.9	4.7	4.8	3.7
50	5.8	4.8	4.9	4.0
55	5.7	4.9	5.0	4.2
60	5.5	4.8	4.9	4.3
70	5.0	4.7	4.7	4.2
80	4.5	4.3	4.3	4.1
90	4.1	4.0	4.0	3.8
100	3.7	3.7	3.7	3.6

Table C3: Data for specific heat against absolute temperature (E_p = 7.5 x 10^{-6} eV and u_d = 6.5 x 10^{-6} eV) for YBaCuO.

Temperature , T(K)	Specific Heat, C_v x 10^{-3}(eV/kgK)			
	$t_{pd} = 0.0\ eV$ $g_{ep} = 0.0 eV$	$t_{pd} = 0.0 eV$ $g_{ep} = 2.0\times10^{-6} eV$	$t_{pd} = 1.6\times10^{-6} eV$ $g_{ep} = 0.0 eV$	$t_{pd} = 1.6\times10^{-6} eV$ $g_{ep} = 2.0\times10^{-6} eV$
15	0.3	0.2	0.1	0.1
20	1.2	0.7	0.6	0.3
25	2.3	1.5	1.3	0.8
30	3.2	2.3	2.1	1.4
35	4.0	3.1	2.8	2.0
40	4.5	3.6	3.4	2.5
45	4.8	4.0	3.8	2.9
50	4.9	4.3	4.1	3.3
55	5.0	4.4	4.2	3.5
60	4.9	4.5	4.3	3.7
70	4.7	4.4	4.2	3.8
80	4.3	4.1	4.1	3.7
90	4.0	3.9	3.8	3.6
100	3.7	3.6	3.6	3.4
110	3.3	3.3	3.3	3.2

Table C4: Data for entropy against absolute temperature (E_p = 3.5 x 10^{-6} eV and u_d = 2.5 x 10^{-6} eV) for YBaCuO.

Temperature, T(K)	Entropy, S x 10^{-3}(ergs/K)			
	$t_{pd} = 0.0\,eV$ $g_{ep} = 0.0\,eV$	$t_{pd} = 0.0\,eV$ $g_{ep} = 2.0\times10^{-6}\,eV$	$t_{pd} = 1.6\times10^{-6}\,eV$ $g_{ep} = 0.0\,eV$	$t_{pd} = 1.6\times10^{-6}\,eV$ $g_{ep} = 2.0\times10^{-6}\,eV$
20	3.7	1.4	1.6	0.7
25	5.6	2.5	2.7	1.3
30	7.2	3.7	4.0	2.1
35	8.8	4.7	5.1	2.9
40	9.9	5.7	6.1	3.6
45	10.7	6.5	6.8	4.3
50	11.6	7.2	7.5	4.9
60	12.9	8.4	8.9	6.0
70	13.6	9.2	9.8	6.8
80	14.5	9.9	10.5	7.4
100	15.1	10.8	11.5	8.4

Table C5: Data for entropy against absolute temperature (for E_p = 5.5 x 10^{-6} eV and u_d = 5.5 x 10^{-6} eV) for YBaCuO.

Temperature, T(K)	Entropy, S x 10^{-3}(J/K)			
	$t_{pd} = 0.0\,eV$ $g_{ep} = 0.0\,eV$	$t_{pd} = 0.0\,eV$ $g_{ep} = 2.0\times10^{-6}\,eV$	$t_{pd} = 1.6\times10^{-6}\,eV$ $g_{ep} = 0.0\,eV$	$t_{pd} = 1.6\times10^{-6}\,eV$ $g_{ep} = 2.0\times10^{-6}\,eV$
30	2.00	1.08	1.12	0.60
40	3.52	2.18	2.24	1.38
50	4.83	3.22	3.30	2.20
60	5.87	4.12	4.21	2.96
70	6.70	4.86	4.95	3.62
80	7.35	5.46	5.56	4.17
90	7.87	5.95	6.05	4.64
100	8.29	6.36	6.46	5.03
110	8.63	6.69	6.79	5.36

Table C6: Data for entropy against absolute temperature (E_p = 7.5 x 10^{-6} eV and u_d = 6.5 x 10^{-6} eV) for YBaCuO.

Temperature, T(K)	Entropy, S x 10^{-3}(ergs/ K)			
	$t_{pd} = 0.0\,eV$ $g_{ep} = 0.0\,eV$	$t_{pd} = 0.0\,eV$ $g_{ep} = 2.0\times10^{-6}\,eV$	$t_{pd} = 1.6\times10^{-6}\,eV$ $g_{ep} = 0.0\,eV$	$t_{pd} = 1.6\times10^{-6}\,eV$ $g_{ep} = 2.0\times10^{-6}\,eV$
30	1.12	0.62	0.71	0.34
40	2.24	1.41	1.57	0.90
50	3.30	2.24	2.45	1.55
60	4.20	3.01	3.26	2.18
70	4.95	3.67	3.94	2.76
80	5.56	4.22	4.50	3.26
90	6.04	4.69	4.98	3.70
100	6.46	5.08	5.37	4.07
110	6.79	5.40	5.70	4.39